CFD Simulations for the Effect of Unsteady Wakes on the Boundary Layer of a Highly Loaded Low-Pressure Turbine Airfoil (L1A)

Final Report

Samuel J. Vinci
Cleveland State University, Cleveland, Ohio

NASA STI Program . . . in Profile

Since its founding, NASA has been dedicated to the advancement of aeronautics and space science. The NASA Scientific and Technical Information (STI) program plays a key part in helping NASA maintain this important role.

The NASA STI Program operates under the auspices of the Agency Chief Information Officer. It collects, organizes, provides for archiving, and disseminates NASA's STI. The NASA STI program provides access to the NASA Aeronautics and Space Database and its public interface, the NASA Technical Reports Server, thus providing one of the largest collections of aeronautical and space science STI in the world. Results are published in both non-NASA channels and by NASA in the NASA STI Report Series, which includes the following report types:

- TECHNICAL PUBLICATION. Reports of completed research or a major significant phase of research that present the results of NASA programs and include extensive data or theoretical analysis. Includes compilations of significant scientific and technical data and information deemed to be of continuing reference value. NASA counterpart of peer-reviewed formal professional papers but has less stringent limitations on manuscript length and extent of graphic presentations.

- TECHNICAL MEMORANDUM. Scientific and technical findings that are preliminary or of specialized interest, e.g., quick release reports, working papers, and bibliographies that contain minimal annotation. Does not contain extensive analysis.

- CONTRACTOR REPORT. Scientific and technical findings by NASA-sponsored contractors and grantees.

- CONFERENCE PUBLICATION. Collected papers from scientific and technical conferences, symposia, seminars, or other meetings sponsored or cosponsored by NASA.

- SPECIAL PUBLICATION. Scientific, technical, or historical information from NASA programs, projects, and missions, often concerned with subjects having substantial public interest.

- TECHNICAL TRANSLATION. English-language translations of foreign scientific and technical material pertinent to NASA's mission.

Specialized services also include creating custom thesauri, building customized databases, organizing and publishing research results.

For more information about the NASA STI program, see the following:

- Access the NASA STI program home page at *http://www.sti.nasa.gov*

- E-mail your question to *help@sti.nasa.gov*

- Fax your question to the NASA STI Information Desk at 443–757–5803

- Telephone the NASA STI Information Desk at 443–757–5802

- Write to:
  STI Information Desk
  NASA Center for AeroSpace Information (CASI)
  7115 Standard Drive
  Hanover, MD 21076–1320

NASA/CR—2012-217417

CFD Simulations for the Effect of Unsteady Wakes on the Boundary Layer of a Highly Loaded Low-Pressure Turbine Airfoil (L1A)
Final Report

Samuel J. Vinci
Cleveland State University, Cleveland, Ohio

National Aeronautics and
Space Administration

Glenn Research Center
Cleveland, Ohio 44135

September 2012

Acknowledgments

Level of Review: This material has been technically reviewed by NASA technical management.

Available from

NASA Center for Aerospace Information	National Technical Information Service
7115 Standard Drive	5301 Shawnee Road
Hanover, MD 21076–1320	Alexandria, VA 22312

Available electronically at http://www.sti.nasa.gov

CFD SIMULATIONS FOR THE EFFECT OF UNSTEADY WAKES ON THE BOUNDARY LAYER OF A HIGHLY LOADED LOW PRESSURE TURBINE AIRFOIL (L1A)

SAMUEL J VINCI

ABSTRACT

The study of a very high lift, low-pressure turbine airfoil in the presence of unsteady wakes was performed computationally and compared against experimental results. The experiments were conducted in a low speed wind tunnel under high (4.9%) and then low (0.6%) freestream turbulence intensity conditions with a flow coefficient (ζ) of 0.7. The experiments were done on a linear cascade with wakes that were produced from moving rods upstream of the cascade. The flow coefficient was kept at 0.7 while the rod to blade spacing was changed from 1 to 1.6 to 2 blade spacings. These cases were conducted for Reynolds number equal to 25,000 and 50,000, based on the suction surface length and the nominal exit velocity from the cascade.

The experimental and computational data have shown that in cases without wakes, the boundary layer separated and did not reattach. The CFD was done with LES and URANS utilizing the finite-volume code ANSYS Fluent under the same freestream turbulence and Reynolds number conditions as the experiment but only at a rod to blade spacing of 1.

With wakes, separation was largely suppressed, particularly if the wake passing frequency was sufficiently high. This was validated in the 3D CFD efforts by comparing the experimental results for the pressure coefficients and velocity profiles, which were reasonable for all cases examined. The 2D CFD efforts failed to capture the three

dimensionality effects of the wake and thus were less consistent with the experimental data. The effect of the freestream turbulence intensity levels also showed a little more consistency with the experimental data at higher intensities when compared with the low intensity cases.

As a further computational study, cases were run to simulate higher wake passing frequencies which were not run experimentally. The results of these computational cases showed that an initial 25% increase from the experimental wake passing frequency of F=0.548 greatly reduced the size of the separation bubble, nearly completely suppressing it, however an additional 33% increase on top of this did not prove to have much of an effect.

TABLE OF CONTENTS

Re50,000, High Free Stream Turbulence Intensity

LIST OF TABLES

LIST OF FIGURES

NOMENCLATURE

Cp $2(P_T - P)/\rho U_e^2$, pressure coefficient

C_x axial chord length

F $fL_{j\text{-}te}/U_{ave}$, dimensionless wake passing frequency

f frequency

HFSTI   High Freestream Turbulence Intensity (4.9%)

$L_{j\text{-}te}$ length of adverse pressure gradient region on suction surface

LFSTI   Low Freestream Turbulence Intensity (0.6%)

L_s suction surface length

L_ϕ blade spacing (pitch)

P pressure

P_S upstream static pressure

P_T upstream stagnation pressure

P_{Te} downstream stagnation pressure

Re $U_e L_s/\nu$, exit Reynolds number

s streamwise coordinate, distance from leading edge

T period of wake passing cycle

t time

TI background freestream turbulence intensity

U local mean velocity

U_{ave} average freestream velocity in adverse pressure gradient region

U_i inlet freestream velocity

U_e nominal exit freestream velocity, based on inviscid solution

u' rms fluctuating streamwise velocity

x axial distance from leading edge

ϕ coordinate along blade spacing, normal to axial chord

ν kinematic viscosity

ρ density

ψ $(P_T\text{-}P_{Te})/(P_T\text{-}P_S)$, total pressure loss coefficient

ζ $U_i\cos(\alpha_i)/U_{rod} = U_{axial}/U_{rod}$, flow coefficient

Chapter I

Introduction

The desire to reduce fuel costs and improve engine performance in the gas turbine industry has led many to do experimental and computational fluid dynamics (CFD) research on the effects of flow over the airfoils of the low-pressure turbine blades. These experiments have shown that separation of the flow can occur on the suction surface of these blades due to the presence of adverse pressure gradients. This separation can result in partial loss of lift and higher aerodynamic losses at high altitude cruise conditions and becomes increasingly more severe as the aft loading of the airfoils increases.

The desire to reduce the airfoil count and thus make a more cost efficient engine outweighs the losses associated with increasing the loading of airfoils, thus studying and accurately predicting the size and severity of the separation associated with a given loading is required in order to make improved designs in these high lift airfoils. This has led many in the field of computational fluid dynamics to create models that match the experimental data of these high lift airfoils. However, much like the airfoils themselves, an efficient model being low in computational time is as desirable as an accurate one. This is because the flow can be modeled directly using a direct numerical simulation technique, however the grid size and resulting computational time associated with such models is far too expensive to be useful in industry. This has lead to a number of different turbulence models, which use approximations of the flow in different regions to model the flow rather than directly compute what is occurring, thus decreasing the computational costs. These models vary in success, especially since the flow over an airfoil is very complex. It is the goal of this report to show which turbulence models

accurately model available experimental data. Once a model is proven to provide

accurate results, further insight to the physics of the flow over the airfoil is capable of

being examined. In this report, a review of previous studies examining different laminar

to turbulent transitions will be reviewed, along with the relevant computational studies of

these flows, which have provided the base of this study. A detailed description of the

experimental set up and the results that were used as the data to validate the

computational models will be provided as well as a detailed description of the

computational domain created to run these models. Finally an examination of the

computational results will prove which turbulence models can provide accurate results

and further insight into flow transitioning separation and suppression.

Chapter II

Literature Review

The transition from a laminar to a turbulent flow over the airfoil blade is described by Langtry [2006]. Here it is described that there are several different transitions that can cause the flow to become turbulent. The first is a "Natural" transition that occurs when the freestream turbulence has a relatively low intensity that allows for the growth of Tollmien-Shlichting two-dimensional waves. In general it is assumed that the freestream turbulence intensity levels in real turbomachinery is rather high, thus the presence of this form of transition is only partially present. However, since there are the adverse pressure gradients that are created over these highly loaded airfoils, this form of transition will still be considered to play an effect over the airfoils in this study. The second form of transition is a result of the high freestream turbulence in the flow and is called "bypass transition." This form of transition is a result of rapidly growing three dimensional instabilities, which disturb the boundary layer and cause the flow to become turbulent. The later form of transition is the type that is the main focus of this paper.

Early experimental and computational studies of the flow over these high lift airfoils were performed by examining the airfoils by themselves in a wind tunnel with varying levels of freestream turbulence intensities applied to the upstream flows. However, it has become evident that the presence of the forward stages of stator blades in front of the rotor airfoil blades creates wake shedding vortices, which play a big role on the boundary layer of these rotor blades. The velocity deficit in these wakes cause flow outside of the wake to accelerate and impinge on the suction surface of stator blades

creating a sort of "negative jet" [Hodson and Howell, 2005]. The study of this wake and the wake induced transition associated with it has started to become the topic of study in a number of experimentals, however this type of flow has yet to be extensively modeled computationally due to the difficulties associated with creating these models, which will be explained in more detail below.

The creation of the impinging wake on a stator has been studied by Pluim et al. [2009] and it was shown that a circular rod provides a sufficient representation of the form of the true wake that comes off the rotor blade. Thus experimental data is collected by passing a line of circular rods upstream of a cascade of airfoils with data collected by hot wire anemometers over the suction side of these airfoils. Many experiments have been run analyzing the wake/blade interaction effects; see Bons et al. [2008] and Pluim et al. [2009], however in this study direct experimental data was provided from Volino [2010]. Thus it was these experiments that the focus of this computational study will be based on.

In Volino [2010] the study of the effect of different rod to blade spacings was studied. The data behind the results of this experiment was available for this report and thus these cases are the basis of what this report attempted to numerically model. The details of the experimental domain and results are given in more detail below.

Numerical studies of the wake and its subsequent interaction with an airfoil was studied in Sakar [2009]. In this study, the wake was created via a circular rod in its own computational domain and then interpolated into a domain containing the airfoil. The analysis of a circular wake generating rod and its effect on a downstream airfoil was examined for a Reynolds number of 78,000 (based on the axial chord and the inlet

velocity). The airfoil used is T106 [Stieger et al., 2003] with flow coefficient (ζ) of 0.83 and reduced blade passing frequency of 0.68. The wake was originally generated in both a 2D and 3D simulation using URANS and LES turbulence models respectively. These results were then interpolated into a 3D airfoil geometry and the effects of the wake/airfoil interaction were studied in LES. It was shown that the wakes produced in LES and interpolated into the airfoil domain produced smaller scale eddies and thus produced more accurate predictions of separation flow control than the 2D wakes.

Suzen and Huang [2005] numerically studied unsteady wake/blade interactions in LPT PAK-B flows using an intermittency transport equation. They followed experiments of Kaszeta et al. [2001, 2002] and Stieger [2002]. In that study predictions of the flow with the Intermittency Transport model were in a good agreement with experimental data for pressure coefficient. Differences in velocity predictions in the separated region were attributed to the inability of hot wire anemometry, used in experiment, to measure negative velocities. The observation was made that high wake passing frequency resulted in suppression of the separation zone due to higher turbulence levels generated in the wake.

Rodi [2006] conducted DNS and LES studies of the flow past turbine blades with incoming wakes. Reynolds number based on axial chord and inlet velocity was 51,800 in the low Re case and 148,000 in the high Re case. In both cases DNS and LES showed similar results for the pressure coefficient, which were in a reasonable agreement with experimental data. Some disagreement in pressure coefficient near the leading edge on the suction side was attributed to the difference in the inlet flow angle and compressibility effects of the flow, which was modeled as incompressible. In the high Re

case, where the flow was attached, LES predicted transition a little later compared to DNS and therefore it was concluded that LES is not a good tool for predicting this type of flow. However, it is necessary to mention that DNS required 10 times longer to compute, compared to LES and it cost the author several months of calculations on a supercomputer.

Ladreau [2005] took an Unsteady Reynolds Averaging Navier Stokes (URANS) turbulence model and applied it to a moving wake generating rod and airfoil blade geometry. Here it was shown that the URANS models were very sensitive to the grid size and the time step size of the calculation. The results showed that with too coarse of size of either one of these results in the wake structure, with vortex shedding, not developing due to the small length scale of the circular wake generating rod as compared to the blade.

Chapter III

Experimental Facility and Measurements

The experimental data used for comparison in this study came from experiments

by Volino [2010] on a very highly loaded LPT airfoil L1A. This airfoil was designed at

the Air Force Research Laboratory (AFRL) and is available on a limited basis from Clark

[2007]. The L1A is aft loaded which makes the boundary layer more prone to separation

[Bons et al., 2008, Ibrahim et al., 2008 and Volino et al., 2008]. As described in Volino

[2010], experiments were conducted in a closed loop wind tunnel with a seven blade

linear cascade as shown in Fig. 1 with the dimensions shown in Table 1. The streamwise

component of the turbulence intensity was 0.6% with the integral length scale of 6.3 cm.

A tailboard, shown on Fig. 1, was used to ensure the correct flow angle from the cascade

with periodicity at high Reynolds numbers. At low Reynolds numbers the periodicity was

not as good because large separation was present and due to suppression of the separation

on the blades closest to the tailboard.

The wake generator includes a chain near each endwall of the cascade that passes

$0.54C_x$ upstream of the leading edges of the cascade blades. The chain links have hollow

pins, through which the wake generator rods are attached. The diameter of each rod is 4

mm. Tests were run with average distances between rods of 136 mm, 221 mm, and 272

mm, which correspond to $1L_\varphi$, $1.6L_\varphi$ and $2L_\varphi$, where L_φ is the blade spacing in the

cascade. These ratios of rod to blade spacing are in the range expected for vane to rotor

blade spacing in an engine. This wake was initially examined to determine if the wake

shedding produced similar velocity and RMS profiles to that from an airfoil. These

results were compared against downstream profiles from airfoil designs with and without vortex generator jets showing similar profiles, thus proving the circular rod to be a sufficient simulator of an upstream wake generator. Flow coefficients were varied from 0.35 to 1.4 and wake spacing was varied from 1 to 2 blade spacings, resulting in dimensionless wake passing frequencies $F=fL_{j\text{-}te}/U_{ave}$ (f is the frequency, $L_{j\text{-}te}$ is the length of the adverse pressure gradient region on the suction surface of the airfoils, and U_{ave} is the average freestream velocity) ranging from 0.14 to 0.56.

For most tests, the rods were driven at a velocity of 1.18 times the cascade inlet velocity, U_i. This gives a flow coefficient, $\zeta = U_i \cos(\alpha_i)/U_{rod} = 0.7$, where α_i is the inlet flow angle. This is also in the expected range for an engine.
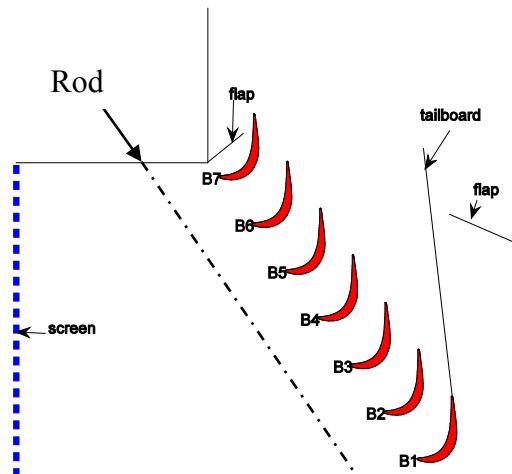
Fig. 1a. Schematic of the linear cascade

Table I: Cascade parameters

Axial Chord, C_x [mm]	True Chord [mm]	Pitch, L_ϕ [mm]	Span [mm]	Suction side, L_s [mm]	Inlet flow angle	Exit flow angle
134	146	136	724	203	35°	60°

The results of this experiment showed that flow over an L1A airfoil is separated without reattachment for Re = 25,000 and 50,000 (based on the suction surface length and the nominal exit velocity from the cascade) [Ibrahim et al., 2008 and Volino et al., 2008]. Volino [2010] observed that in the presence of the wakes passing with high frequencies separation on this airfoil was largely suppressed for Re = 25,000 and 50,000. At lower frequencies the boundary layer separated between wakes.

Chapter IV

Numerical Models and Domain

The numerical simulations were conducted utilizing the finite-volume code

ANSYS FLUENT [2009]. Cases were run at different Reynolds numbers, wake passing

frequencies, and free stream turbulence intensity levels. Table 2 shows a summary of all

CFD conducted in this study.

The computational domain was based off of Ibrahim et al. [2010, however the grid

was then sub-divided into three cell-zone domains, a stationary inlet zone, a moving via a

sliding, periodically repeating translational zone with the circular wake generating rod in

it, and a stationary zone with the airfoil and rest of the downstream domain in it. The

mesh generated around the rod was refined until it showed a wake that was produced and

did not dissipate as it propagated downstream. The interaction between the interface

zones was set up so the conditions periodically repeated themselves allowing for the

wake to carry between zones even as the interfaces became unaligned. The inlet and

outlet conditions varied based on Reynolds' number and the freestream turbulence

intensity of the flow and the boundaries on each face of the grid were set up as periodic in

order to simulate a full blade and a full cascade. For the two dimensional cases this

assumed no variation in the z direction, which will prove to cause modeling issues.

For the two dimensional cases, a URANS calculation utilizing the Transition-SST

turbulence model of Menter et al. [2006] was used. The three dimensional computational

domain was used for both the same URANS calculations and LES calculations. The

number of passages used varied based on a two dimensional or three dimensional domain

and will be explained further below (see Table 1. for cascade parameters). A uniform velocity inflow condition is specified 1.9 C_x upstream of the blade leading edge in the flow direction. The inlet flow angle is set to 33° based on an inviscid calculation of the full cascade used in the experiment [Ibrahim et al., 2008]. This angle agrees with the experimentally measured inlet angle to within the experiment uncertainty. The exit boundary is located 3.8 C_x downstream of the trailing edges in the flow direction. The boundary conditions on the sides of the passage are periodic.

Convergence was established when: 1) residuals reduced to a value 10^{-5}, 2) no change was observed in any field results, and 3) the mass imbalance was less than 0.01 %.

For the 2-D cases, a two-channel domain was designed, having an entire airfoil in the middle, with two rods spaced equally one blade spacing apart as seen in Fig 1b with the details of this grid given in Table II. In the 3-D simulations, with rod to blade spacing of 1 a single airfoil with half a channel spacing above and below was used. Periodic boundary conditions were applied to simulate the entire cascade (Fig. 1b.) and in order to save on computational time. Adding multiple rods to a single domain (in the 2D cases) did not increase the mesh size significantly nor computational time, therefore two blade passages with two rods were used, however for the 3D domain one full blade passage (half a blade passage above and below an airfoil) was simulated to keep the mesh size at a minimum.

Table III summarizes cases examined in this paper, with the same cases also studied experimentally by Volino, [2010] indicated. A combination of variation in Re (25,000, and 50,000), free stream turbulence intensities (LFSTI and HFST) and turbulence modeling approach (URANS-Transition-SST and LES) was considered to match

experimental data. Additional cases with increased rod speeds, and thus increased wake

passing frequency values (F) were studied to examine what effect having a more frequent

wake passing over the blade would cause.

Table II: Grid Refinement Parameters

Grid #	Size (Cells)	Number of grids in z direction	y+	$\Delta z+$	$\Delta x+$
1 (2-D)	60,600	NA	0.132	NA	< 28
2* (2-D)	122,000	NA	0.115	NA	< 10
3 (2-D)	200,000	NA	0.113	NA	< 4
4* (3-D)	1.7 million	32	0.117	<1	< 18

*Grid Used in Computations.

Details of Grid 4

Number of cells (million)	1.7
Number of nodes on the suction surface	292
Number of nodes on the pressure surface	240
Number of nodes in span direction	32
y+	0.117
$\Delta z+$	< 1
$\Delta x+$	< 18
Distance from inlet boundary to the leading edge	3.8 C_x
Distance from the trailing edge to the outlet boundary	1.9 C_x
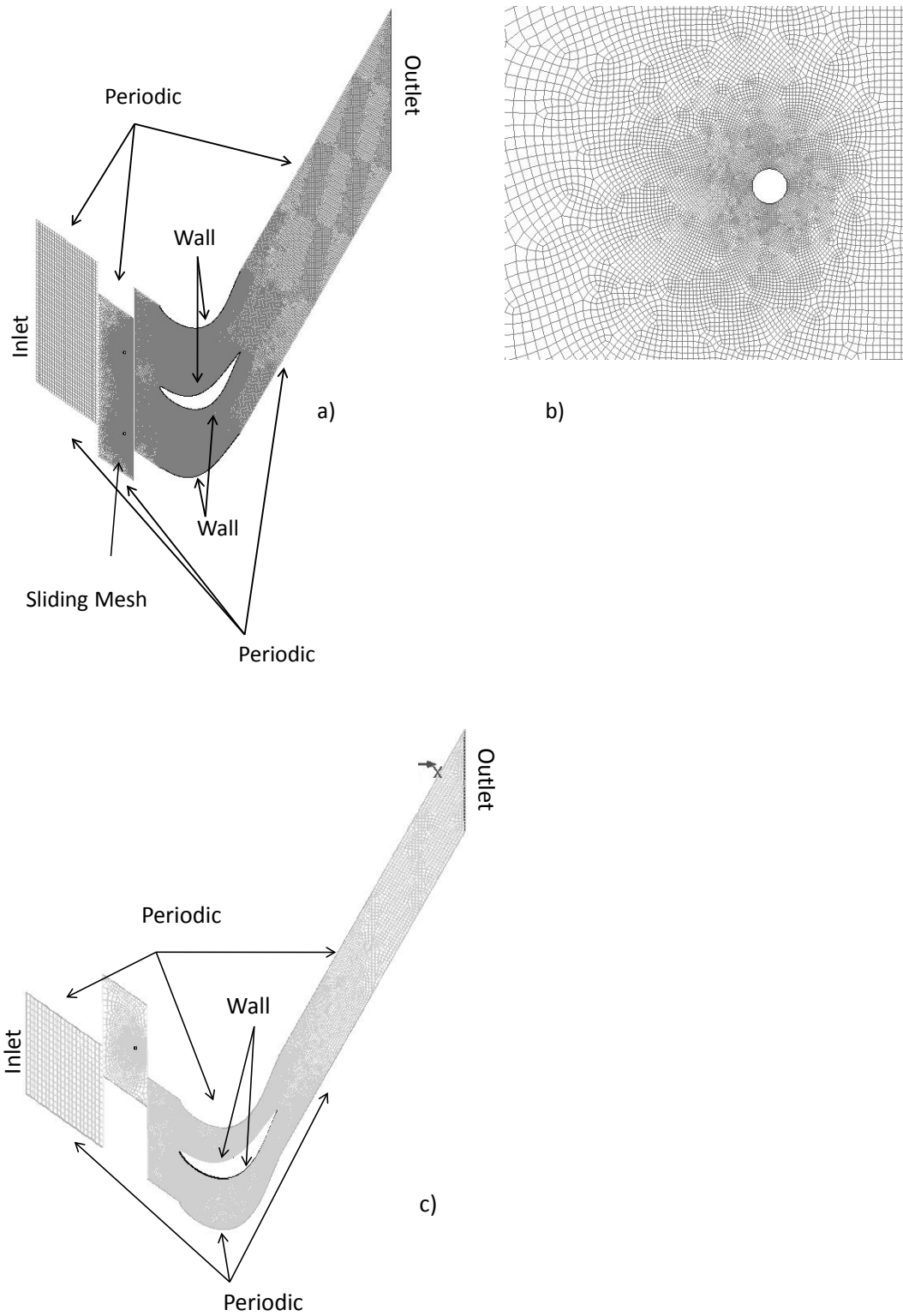
Fig 1b. Schematic of Computational Domains and mesh: a) 2D Domain b) Refined
Rod Mesh c) 3D Computational Domain

Table III. CFD Test matrix

Case	Re	Free Stream Turbulence Intensity	Dimensionless Frequency, F	Turbulence Model
1	25,000	LFSTI*	0.513	Trans-SST (2D)
2	50,000		0.548	
3	25,000	LFSTI*	0.513	LES
4		HFSTI*		
5	50,000	LFSTI*	0.548	
6		HFSTI*		
7		HFSTI	0.698	
8			0.917	

*Experimental data available from Volino [2010].

TURBULENCE MODELS

LES with Dynamic Kinetic Energy Subgrid-Scale model

The governing equations employed for LES are obtained by filtering the time-dependent Navier-Stokes equations in either Fourier (wave-number) space or configuration (physical) space. The filtering process effectively filters out eddies whose scales are smaller than the filter width or grid spacing used in the computations. The resulting equations thus govern the dynamics of large eddies. The subgrid-scale stresses resulting from the filtering operation are unknown, and require modeling. The subgrid-scale turbulence models in Fluent employ the Boussinesq hypothesis as in the RANS models.

The dynamic subgrid-scale kinetic energy model, used in the present study, is based on the model proposed by Kim and Menon [1997]. In this model a separate transport equation is solved for subgrid-scale kinetic energy. The model constants are determined dynamically. The details of the implementation of this model in ANSYS FLUENT and its validation are given by Kim [2004].

Transition-SST (4 equation) model of Menter [2006]

A correlation-based transition model was proposed by Menter et al. [2006]. This model is based on two transport equations. The intermittency transport equation is used to trigger the transition onset. The transport equation for the transition momentum thickness Reynolds number ($Re_{\theta t}$) is used to capture non-local effects of freestream turbulence intensity and pressure gradient at the boundary layer edge. Outside the boundary layer the transport variable was forced to follow the value of $Re_{\theta t}$ given by correlations. Those two equations were coupled with the shear stress transport turbulence model (SST). This model is available in ANSYS FLUENT V-13 as Transition-SST (4 equation) turbulence model.

Chapter V

Results and Discussion

As further validation of the computational domain, the initial cases run were those that a direct comparison with the experimental data provided by Volino [2010] was possible. In all cases, the data will be presented first with the time average statistical data to show how consistent the model is overall. For the cases that proved exceptionally accurate, further analysis and instantaneous data is examined to help better understand the wake interaction over the suction side surface of the airfoil. Using this comparison with the experimental data to validate the accuracy of the results, further cases where simulated to see how changing the rod speed, and thus the wake passing frequency, would then effect the separation and reattachment of the boundary layer. For all the cases presented, a discussion of the results will be given with all the figures associated with the given case presented at the end of each section.

For each case plots of the rod wake velocity profile, C_p, and Total Pressure Loss are compared directly with experimental data for a rod to blade spacing of 1. For the cases which showed exceptional consistency with the experimental data, plots of six streamwise velocity profiles are compared against data for rod to blade spacings of 1.6 and 2. Thus, the CFD results will be analyzed versus the trend of the experimental data, but a direct comparison is not possible.

In computing the Cp plots, the plots were created to match the experimental data, thus:

$$Cp = \frac{(P_{inlet} - P)}{\frac{1}{2}*\rho*U_{ave}^2}$$ (where U_{ave} is the mean freestream velocity between blades.)

However, when creating the contours of Cp, Ansys Fluent utilizes the equation:

$$Cp = \frac{(P - P_{inlet})}{\frac{1}{2} * \rho * v^2}$$

Thus, the contour color values are in reverse of the typical, where blue represents the suction peak and positive values and red is zero to negative.

Further analysis of the wake passing through the cascade passage is done by plotting the second invariant of the velocity gradient tensor, Q-Criterion, iso-surfaces on a mid-z plane, colored by x-velocities in one and Cp values in another plot. This is done to capture the turbulence and vortex shedding of the wake since the definition of Q-Criterion is:

$$Q = -\frac{1}{2} \frac{\partial \overline{u_i}}{\partial x_j} \frac{\partial \overline{u_j}}{\partial x_i} = -\frac{1}{2} (\overline{S}_{ij} \overline{S}_{ij} - \overline{\Omega}_{ij} \overline{\Omega}_{ij})$$

where, $\overline{S}_{ij} = \frac{1}{2} (\frac{\partial \overline{u_i}}{\partial x_j} + \frac{\partial \overline{u_j}}{\partial x_i})$, and $\overline{\Omega}_{ij} = \frac{1}{2} (\frac{\partial \overline{u_i}}{\partial x_j} - \frac{\partial \overline{u_j}}{\partial x_i})$

A two dimensional mesh was first generated to establish a grid that was refined enough to capture the wake vortex shedding and allow for the wake to proceed through the entire blade passage. Figure 2 shows that the initial mesh would capture the shedding, but the wake would quickly dissipate downstream. Therefore a finer mesh was created, allowing for not only the vortex shedding to be captured, but then to continue onward toward the blade passage. A further refinement was then made (not pictured) to see if the results would be improved, however, the results remained consistent with the initial refinement, thus any additional refinements only added computational time without adding any extra benefit. Once this two dimensional grid proved effective, it was used as the base for the projection into the three dimensional grid domain.

It has been shown by Sakar [2009] and Ladreau[2005] that a two dimensional domain would capture the wake effects on a separated boundary layer.   However due to the lack of ability to capture the three dimensionality of a wake vortex and the small scale eddies associated with them, as shown in Figure 3, the effects of the wake only show the proper trends, but the overall magnitude and shape of the wake impinging on a boundary layer are not consistent.   The 2D results under-predict the suction peak value by about 15% and has the peak location 4% too far downstream. It also predicts reattachment to occur about 6% further upstream than the experimental data shows, thus predicting overall a smaller, less intense separation bubble. The three dimensional domain with the LES turbulence model is much more consistent as show in Figure 4, which validates the reason for this domain and turbulence model. It predicts a suction peak value less than 2% less than the experimental and has nearly the same reattachment point. The size and intensity of the separation bubble is also very consistent with the experimental data, as well as the trailing edge values.

 However, the two dimensional results did show some good promise with the Unsteady Reynolds Averaging Navier Stokes (URANS) code. The overall trend was accurate and the results will be further discussed some since the computational time for these cases were on order of 90% faster.
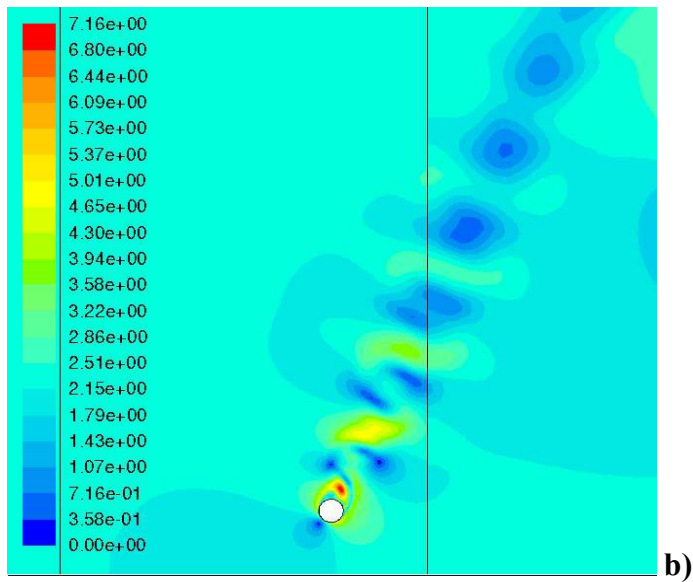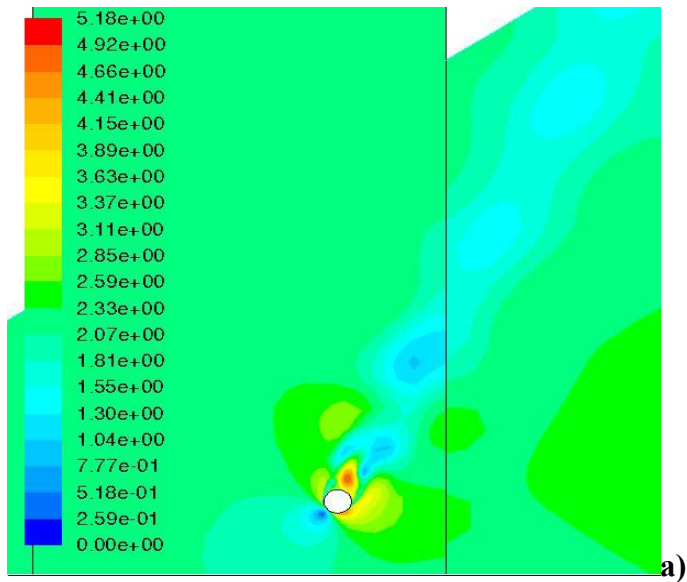
Fig. 2 Rod Wake Velocity Magnitude Contours for Re 50,000: Comparison between a) Grid 1 and b) Grid 2.

5,500

3,850

1,920

825

0

a)

b)
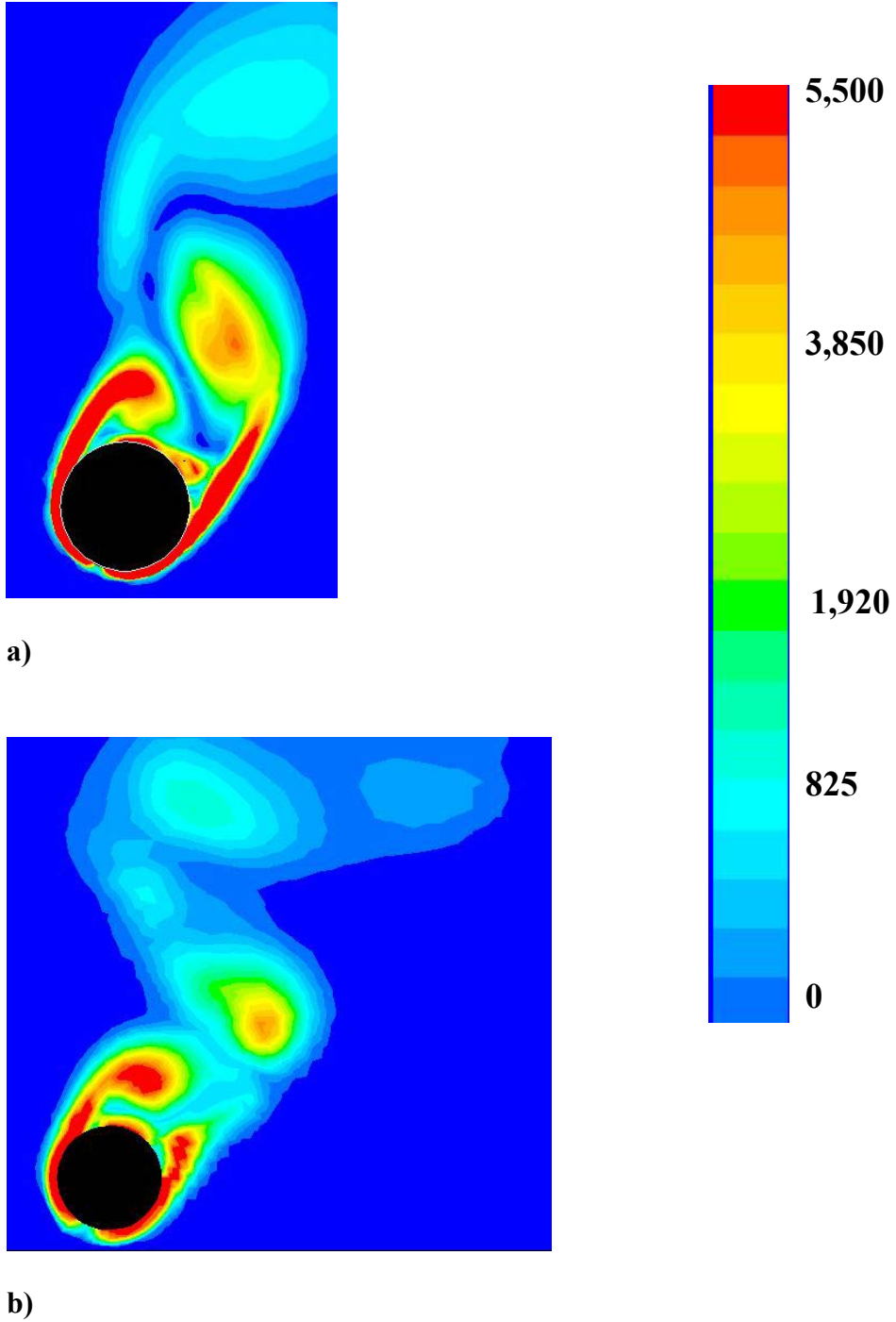
Fig. 3 Vorticity Contours for Re = 50,0000: Comparison between a) 2D (Trans-SST) Spacing 1 versus b) 3D (LES) Spacing 1
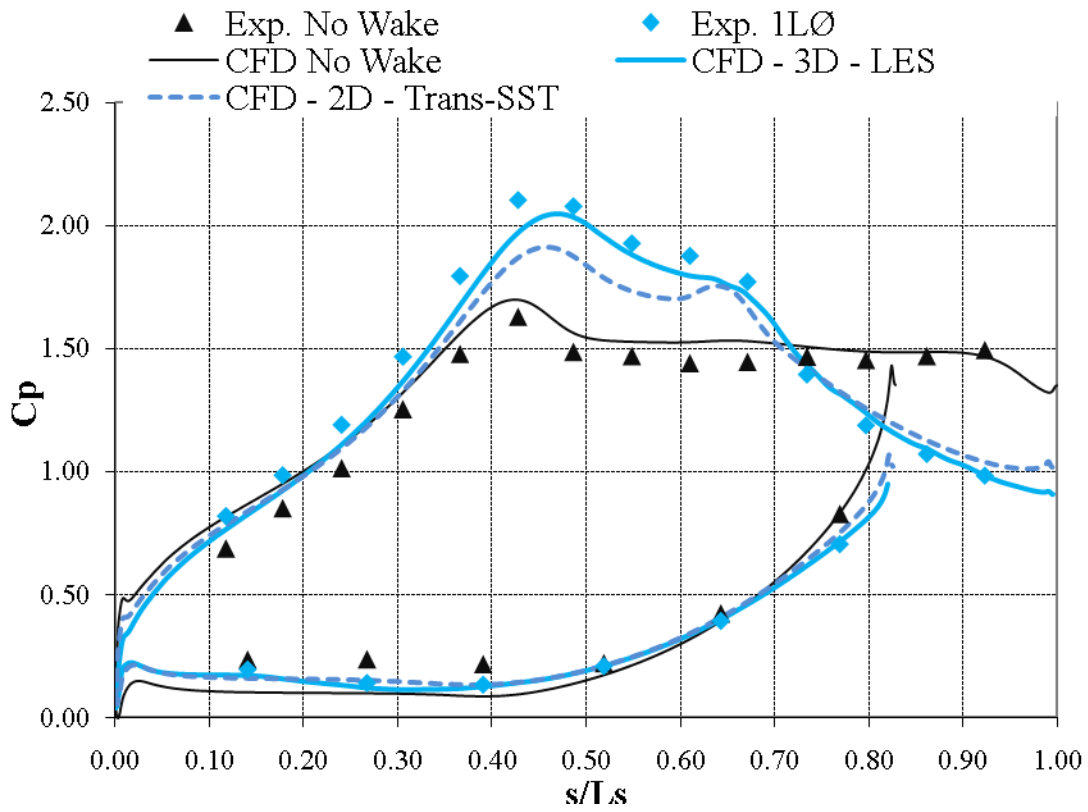
Fig. 4 Code Validation: Comparison of Trans-SST (2D) $1L_\varphi$ results with LES (3D) $1L_\varphi$ and Experimental Data $1L_\varphi$.

2D Results

The Re=25,000, LFSTI Cp values found in Figure 5 shows that the overall shape and trend of the pressure distribution over the suction side of the airfoil is accurately predicted, the magnitude of these values is where the discrepancies lie. This can be associated with the formation of the wake from the rod which will be discussed further below, since the pressure side values, which are not as affected by the wake, match the experimental data nearly exactly and are on order with the no-wake CFD results.

The total pressure loss values (Figure 6) for the Re=25,000, LFSTI case predict less of a pressure drop, $\Delta \psi = 0.7$ as compared to a 0.8 pressure loss shown in the experiment. This can be attributed to the smaller Cp values and separation bubble size prediction on the suction surface. These values are also shifted due to the lack of ability of the periodic boundary conditions of the CFD model to take into account the tailboard of the experimental domain, as seen and described in Kartuzova [2010].

As for to Re=50,000 LFSTI, the experimental data show (Figure 7) an increase in the suction peak Cp value of about 2%, however the CFD does not predict much of a difference from Re=25,000. This leads to a greater discrepancy between the experimental and CFD results, translating to a greater difference in prediction of the total pressure loss profile (Figure 8). Again the pressure side Cp values match experimental data nearly exactly, and as well, like Re=25,000, the same periodicity of the domain error seems to shift the total pressure loss.

In examining the further detail of the rod wake velocity profile, a very smooth velocity profile that has a symmetric profile about the middle of the wake can be seen in Figure 9. The experimental data available was for a rod of the same size and shape

(circular) however it was simulated at a rod to blade spacing of 1.6, and the speed at which it moved at was also different. These differences would be seen mostly in the wake width, not the magnitude since both cases had the same Reynolds number flow value. Therefore the smoothness of the wake profile can be associated with the lack of three-dimensionality of the wake structure and this lack in three dimensionality in the wake profile would also be the main cause of the difference in magnitude of the pressure profiles on the suction surface seen in Figure 7.

These two dimensional simulations provided good enough results to have the confidence to project this mesh in the z-direction and create the three dimensional domain. It also should be noted that the Reynolds numbers (25,000 and 50,000) along with the LFSTI levels associated with these cases are cases that have been historically noted difficult to simulate. Therefore, further two dimensional studies using the Trans-SST turbulence model with a higher freestream turbulence and a higher Reynolds number may prove this model to be more accurate.
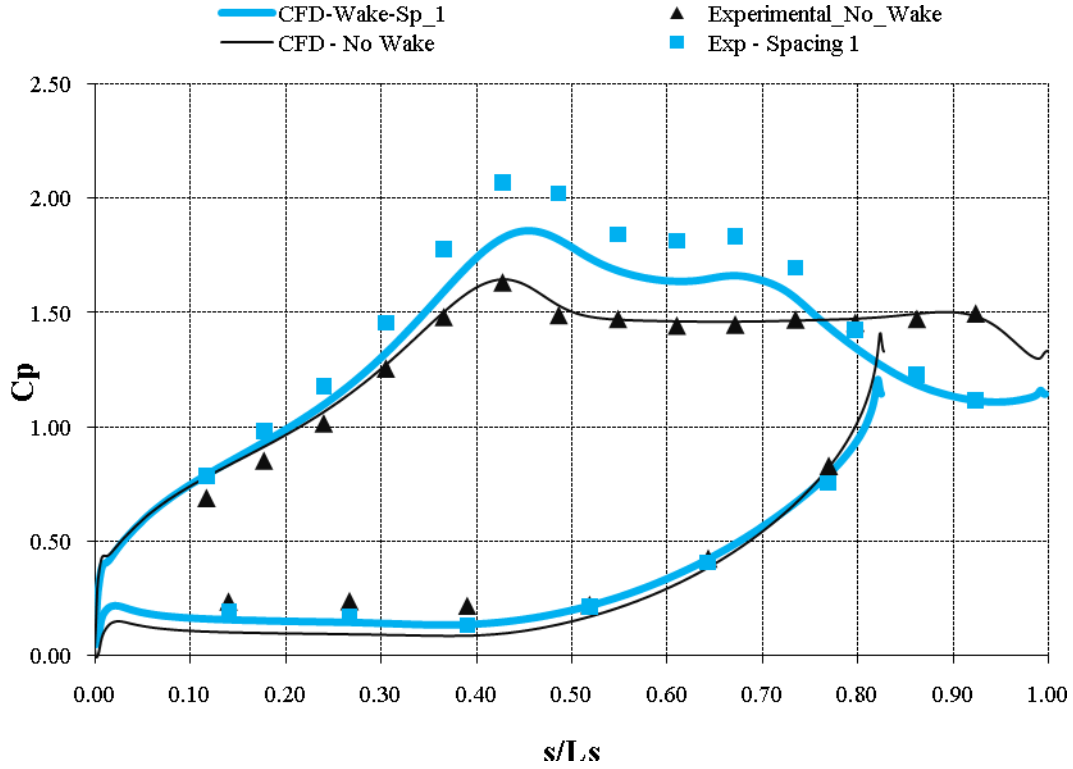
Fig.5 C_p profiles for Re=25,000, LFSTI: Comparison between Trans-SST (2D) and Experimental data
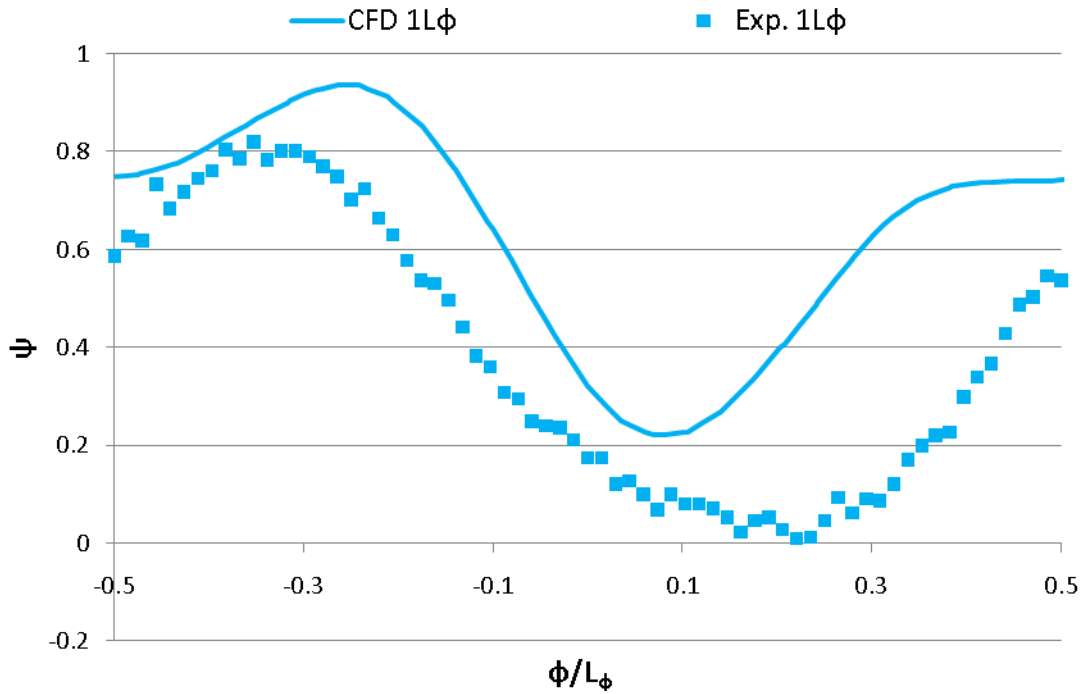
Fig. 6 Total Pressure Loss Coefficient for Re=25,000, LFSTI: Comparison between Trans-SST (2D) and Experimental Data.
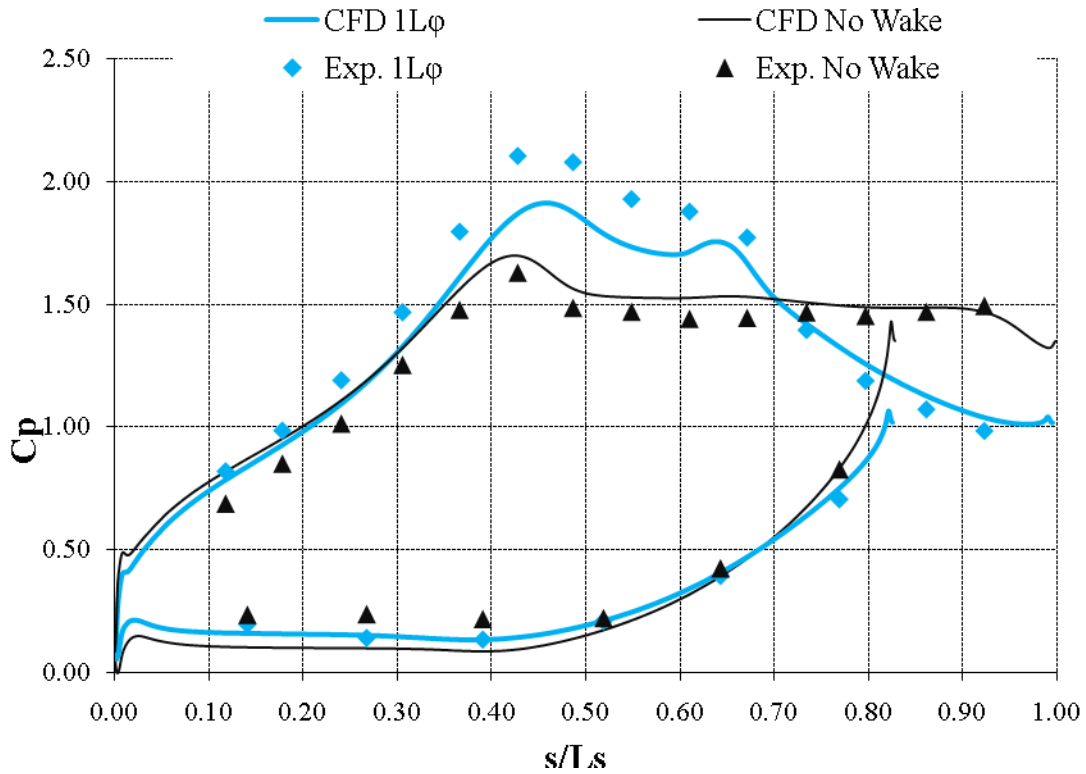
Fig. 7 C_p profiles for Re=50,000, HFSTI: Comparison between Trans-SST (2D) and Experimental data
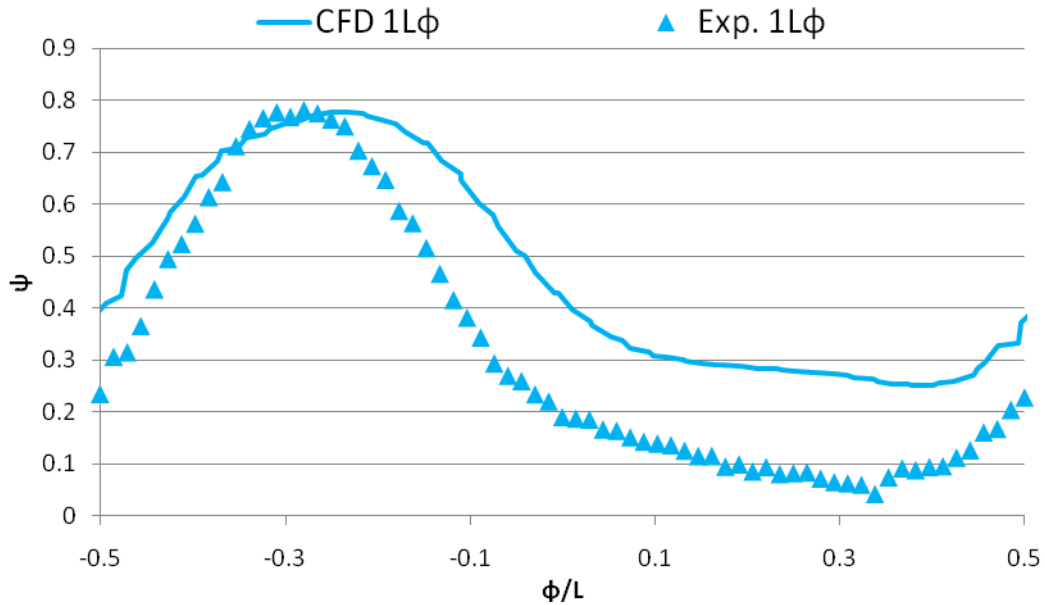
Fig. 8 Total Pressure Loss Coefficient for Re=50,000, HFSTI: Comparison between Trans-SST (2D) and Experimental Data
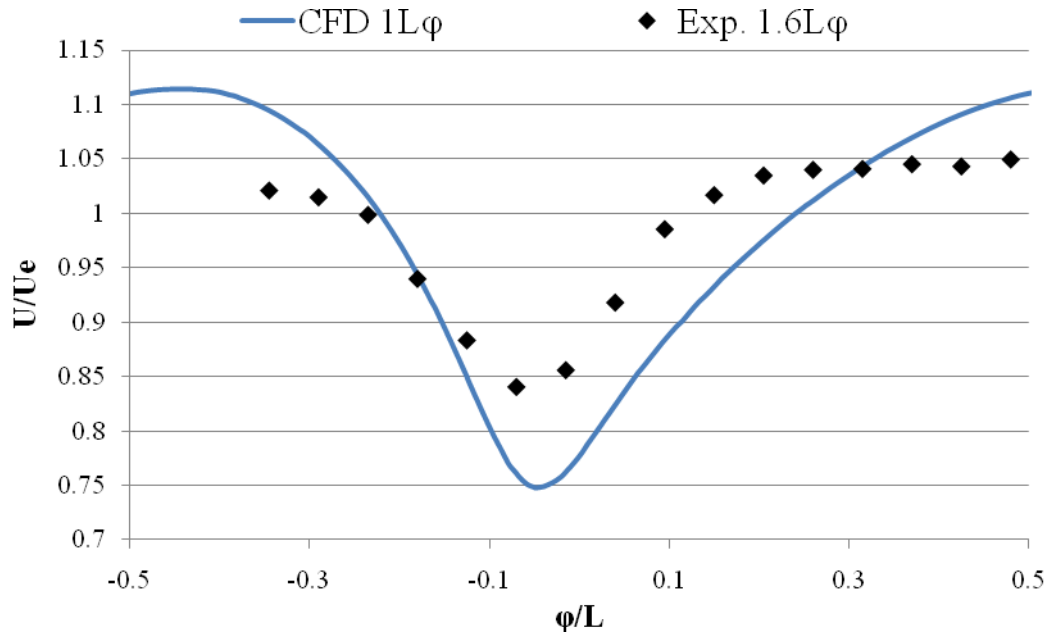
Fig. 9 Rod Wake Velocity Magnitude for Re=50,000, HFSTI: Comparison of Trans-SST (2D), $1L_\varphi$ to Experimental $1.6L_\varphi$

3D Results

Initially the idea was to take the 3D projection of the 2D mesh and keep the same URANS turbulence model to provide further insight into the difference of switching from a 2D mesh to a 3D one. However, when the cases were run with the same time step size as our 2D cases, $\Delta t = .001$, the 3D mesh was unable to capture the vortex shedding off of the rod, as seen in Fig. 10a and 10b. As mentioned, in the study of Ladreau [2008], it was found that URANS turbulence models need a sufficiently fine mesh and time step in order to produce wake shedding due to the small length scale of the rod in the computational domain. Therefore, the need to switch to a time step of $\Delta t=.0001(s)$ eliminated most of the computational cost savings benefit of a 3D URANS turbulence model, thus the 3D cases were subsequently all run using the LES turbulence model with a Δt of .0001(s). This proved to show a much better defined wake, with vortex shedding and wake structures taking a three dimensionality. In Figure 10b, an attempt to display vortex shedding from the Trans-SST model showed that little to no vorticity was produced and that which was produced was uniform in the z-direction. However, by plotting the Q-criterion values colored by vorticity for the LES turbulence model, one can see that the formation of the wake structures vary across the span-wise direction as well as does the magnitude of vorticity. This three dimensionality will play a major role in the interaction of the wake with the suction surface.

a)

b)

c)
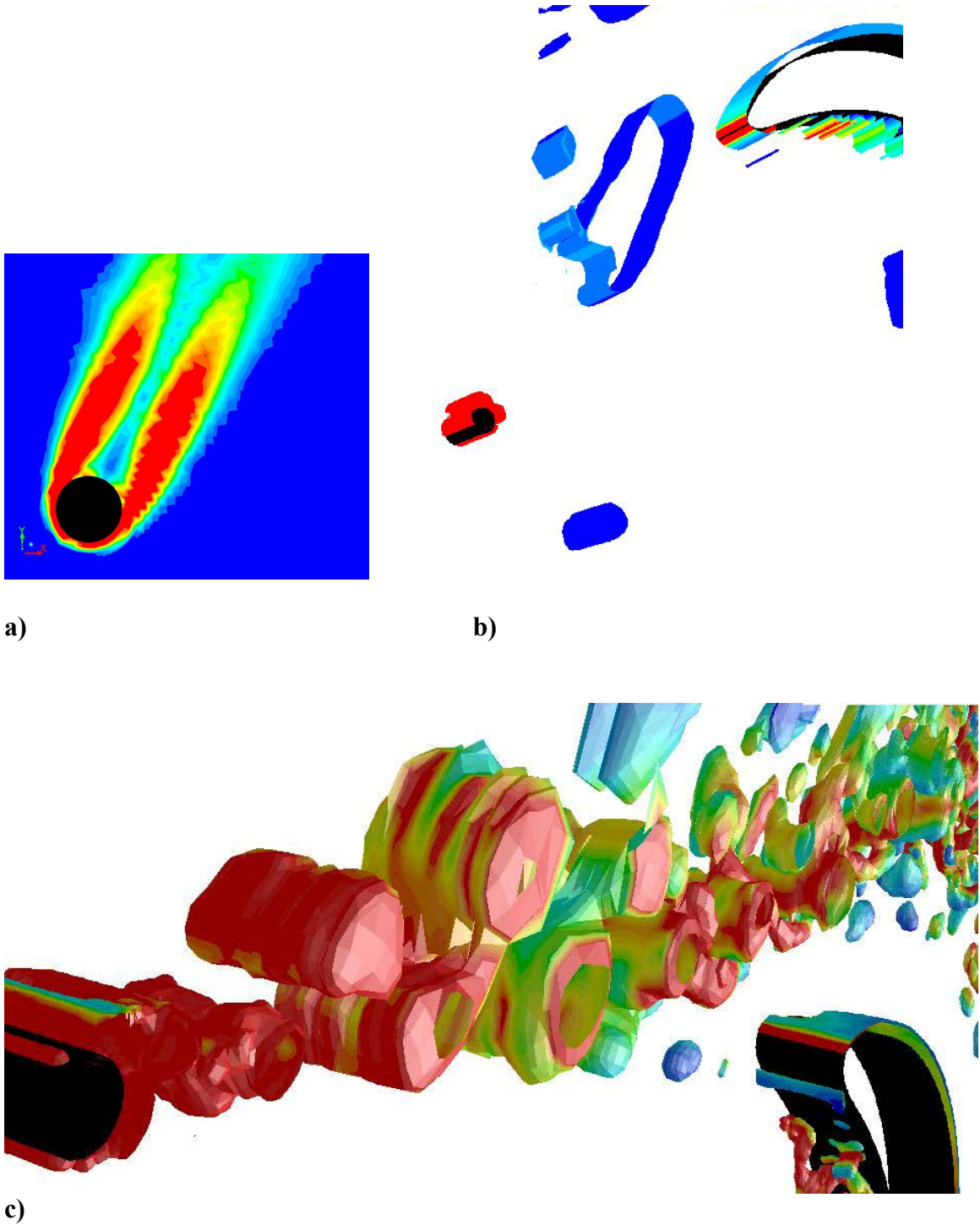
Fig. 10 Vorticity Contours for Re = 50,0000, HFSTI: a) 3D – Trans-SST with time step = .001 seconds, b) 3D – Trans-SST – time step = .001 – Q-criterion colored by Vorticity Contours c) 3D – LES – time step = .0001 – Q-criterion colored by Vorticity Contours

Re=25,000

LFSTI, F=0.513

 In a 3D domain, the rod wake velocity profile seen in Figure 11 shows a wake that has a much less smooth structure to it, yet is still symmetric across the width. The magnitude of the wake matches the trend of the experimental data slightly better, as does the width and shape of the wake. The peak velocity outside of the wake is considerably higher, which is the same for all the wake profiles produced and may be attributed to the difference of taking a time averaged of a line in a computational domain and taking the time averaged results of a single probe point and using the rod speed and cycle time to determine the pitch location of the averaged values. With that said, the wake structure is deemed sufficiently consistent to proceed.

 The fact that the wake shows a profile closer to that which is expected leads to a more consistent Cp prediction with the experimental data, however the CFD predictions still have areas where the consistency with the experimental data lacks. The suction peak is seen to be predicted slightly downstream from that of the experimental and is larger in magnitude. Then as flow proceeds downstream, the point of separation seems to occur earlier than it should as well as reattachment. The magnitude of the pressure bubble is greater and shorter than what the experimental data show. As the flow approaches the trailing edge, the pressure magnitude is underpredicted and seems to be forming another plateau as if to start to form another separated region, near the trailing edge, that is not evident in the experimental data.

 The total pressure loss shown in Figure 13 has a peak that is proportional to the f the experimental data, however the shape is quite different. There seems to exist the same

shift associated with the periodic domain and the sharp decline from the peak to minimum is associated with the sharp decline in the Cp curve as the flow reaches the trailing edge. The difference in the peak value can be also correlated to the over prediction of the size of the separation bubble indicted by the size of the plateau of the Cp curve.

In Figure 14a one can see the contour plots of the time averaged mean skin friction coefficient (C_f) values along with the mean contours associated with the Cp profile over the suction surface of the airfoil. This along with the data plots of these values in the graph above them can lead to further insight in the separation, transition, and reattachment locations. As previously referenced, the separation region has traditionally been associated with a "plateau" of the Cp values on the suction surface of an airfoil. Here one can see that even before the flow gets to the suction peak, the skin friction starts to drop steadily. Slightly after the suction peak, where the Cp values show the start of a plateau, there is a slight inflection in the decreasing C_f values. This point shows where the flow starts to become separated, with full separation reached when C_f hits zero and thus no flow is attached to the surface. Coming out of the separation point there is another inflection at about .63Ls, which indicates an increase in the rate of change of C_f growth and thus the start of transition. At about .65Ls, where the end of the Cp plateau occurs there is again another inflection point to the C_f plot indicating reattachment. Now since this point is predicted too far upstream of the experimental point of reattachment, and the fact that the data fails to be consistent with the flow over the rest of the airfoil, the fact that this point is not the peak, but continues to rise in C_f value, indicates part of the error in this prediction. Better results will be shown in the

case of Re=50,000. However, in speaking to what is shown, the same trend of a peak in C_f, followed by a decrease, inflection point, and zero point coincides with the Cp prediction of a plateau forming on the trailing edge.
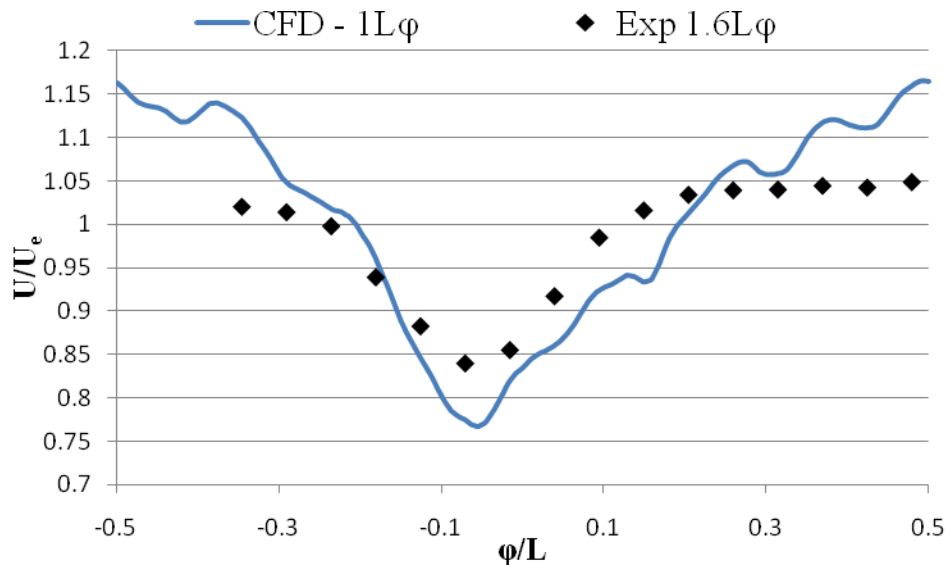
Fig 11 Rod Wake Velocity Magnitude for Re=25,000, LFSTI: Comparison of LES, $1L_\varphi$ to Experiment $1.6L_\varphi$
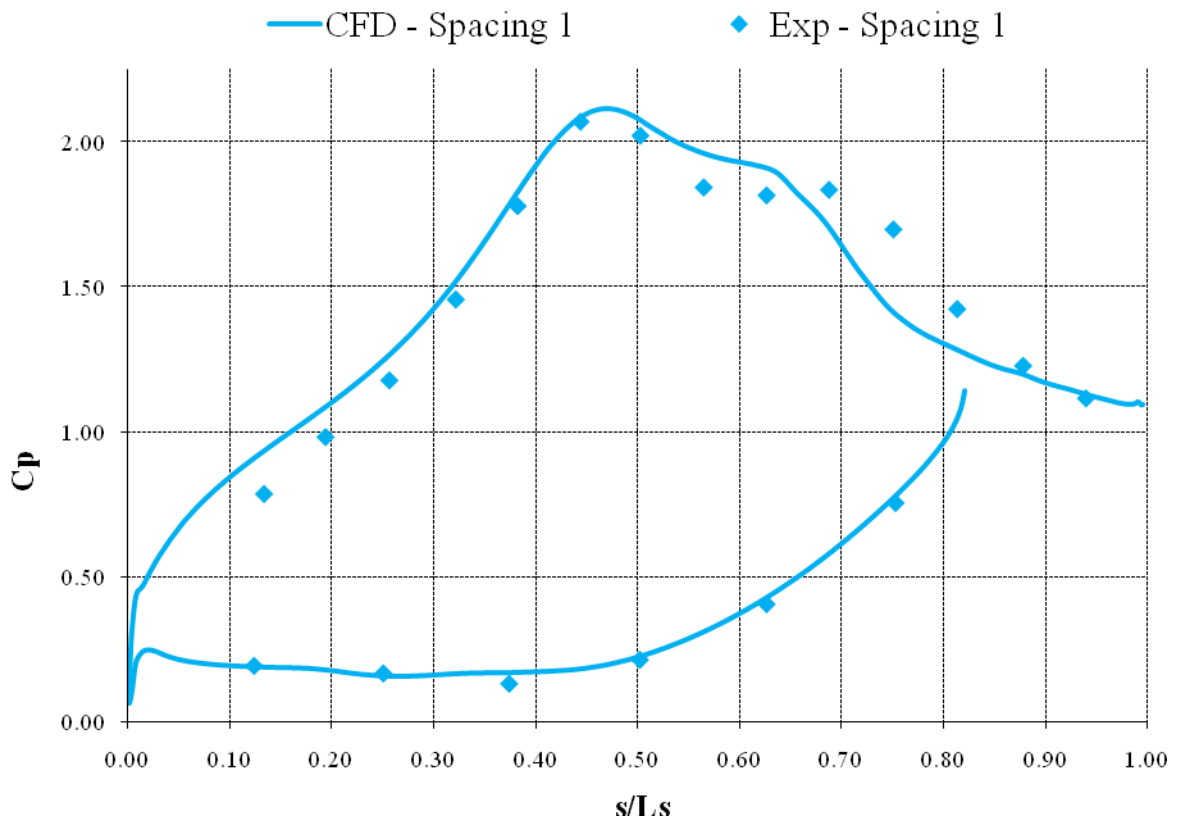
Fig. 12 C_p profiles for Re=25,000, LFSTI: Comparison between LES and Experimental data
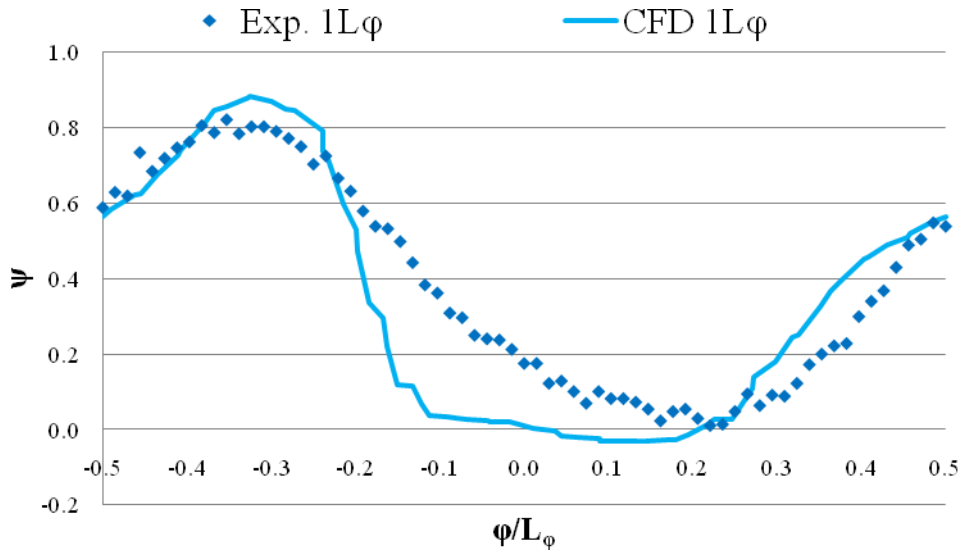
Fig. 13 Total Pressure Loss Coefficient for Re=25,000, LFSTI: Comparison between LES and Experimental Data
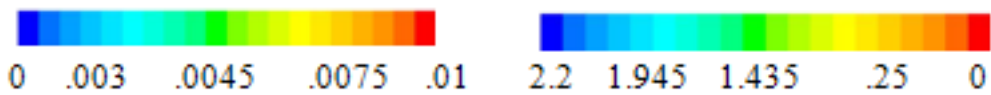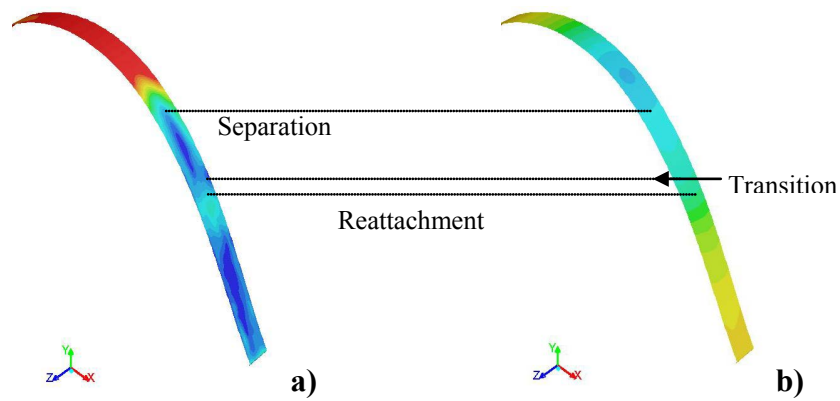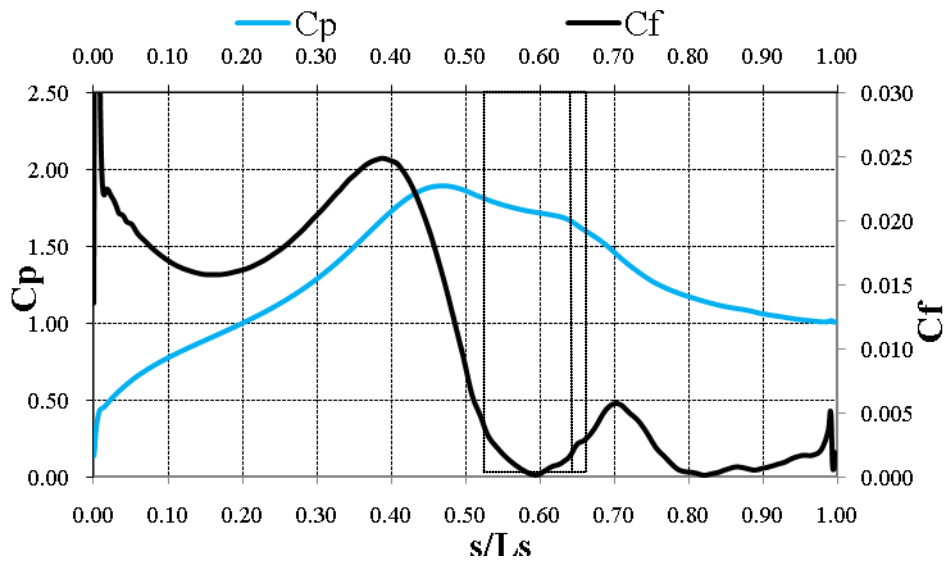
Fig. 14 Comparison of Mean C_p and C_f on suction surface for Re=25,000, LFSTI: a) Contours of mean C_f b) Contours of mean C_p

Re=25,000

HFSTI, F=0.513

In changing the free stream turbulence level from low to high, the experimental data showed that the magnitude of the peak Cp value would decrease; however its location along with the location of the separation and reattachment points all remained basically the same, thus giving an overall shape to the curve nearly identical to the low turbulence case The CFD results once again do an insufficient job of capturing these details.

In figure 15, the rod wake profile for the Re=25,000 HFSTI case is nearly identical to the profile for the LFSTI. This is to be expected since the wake shape should be highly dependent on the flow over the cylinder, or on the Reynolds' number, which is seen here. The wake does appear to be slightly wider, but the magnitude is the same. This does not translate though into similar to experiment Cp results.

In Figure 16, one can see that the predicted peak magnitude of Cp decreased from the LFSTI case, as did the experimental, but the proportion with which it decreased is less, thus causing the already over-predicted peak value to be even larger for the HFSTI case. The point of the peak did remain the same, which is expected from the experimental data. Moving downstream, the experimental data shows a very well defined drop in Cp, with a plateau, or prediction of a separation bubble, and then reattachment. The CFD results show a much slower decrease from the Cp maximum, with only a slight, small plateau and then quick reattachment. After reattachment the results remain below

the experimental data, however this time it does not incorrectly show the formation of another separation bubble at the trailing edge.

The fact that the separation bubble predicted by the CFD is very small, and the fact the pressure drops steaper near the trailing edge, leads to a total pressure loss prediction that is smaller in amplitude than the experimental and has a quicker drop (Figure 17). The same effect, shown earlier in Figure 6,of a shift in the profile due to the periodic boundary conditions in once again also present.

In an attempt to determine the locations of predicted separation, transition and reattachment, the Cp profile is difficult to use due to its small, non-dominate bubble plateau. However, when looking at the C_f curve inf Figure 18, the same points of inflection as seen in the LFSTI case are present and indicated in Fig. 18. Once again, from the C_f peak, a steady decrease is observed through the suction peak, then at about .54Ls, there is an inflection coinciding with the beginning of a slight plateau to the Cp profile. Then, after C_f hits zero, it quickly increases to another inflection indicating transition and then reattachment can be seen by a peak in the C_f. Upon examining the contours, it can be seen that this separation bubble is not even indicated across the span of the airfoil, thus resulting in more of a local, less defined separation as compared to a full separation bubble Again, the trend of another C_f zero point with inflections around it is not seen, nor is the formation of a plateau on the trailing edge.

These results give a good indication of what to look for in the data to come, however, as stated, they do not correlate very well with the experimental data results. From the literature review it was found that low Reynolds number flows have been deemed difficult to model, thus the fact that the trends are predicted correctly is

sufficient, but it is not surprising that the Re=25,000 results are less than exact. An attempt to run a finer mesh was run and did not show any significant improvement in results. A finer time-step may prove more effective however the computational costs would have to increase, rendering using a turbulence model and not a direct numerical simulation useless.
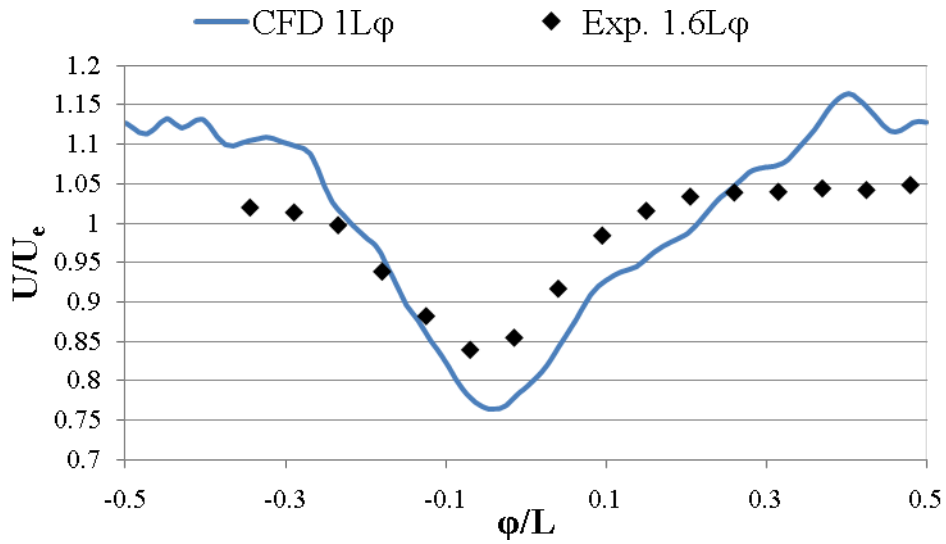
Fig 15 Rod Wake Velocity Magnitude for Re=25,000, HFSTI: Comparison of LES, $1L_\varphi$ to Experimental $1.6L_\varphi$
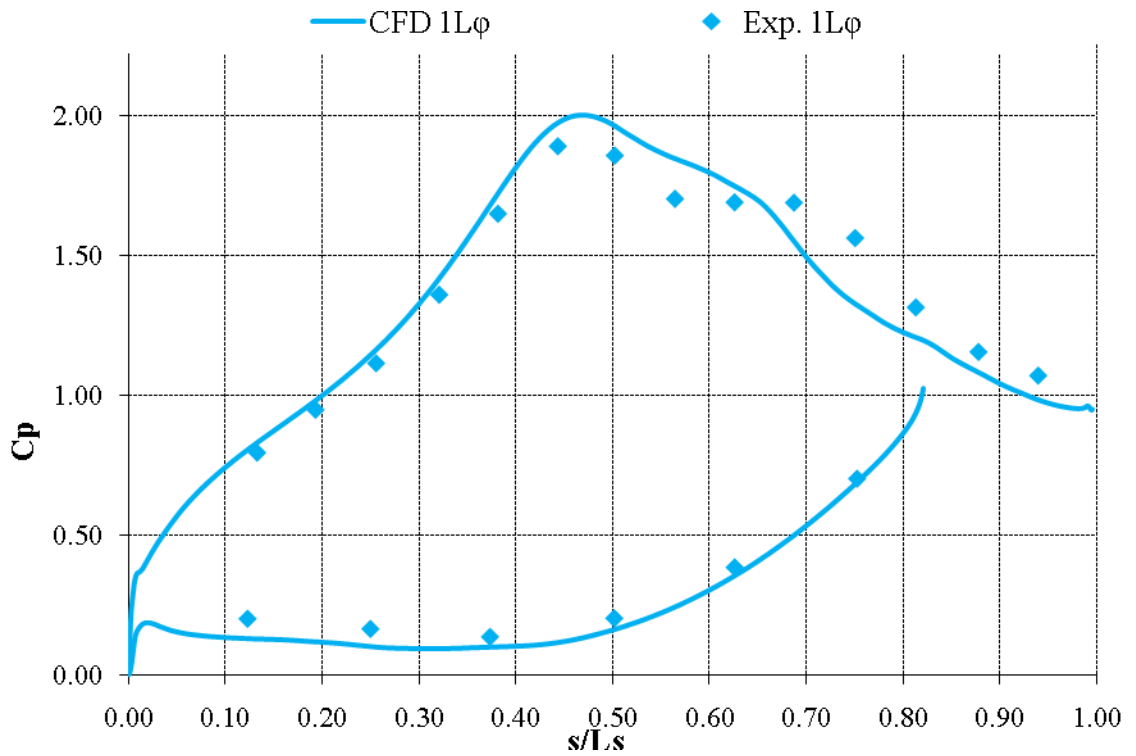
Fig. 16 C_p profiles for Re=25,000, HFSTI: Comparison between LES and Experimental data
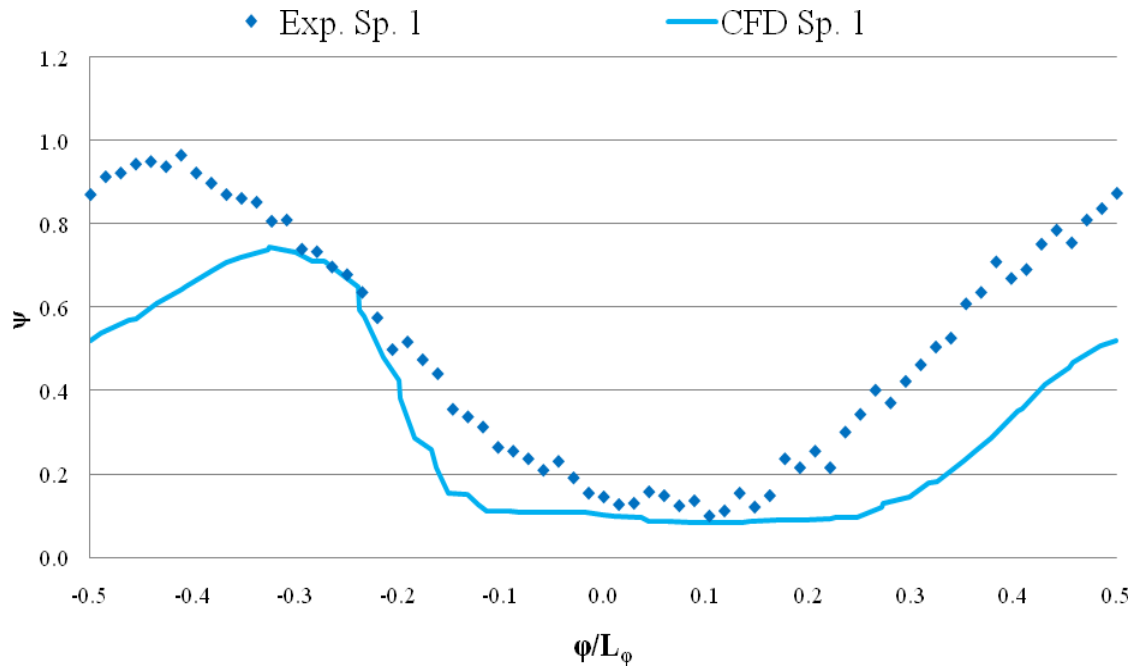
Fig. 17 Total Pressure Loss Coefficient for Re=25,000, HFSTI: Comparison between LES and Experimental Data
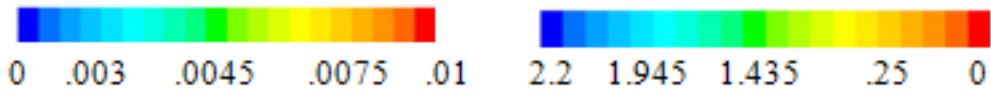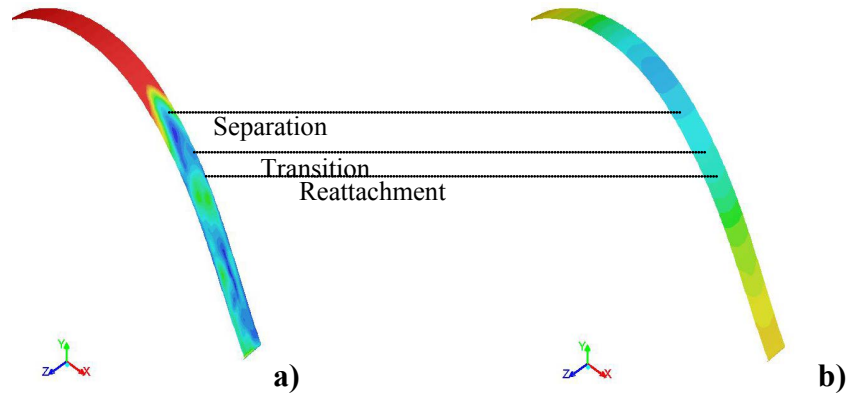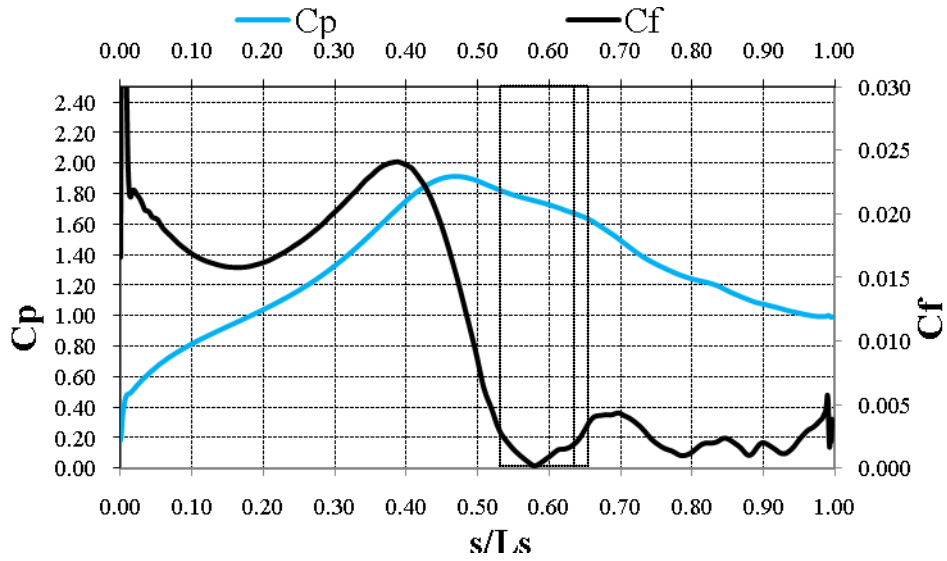
Fig. 18 Comparison of Mean C_p and C_f on suction surface for Re=25,000, HFSTI: a) Contours of mean C_f b) Contours of mean C_p

Re=50000

The Reynolds 50,000 cases proved to be the most consistent with the experimental results and the wake passing over the airfoil will be examined in greater detail. Data were available for HFSTI and LFSTI inlet conditions for a wake passing frequency, F, of 0.548. After confirming that the CFD results for these cases were sufficiently accurate, additional cases where the rod speed was increased to create a greater wake passing frequency were simulated. The desire was to see if when a wake was nearly always impinging on the airfoil could separation be eliminated completely. The two cases that were run were a case that represented a 25% increase in rod speed, resulting in an F = 0.689. The second was run based off the time it took for the wake effects to be eliminated from the base Re=50,000 cases with a rod speed of 2.63 m/s. This resulted in a 40% increase in rod speed and a wake passing frequency of .917 from the base, F=0.548 case, or an additional 33% increase from F=.689.

Re=50,0000

LFSTI, F=0.548

The wake produced by the Re=50,000 LFSTI case shows in Figure 14 a wake that has nearly the same shape and magnitude as displayed in the experimental data, which was an initial indication that the Re=50,000 results will produce results much more consistent with the experimental data. The width of the wake is slightly larger than the experimental rod to blade spacing of 1.6 data, however it is consistent to the width of all the other CFD rod to blade spacing of 1 results.

The result of this wake profile provide Cp values that were in very good agreement with the experimental data. In Figure 20 it can be seen that the CFD results predict a suction peak that is slightly under-predicted in magnitude and slightly downstream. This slight under-prediction persists until reattachment and may be a result of a wake that is greater in magnitude than what the experimental data would show. The prediction of the location of separation, the size of the bubble, and the location of reattachment are all very consistent though with the experimental data. The flow over the trailing edge of the airfoil also matches the data in both location and magnitude.

The consistency of the Cp profiles leads to similar results in the total pressure loss data, Figure 21. Here the magnitudes of the peak and trough of the CFD are under-predicted compared to the experimental data. This is a result of the fact that the Cp values show an under-prediction in the pressure bubble size. The shape of the total pressure loss coefficient profile though shows a much more

consistent result, especially compared to the Re=25,000 results. This is due to the

fact that as the flow passes over the airfoil, even though the magnitudes vary

slightly, the shape and location of different separation and reattachment events is

very well matched.

In Figure 22 suction surface velocity profiles from six streamwise

locations are shown. The CFD data for a rod to blade spacing of 1 is compared

against the available experimental data for cases with rod to blade spacings of 1.6

and 2. Therefore a direct match in these profiles is not expected but it will be

analyzed based on what is seen as the trend of the data as the rod to blade spacing

is reduced from 2 to 1.6. In figure 22a, the mean velocity profiles are plotted with

experimental data in dots and the CFD result in a solid line. The results show that

even though the experimental data does not vary much from rod to blade spacing

of 2 to 1.6, there does seem to be the trend of the magnitude of the U/U_e profiles

to grow as spacing is reduced. The CFD models the shape of the velocity profiles

very well, however it does not show a greater magnitude than the experimental

data until station 5. This is consistent with the fact that the pressure magnitudes

over that span is also less than the experimental data until the trailing edge, this

shows consistent matching and thus also shows a consistent trend in velocity

magnitude at those stations. In figure 22b, the turbulence, or u'/Ue, profiles are

plotted for the same six locations. Here again, the results become more consistent

with the experimental data trends toward the trailing edge where better matching

is observed. Overall, the shape and trend seem to be consistent, however the

magnitude seems to be amplified a bit too much with what the experimental data

trend shows. However, these results are believed to be in good agreement with the data with some of the error due in part to the inability of an anemometer to resolve the difference between attached and reversed flow.

With the Cp results showing very consistent trends with the experimental data, looking at the Cp vs C_f plot in Figure 23 will allow for more confidence in observing what happens to the skin friction as flow proceeds down an airfoil. Here one can see that the skin fiction reaches a peak before the suction peak of the airfoil. The subsequent decline in C_f is very consistent and smooth as flow moves past the suction peak and down the aft side of the airfoil. At about .53Ls, right as the Cp is starting to show the plateau of separation bubble there is a slight inflection in the skin friction plot, leveling out slightly and having the decrease in C_f taking a less negative slope. This continues until C_f hits zero and thus full separation has occurred. While still in the separation bubble, the skin friction increases at a slow rate, staying near zero, until at about .63Ls there is an initial sharp increase in C_f signaling the start of transition. This increase continues until .65Ls where the rate of increase changes and grows even greater signaling the start of reattached flow. By the C_f peak at .68Ls the flow is fully reattached and continues on that way to the trailing edge. As the flow approaches the trailing edge it stay attached due to the presence of turbulence in this region evident by the fluctuations in C_f from .75Ls to the end.

Figure 24-1 through 24-14 represents instantaneous plots and contours of a wake passing over the airfoil. Each separate plot represents a 10% time step of a full cycle, even though there is greater than one cycle shown so the full effect of

the wake can be seen. An instantaneous plot of Cp and C_f values are shown at the top with the corresponding contours of these values over the suction surface shown beneath. Then continuing clockwise, beneath the Cp suction surface contour is another contour plot of Cp values at mid-z span with iso-surfaces of q-criterion also displayed at that instant to show where the wake is currently located and how it is affecting the boundary layer on the suction surface. Finally the last contour is the x-velocity contours at mid-z span with iso-surfaces of Q-criterion for that instant also plotted to give an idea of the magnitude and direction of the flow.

Figure 24-1 starts as a wake is passing through a passage to show the re-growth of the suction peak. Here there is evidence of the last parts of the wake to hit the suction surface (before entirely hitting the pressure side) moving its way up the forward part of the airfoil. The suction peak has been rolled up into three separate peaks, as described in Hodson and Howell [2005], along with their prediction of a calm zone seen following the high turbulence fluctuations in the C_f values. Moving from Figure 24-1 to 24-2 the suction peak of the airfoil continues to be suppressed as is the peak skin friction that is seen before the peak. The rolled up separation bubble is compressed and increases in magnitude as does the magnitude of C_f in this region. Again trailing behind these amplified values of C_f is a low C_f, calm region. From the contours of C_f, it can be seen that the aft side of the suction surface is fully turbulent, with spots of zero skin friction present where the separation bubble is being rolled downstream.

By Figure 24-3, or within 10% of the suction peak hitting its lowest magnitude, the peak begins to reform with a subsequent C_f peak preceding it. From the q-criterion and C_f plot, it is evident that turbulent wake structures are still making their way up the forward side of the airfoil, however their presence seems to play little effect on the growth of the suction peak. The rolled up separation bubble that is making its way down the aft portion of the airfoil continues to be compressed and grow in magnitude along with the C_f values; the calm region still trails.

By Figure 24-4, the suction bubble has completely separated from the surface causing high levels of turbulence to shed off the trailing edge of the airfoil. At this point, where the separation bubble stops drawing the wake towards the surface, the C_f values show less of a turbulent peak and the entire calmed region starts to decrease to zero, with some local values of zero C_f already present. This shows that immediately after the wake influence on the surface ends, the start of formation of another separation bubble begins.

From this point to Figure 24-6, the suction peak continues to grow as does the presence of another separation bubble. The turbulent structures on the forward part of the airfoil have all moved beyond the suction peak and the flow in this area seem to be completely laminar, having no fluctuations present in the C_f plots. By Figure 24-7, the contours of C_f on the suction surface show a point of zero C_f, or separation, that is no longer just a point, but covers the whole span and by Figure 24-8 and 24-9 a more definite zero C_f band is formed over the suction surface with the separation plateau present in the Cp plot. In figure 24-10, the wake

begins to collapse in on the suction peak, putting a shear stress on the separation

bubble, pushing it downstream. The Cp plot still shows separation in the flow

with an abrupt reattachment point.

Figures 24-11 thru 24-14 show the same things as Figure 24-1 thru 4.

They are included to help visualize the full wake/blade interaction.

In this Re=50,000, LFSTI flow, the CFD results are shown to be in very good

agreement with the experimental data. The magnitudes of both the mean Cp values and

total pressure loss are slightly under-predicted, however, the shape and trend of the data

matches the experimental data. In looking at the instantaneous plots, many of the trends

that were evident in the time averaged plots were seen. A peak in the skin friction was

seen slightly upstream of the suction peak, separated flow is marked by zero skin friction

coefficient, and reattachment is seen near a subsequent inflection or near peak of C_f. The

inflections seen that indicated the start of separation and the point of transition are not

always prevalent, but this could be as much associated with a small magnitude in change

which could be too difficult to pick up on the given plots. Ultimately, the flow is seen to

separate and grow a prevalent separation bubble between wakes.
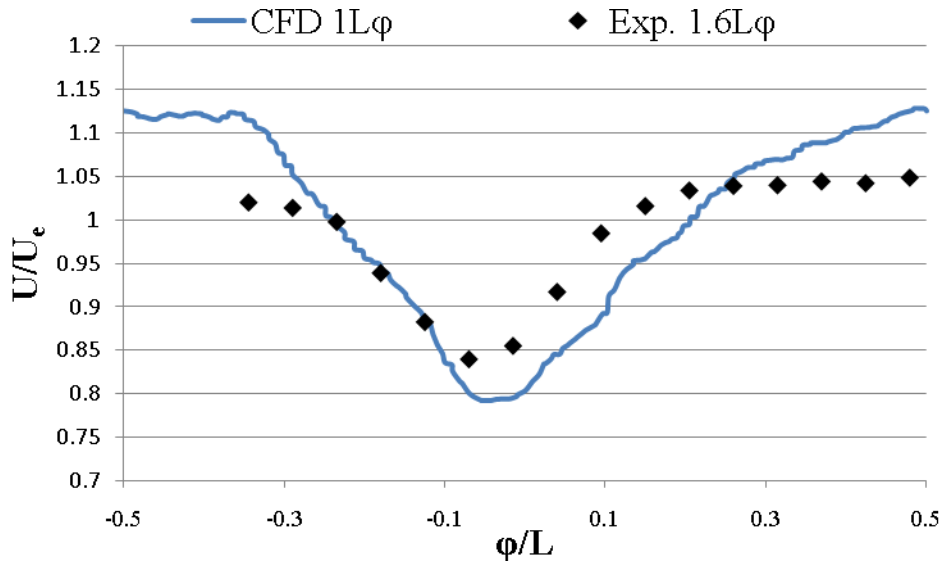
Fig. 19 Rod Wake Velocity Magnitude for Re=50,000, LFSTI: Comparison of LES, 1L_φ to Experimental 1.6L_φ
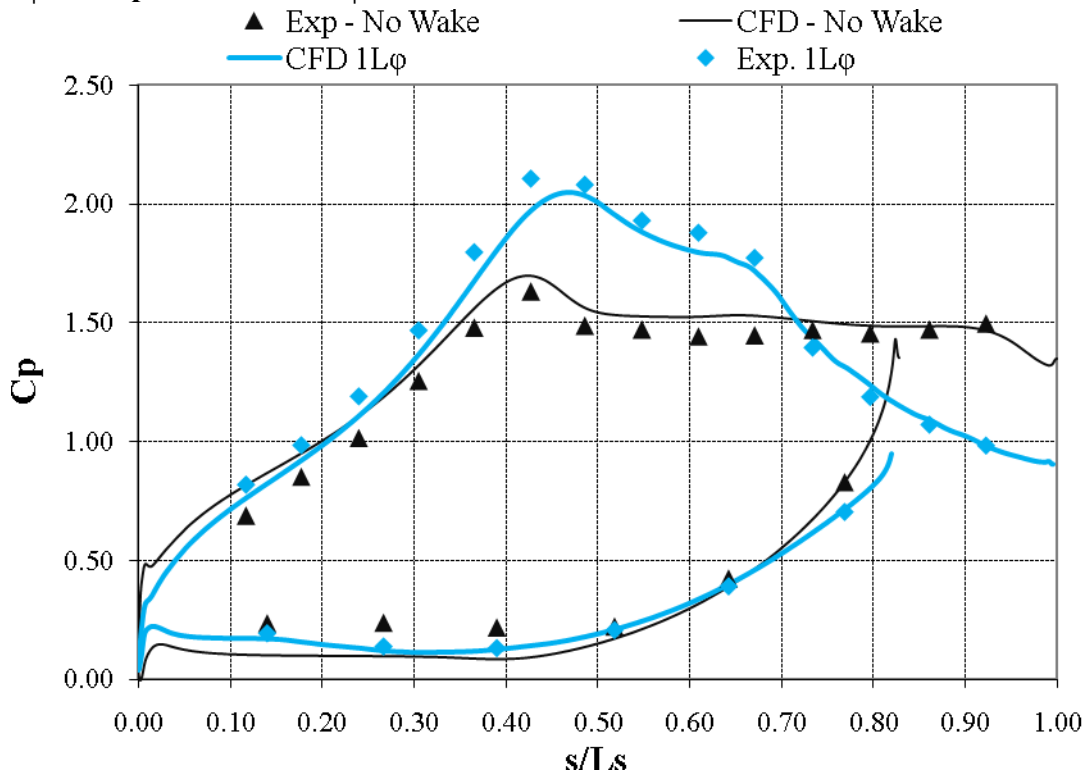
Fig. 20 C_p profiles for Re=50,000, LFSTI: Comparison between LES and Experimental data
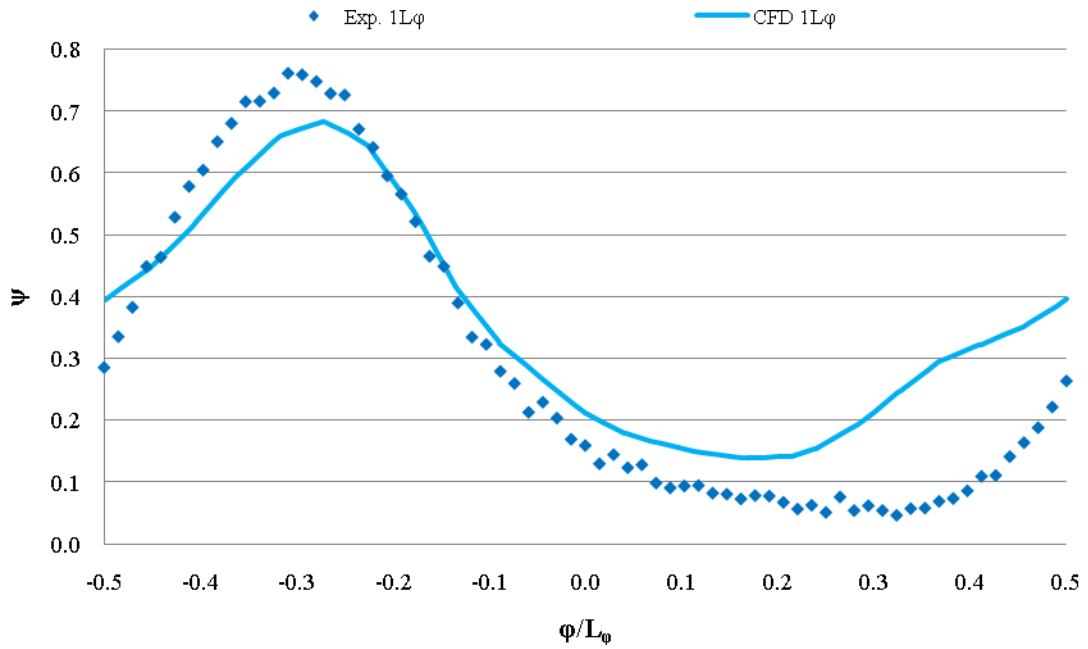
Fig. 21 Total Pressure Loss Coefficient for Re=50,000, LFSTI: Comparison between LES and Experimental Data
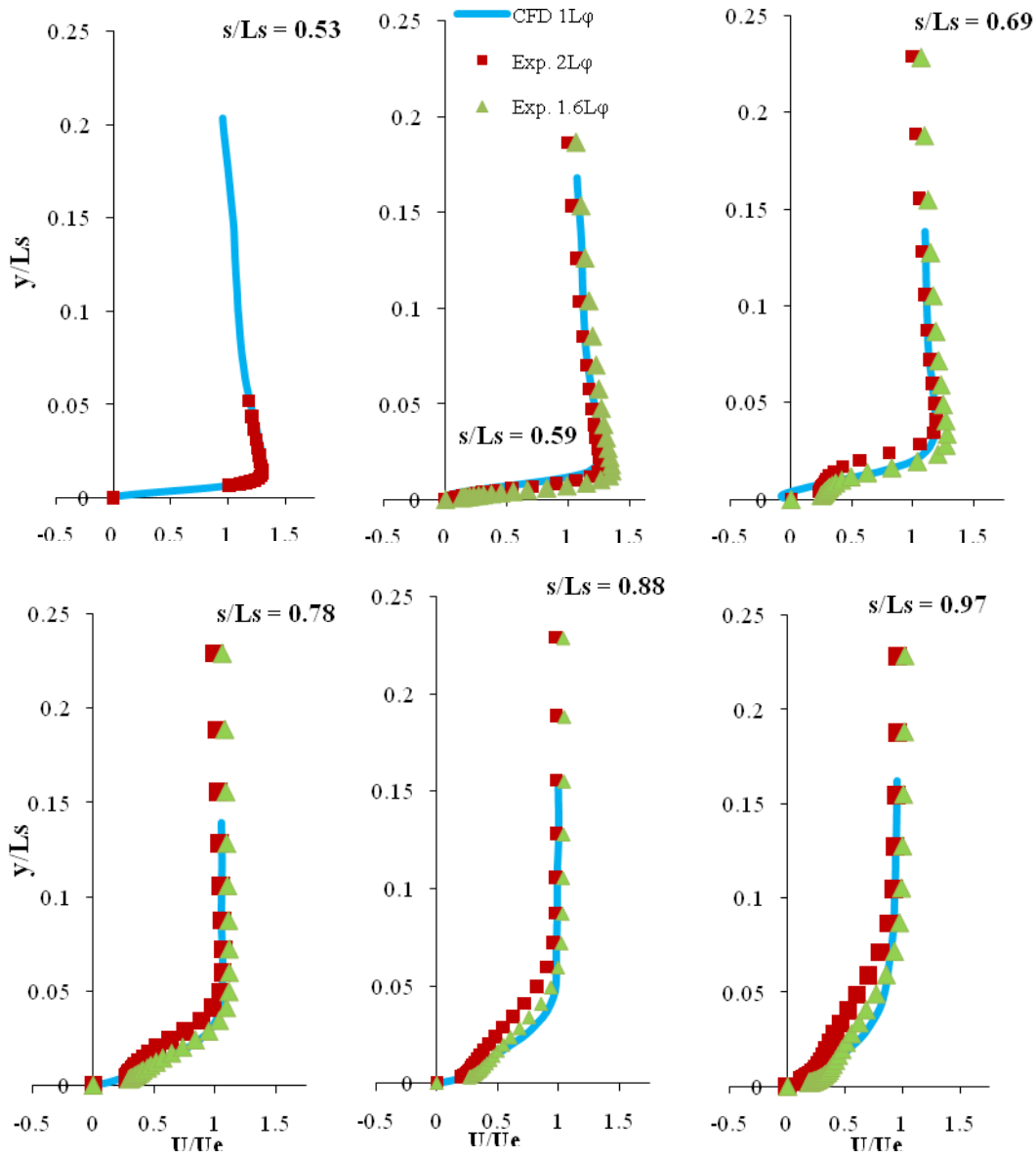
a)

Fig. 22 Time averaged velocity profiles at six streamwise stations for Re=50,000, LFSTI: Comparison between CFD (LES) and Experimental data: a - Mean, b - RMS
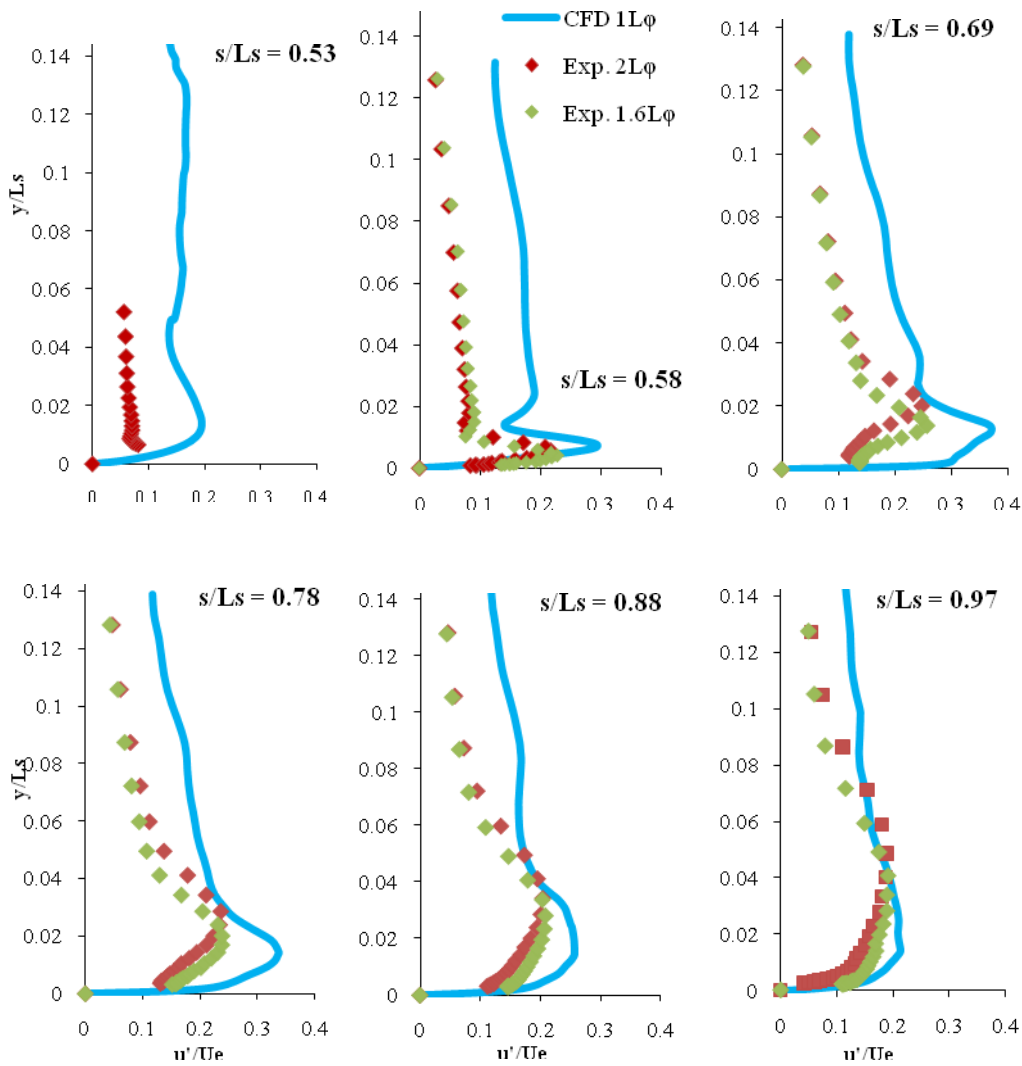
Fig. 22 Time averaged velocity profiles at six streamwise stations for Re=50,000, LFSTI: Comparison between CFD (LES) and Experimental data: a - Mean, b - RMS
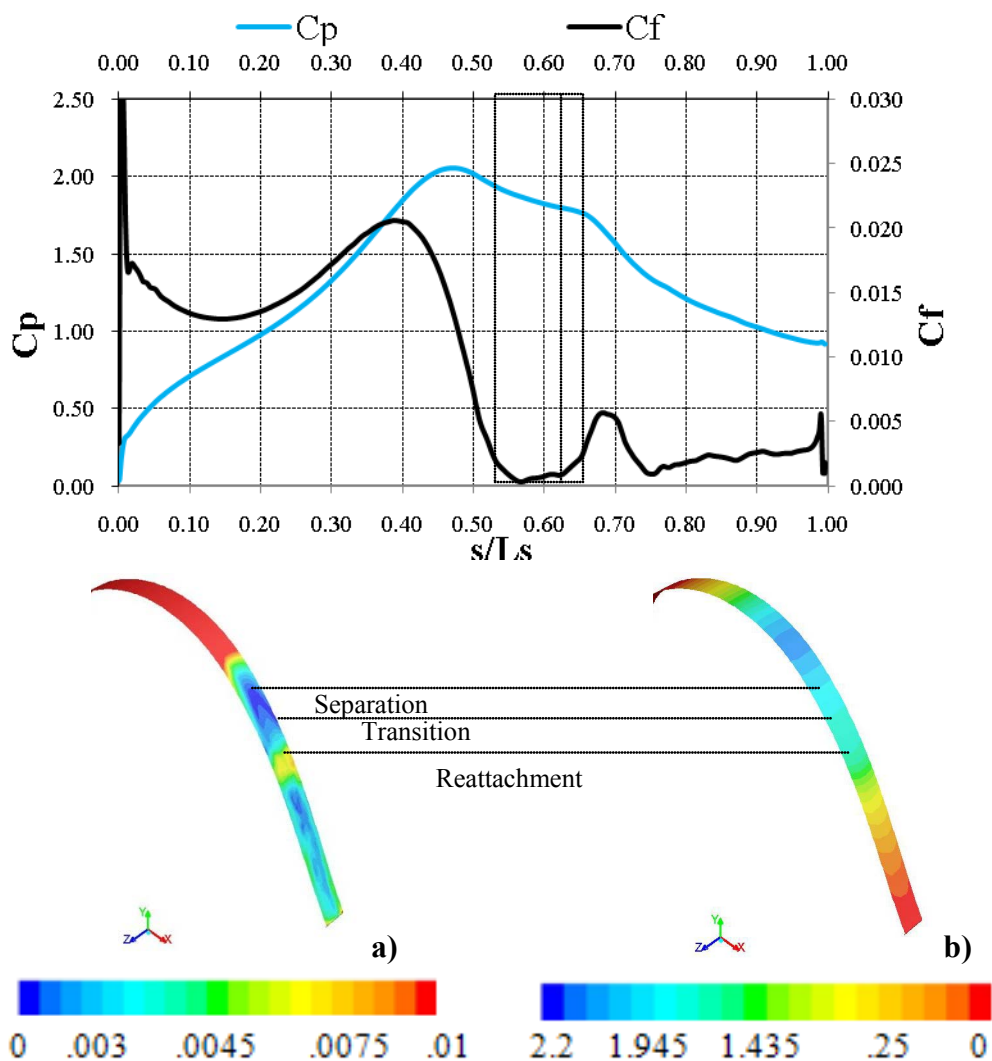
Fig. 23 Comparison of Mean C_p and C_f on suction surface for Re=50,000, LFSTI: a) Contours of mean C_f b) Contours of mean C_p
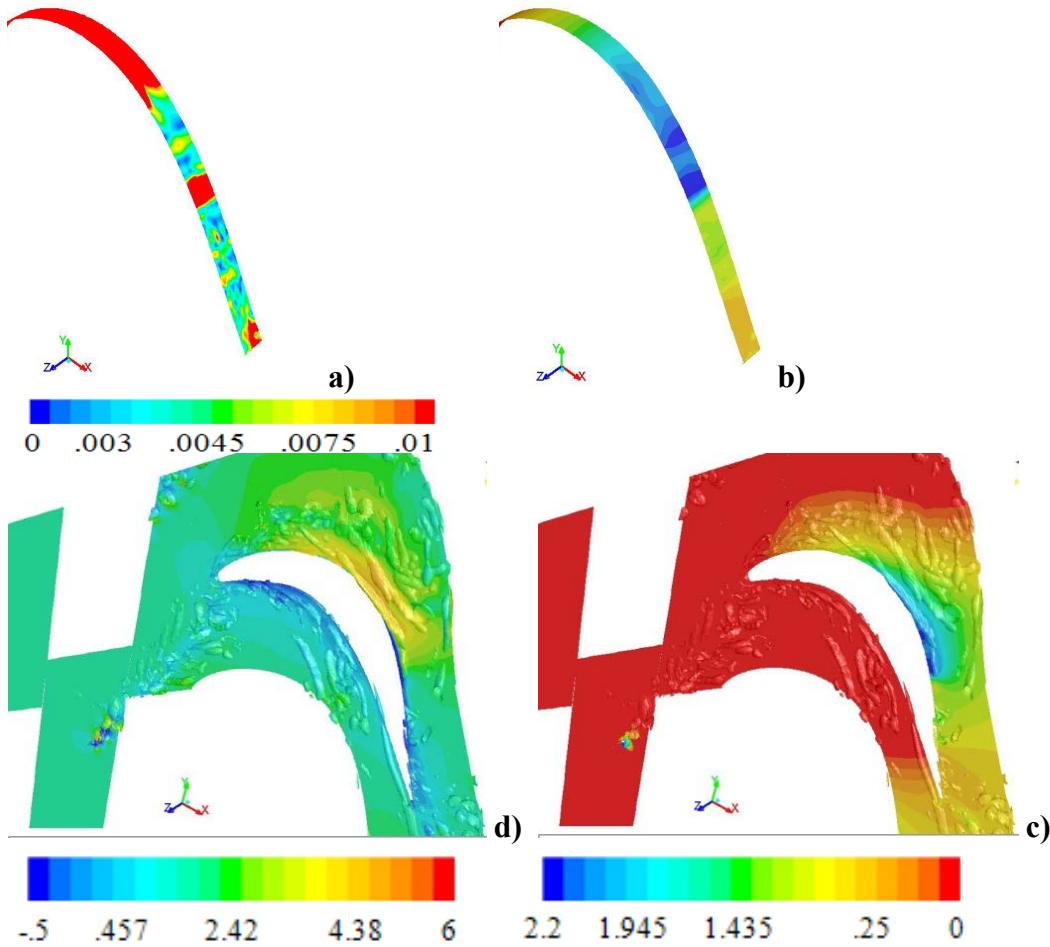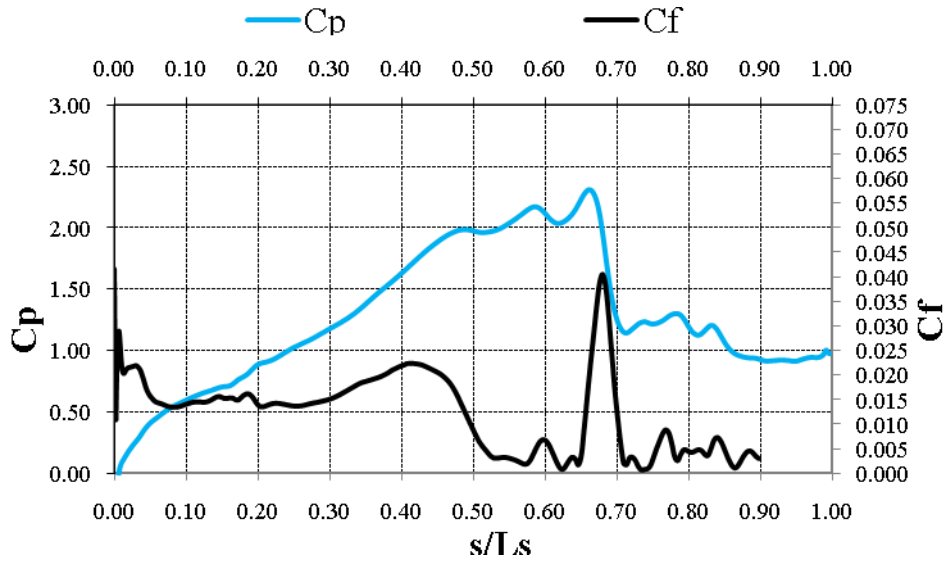
Fig. 24-1 Comparison of Instantaneous C$_p$ and C$_f$ on suction surface for Re=50,000, LFSTI: a) Contours of mean C$_f$ b) Contours of mean C$_p$ c)Q-criterion, Cp Contours d)Q-criterion, x-velocity Contours
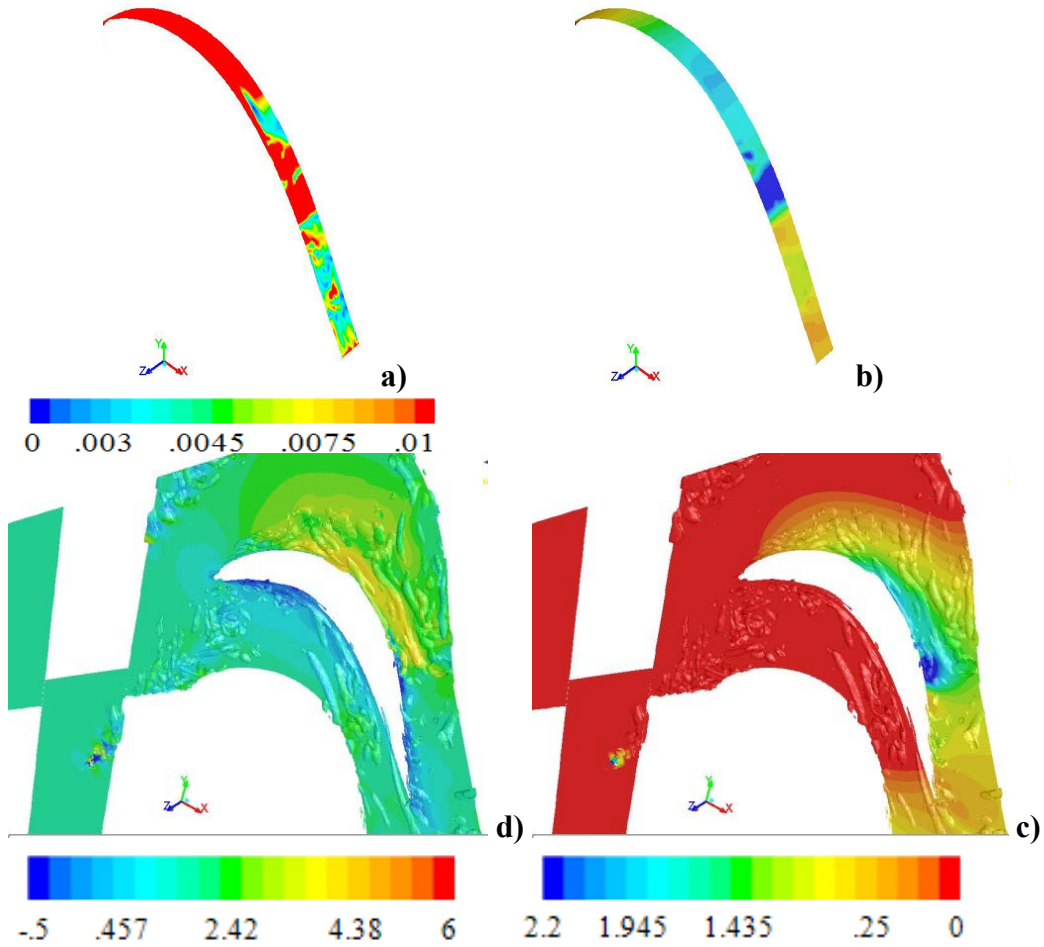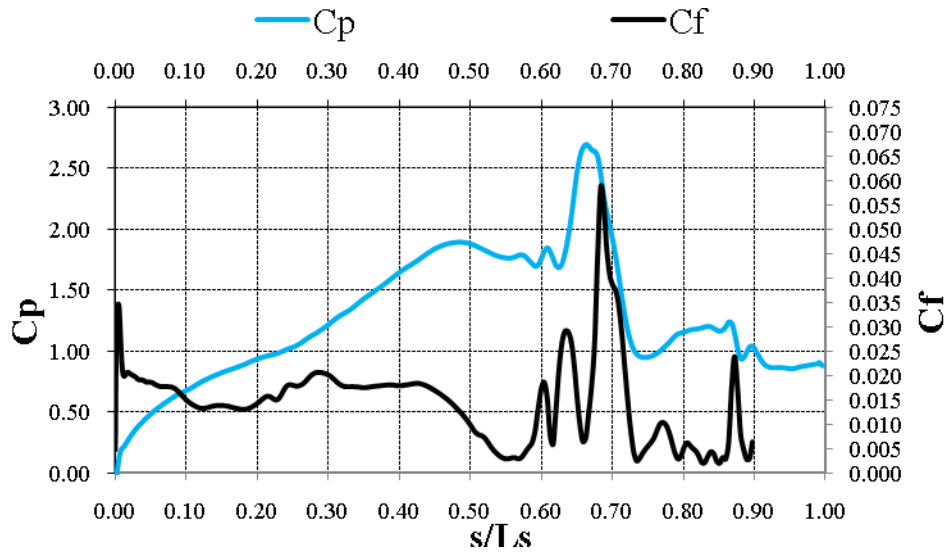
Fig. 24-2 Comparison of Instantaneous C_p and C_f on suction surface for Re=50,000, LFSTI: a) Contours of mean C_f b) Contours of mean C_p c)Q-criterion, C_p Contours d)Q-criterion, x-velocity Contours
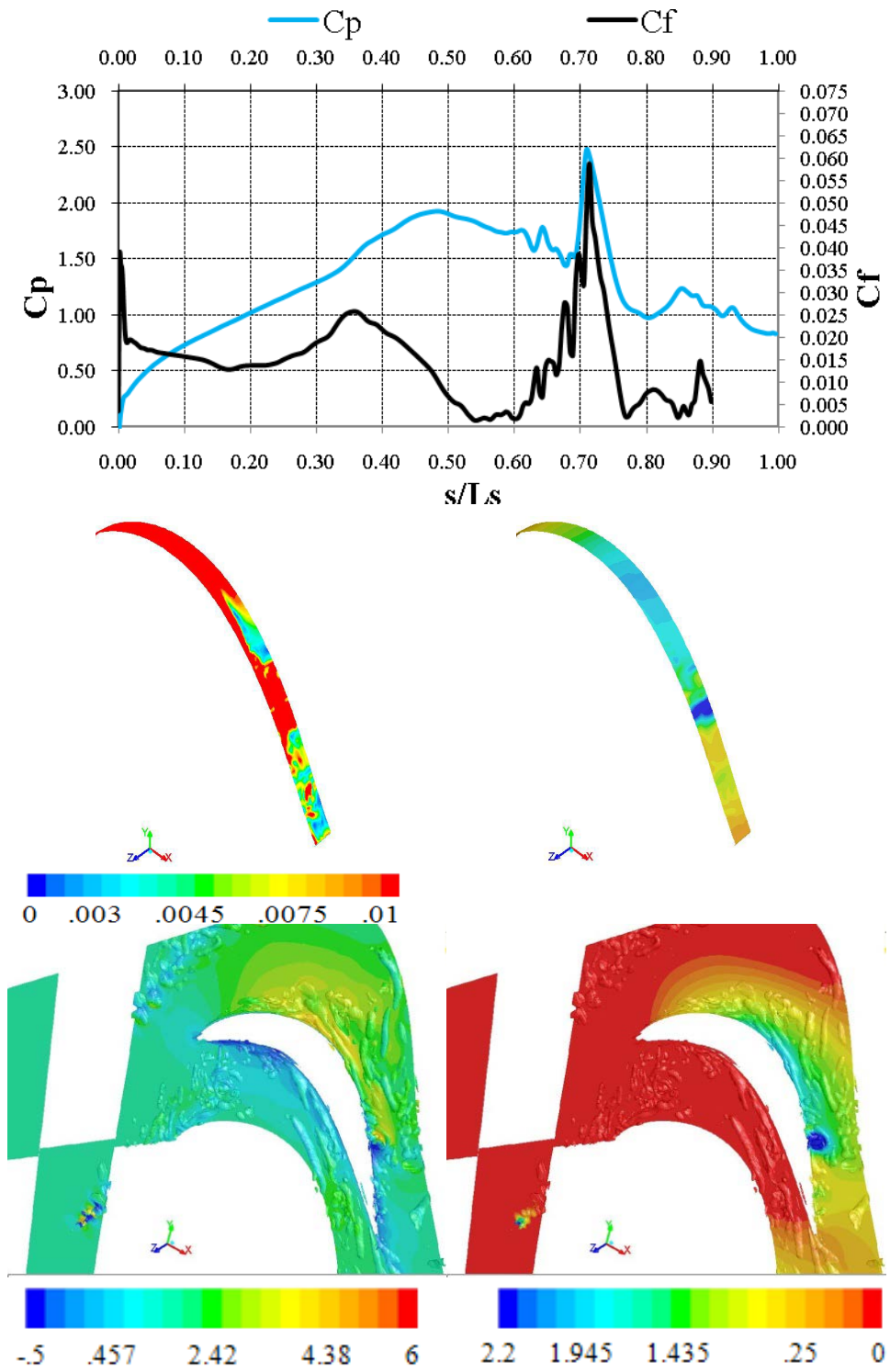
Fig. 24-3 Comparison of Instantaneous C_p and C_f on suction surface for Re=50,000, LFSTI: a) Contours of mean C_f b) Contours of mean C_p c)Q-criterion, Cp Contours d)Q-criterion, x-velocity Contours
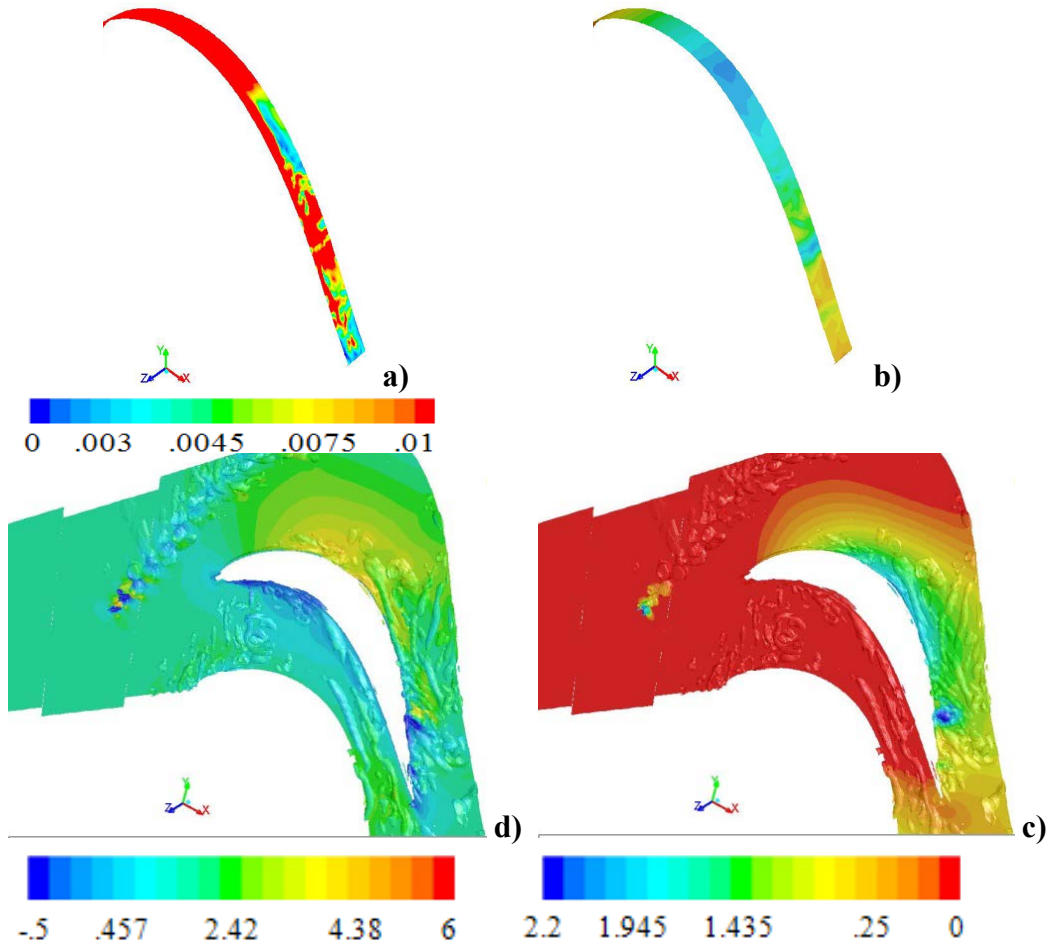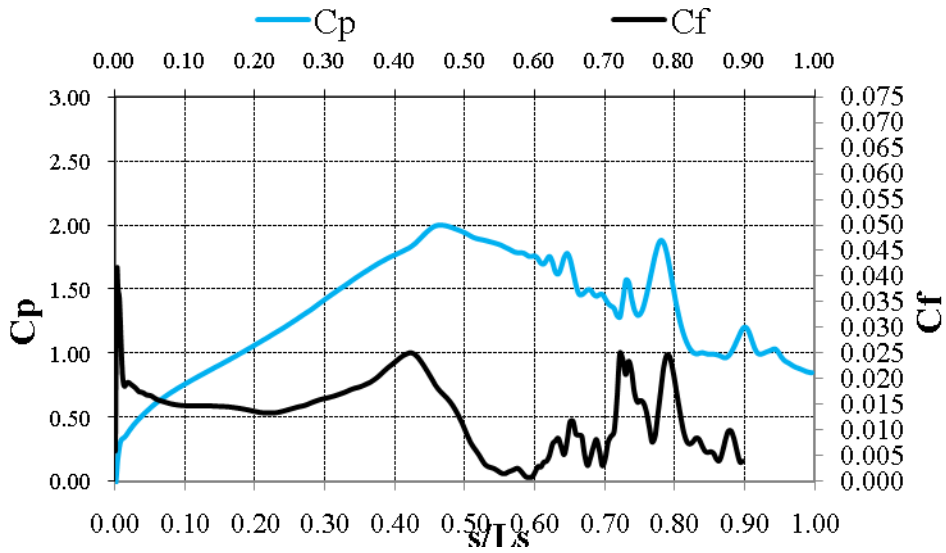
Fig. 24-4 Comparison of Instantaneous C_p and C_f on suction surface for Re=50,000, LFSTI: a) Contours of mean C_f b) Contours of mean C_p c)Q-criterion, Cp Contours d)Q-criterion, x-velocity Contours
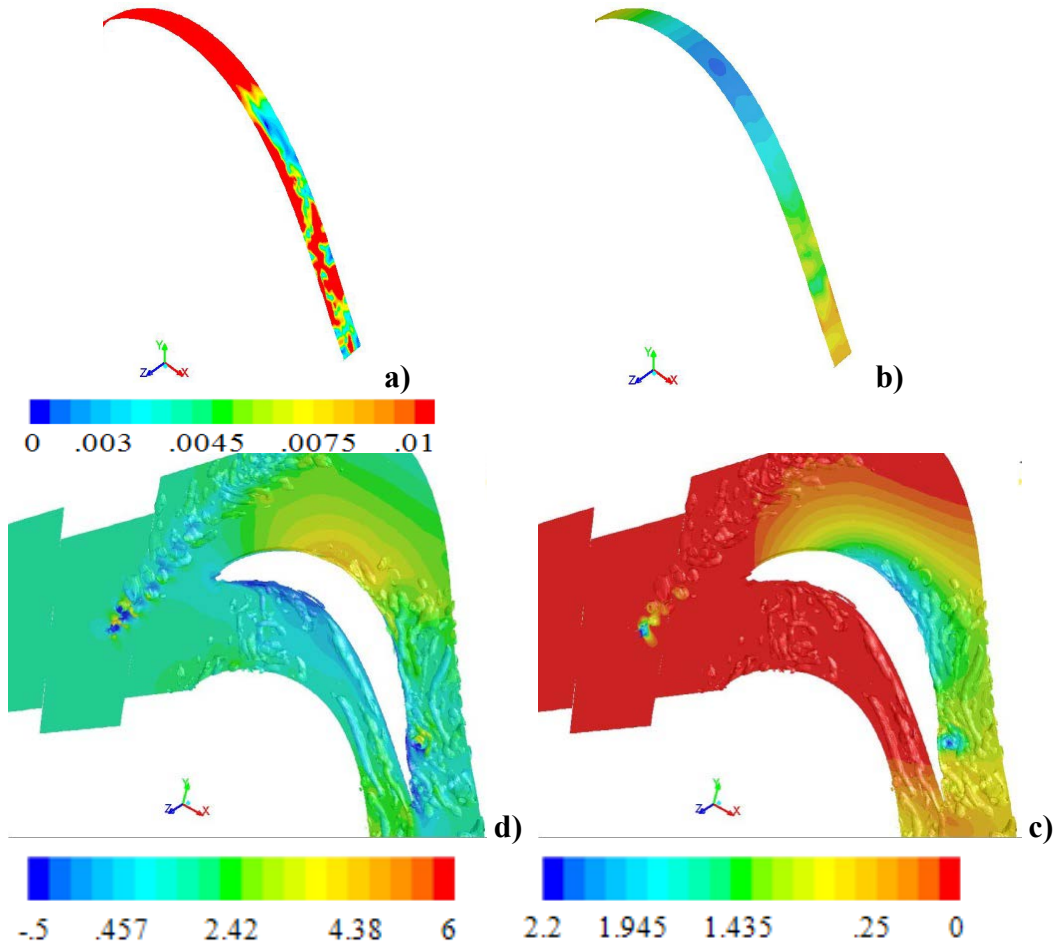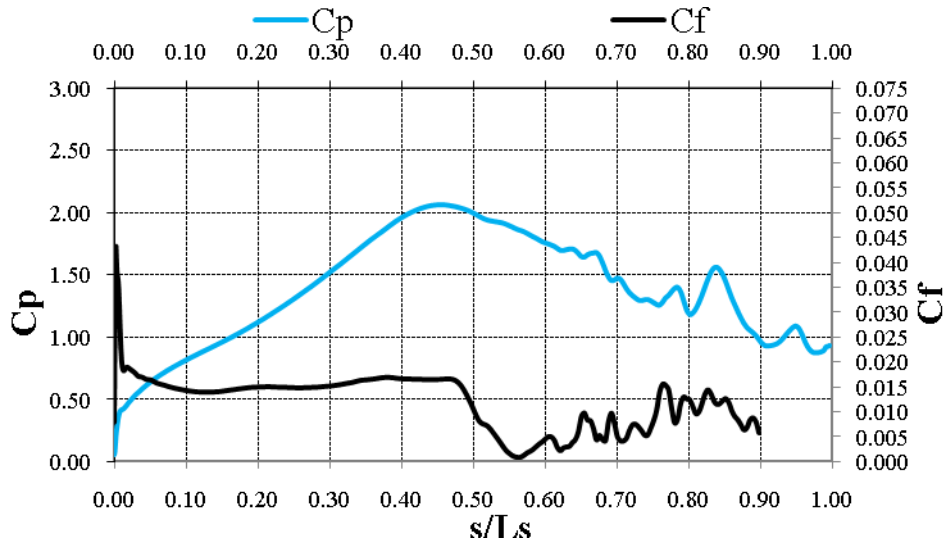
Fig. 24-5 Comparison of Instantaneous C_p and C_f on suction surface for Re=50,000, LFSTI: a) Contours of mean C_f b) Contours of mean C_p c)Q-criterion, Cp Contours d)Q-criterion, x-velocity Contours
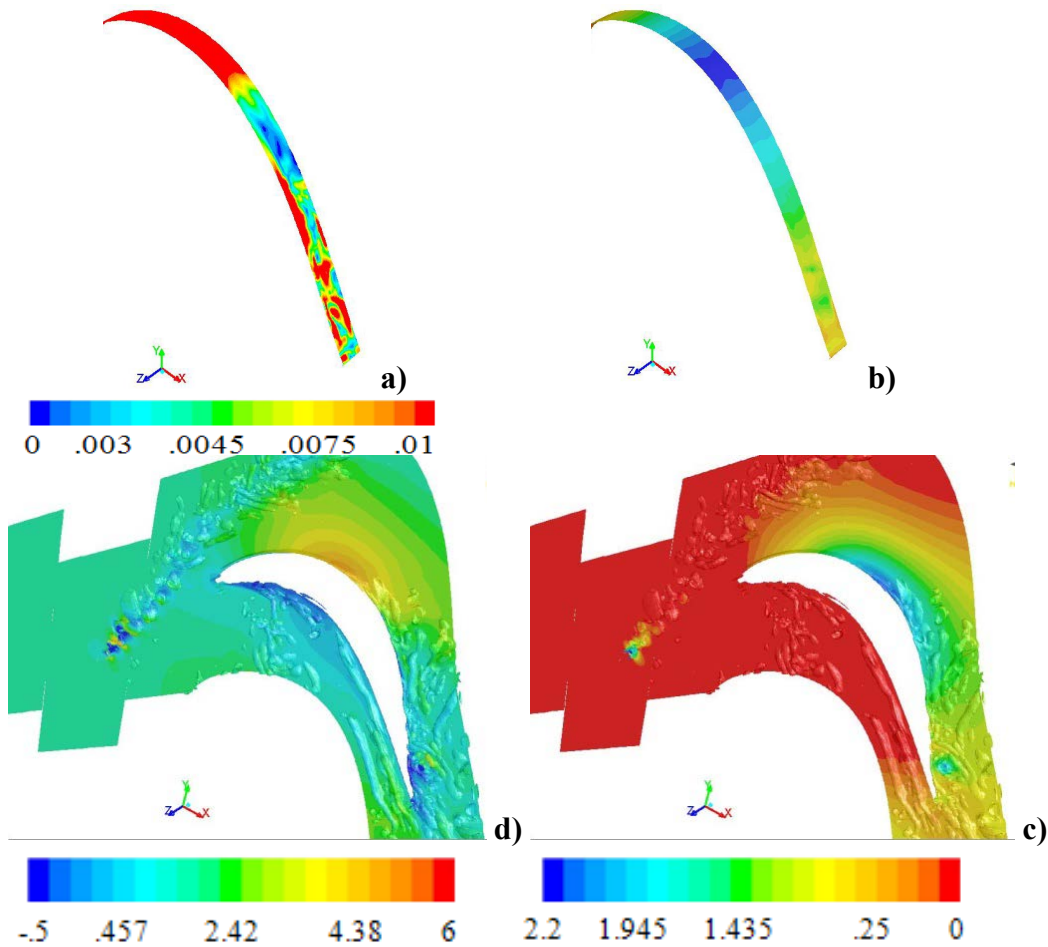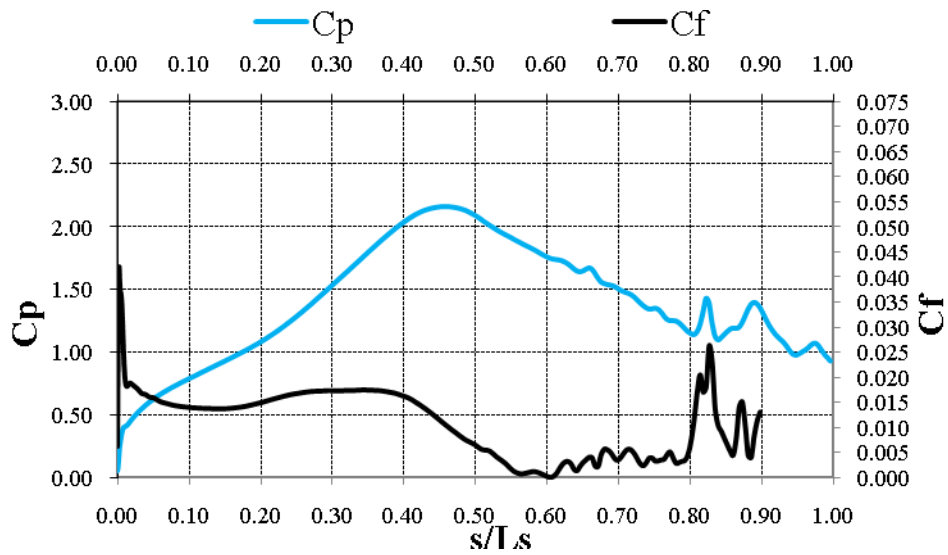
Fig. 24-6 Comparison of Instantaneous C_p and C_f on suction surface for Re=50,000, LFSTI: a) Contours of mean C_f b) Contours of mean C_p c)Q-criterion, Cp Contours d)Q-criterion, x-velocity Contours
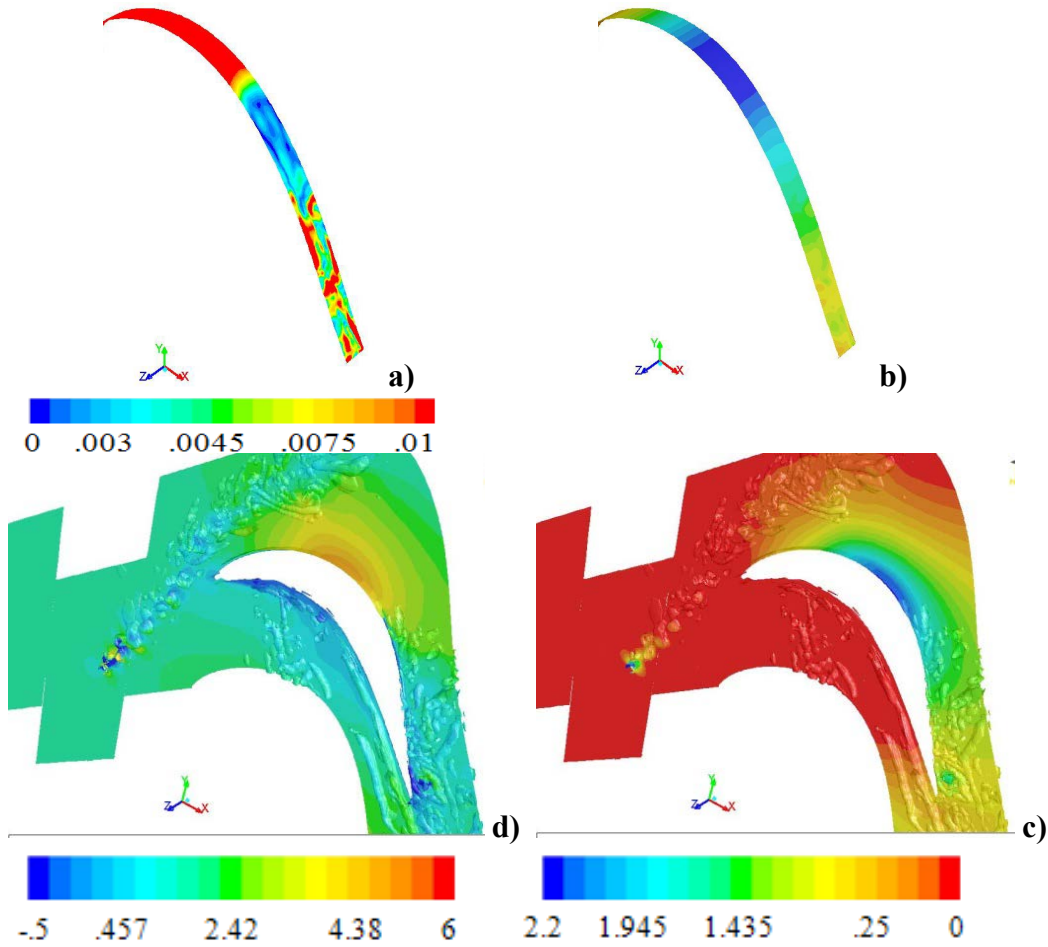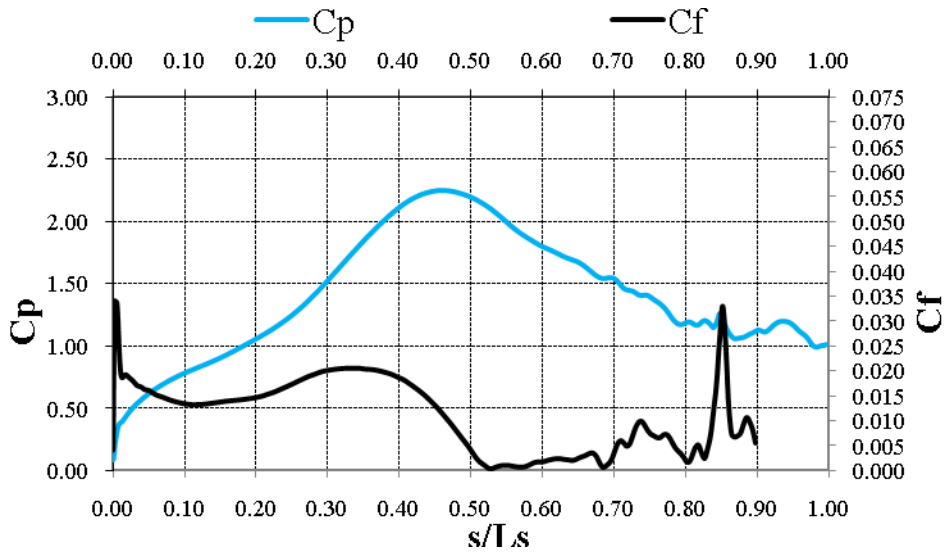
Fig. 24-7 Comparison of Instantaneous C_p and C_f on suction surface for Re=50,000, LFSTI: a) Contours of mean C_f b) Contours of mean C_p c)Q-criterion, Cp Contours d)Q-criterion, x-velocity Contours
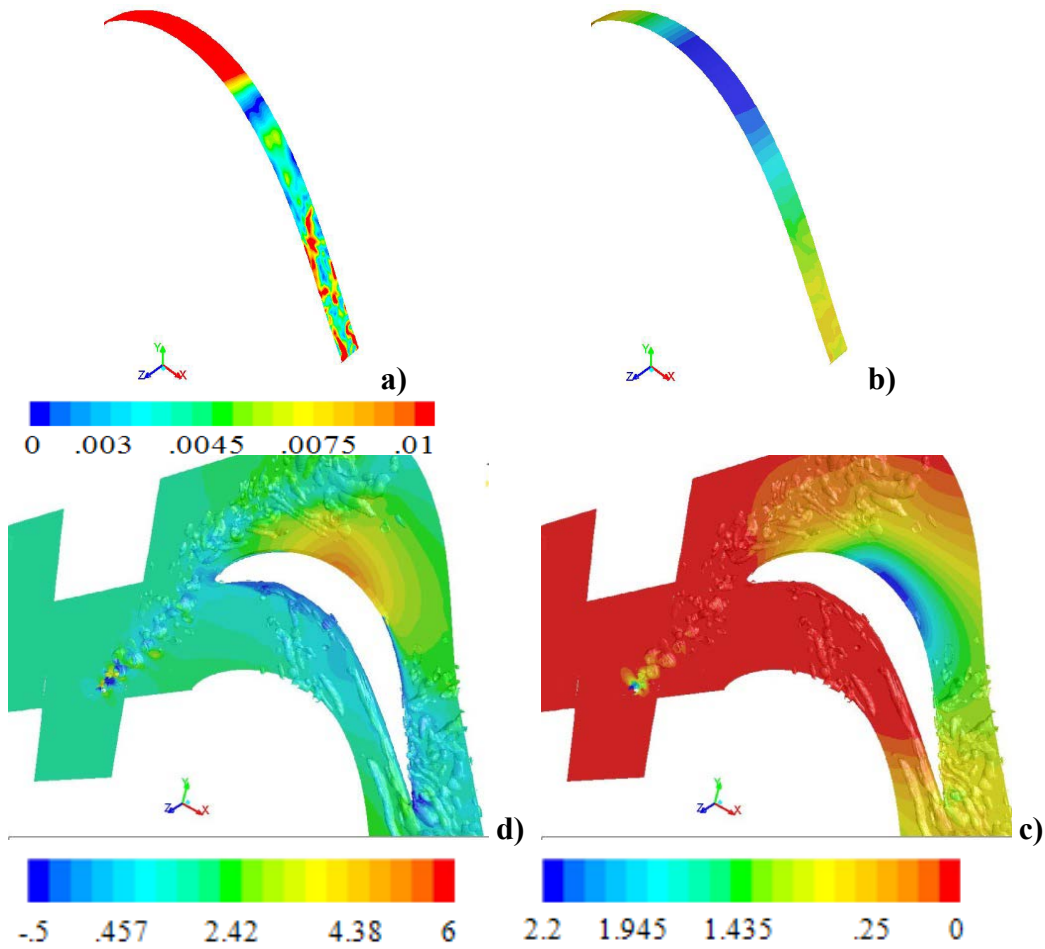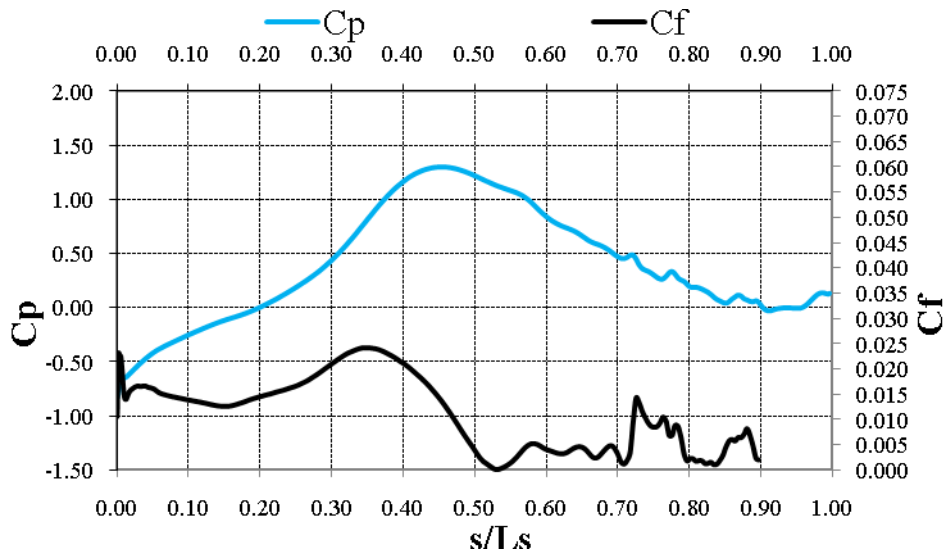
Fig. 24-8 Comparison of Instantaneous C_p and C_f on suction surface for Re=50,000, LFSTI: a) Contours of mean C_f b) Contours of mean C_p c)Q-criterion, Cp Contours d)Q-criterion, x-velocity Contours
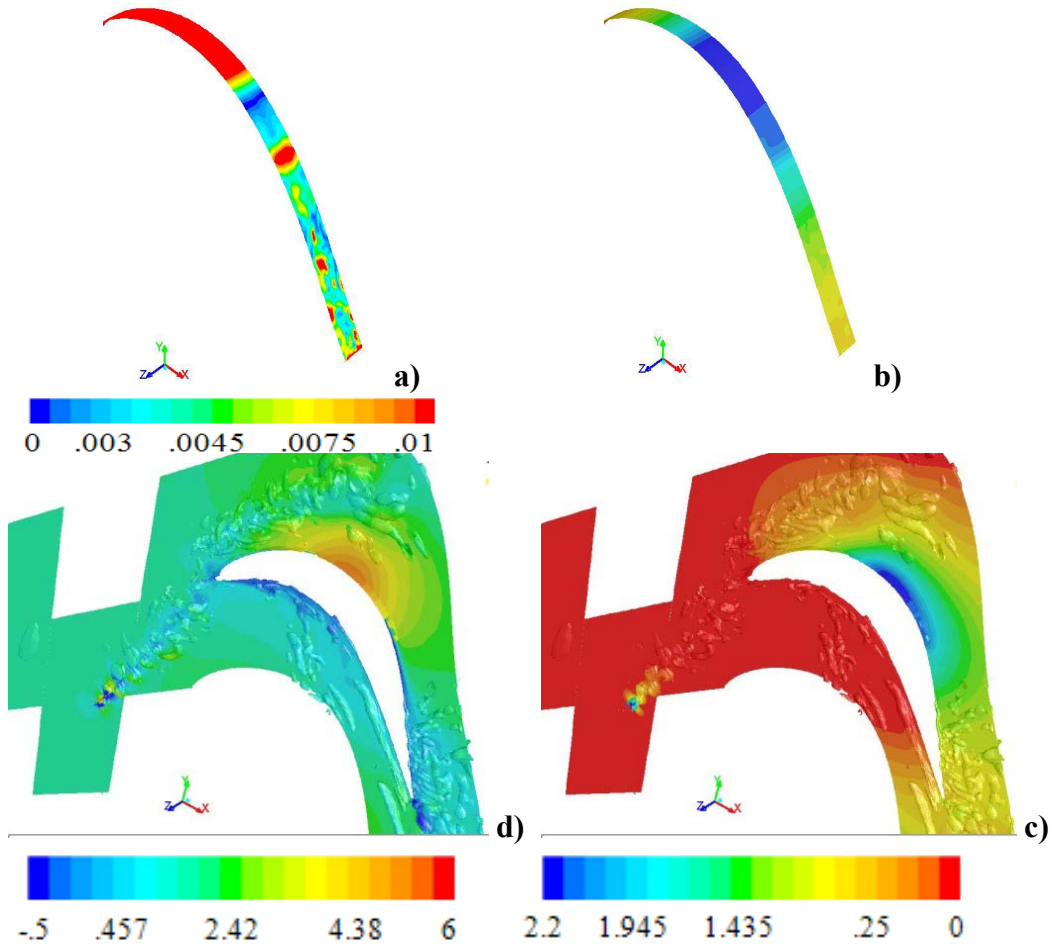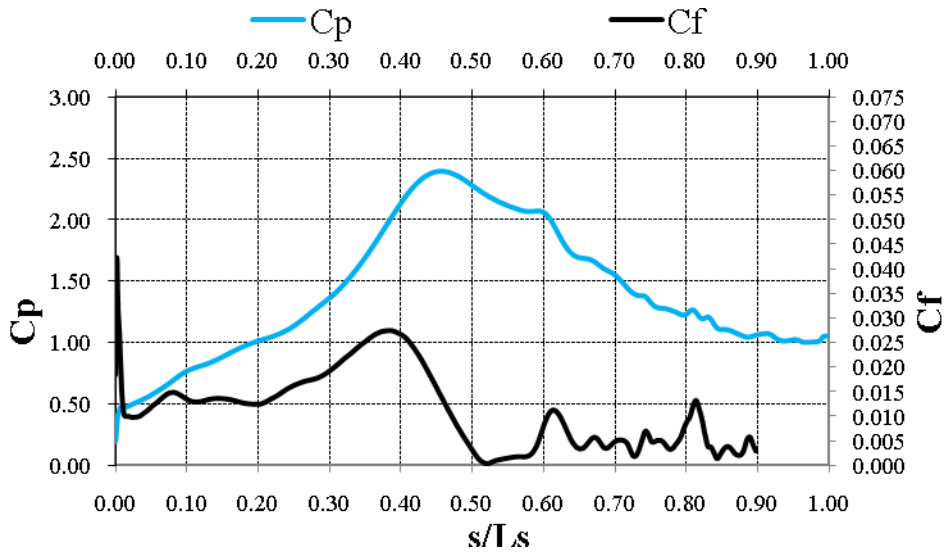
Fig. 24-9 Comparison of Instantaneous C_p and C_f on suction surface for Re=50,000, LFSTI: a) Contours of mean C_f b) Contours of mean C_p c)Q-criterion, Cp Contours d)Q-criterion, x-velocity Contours
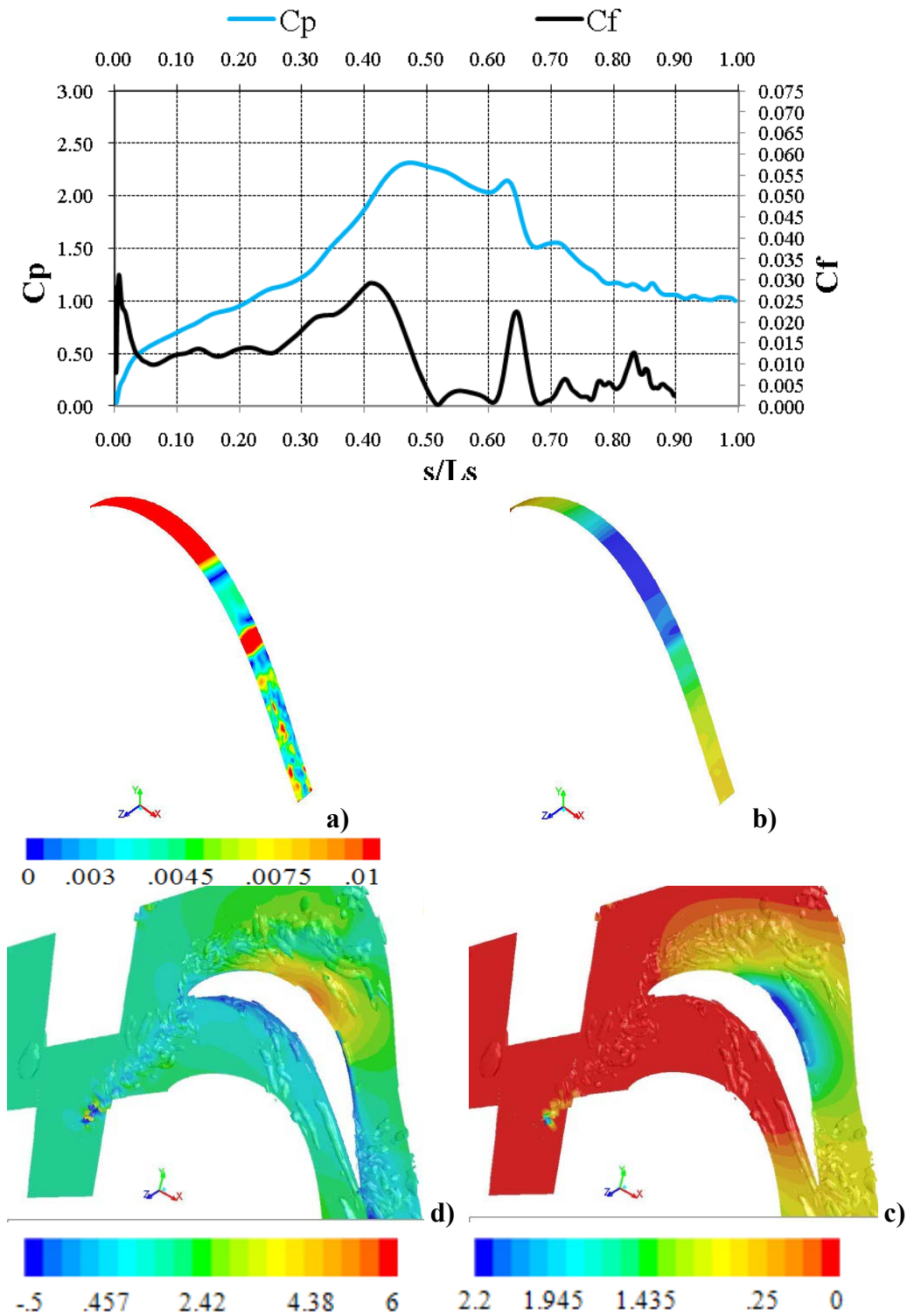
Fig. 24-10 Comparison of Instantaneous C$_p$ and C$_f$ on suction surface for Re=50,000, LFSTI: a) Contours of mean C$_f$ b) Contours of mean C$_p$ c)Q-criterion, Cp Contours d)Q-criterion, x-velocity Contours
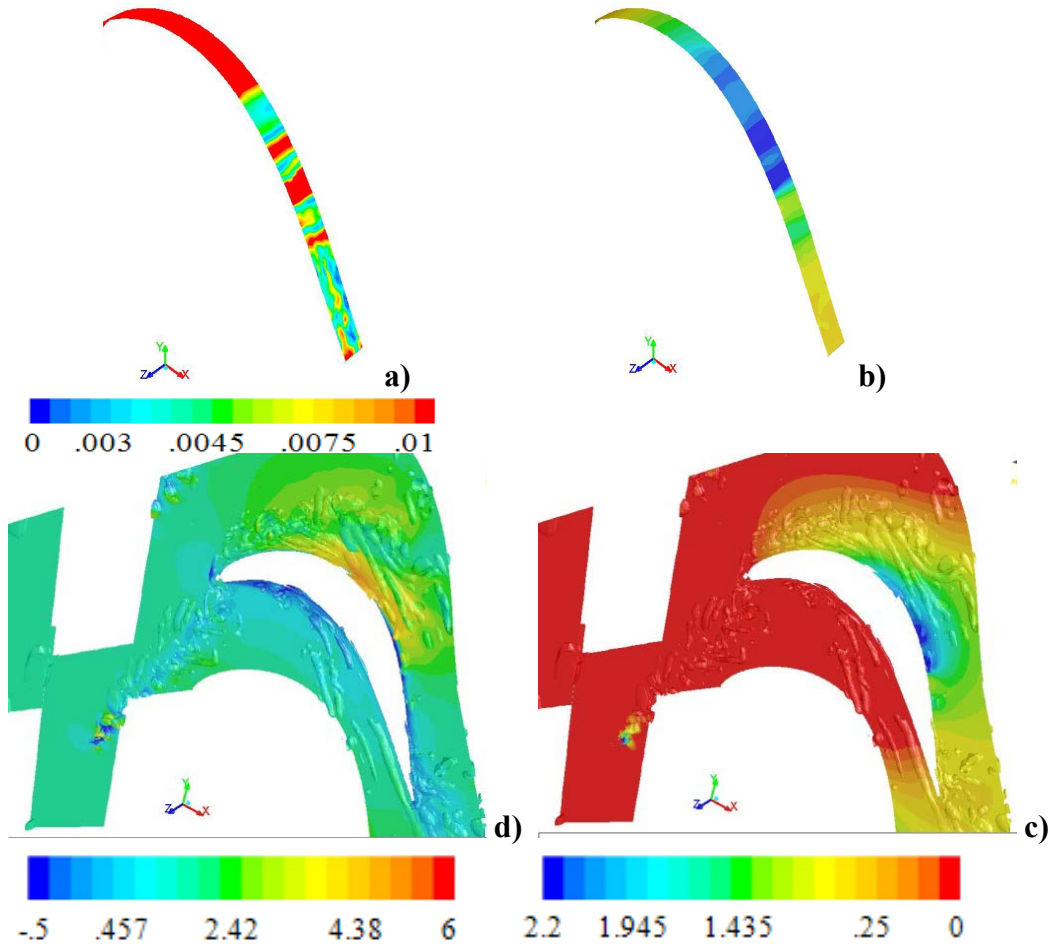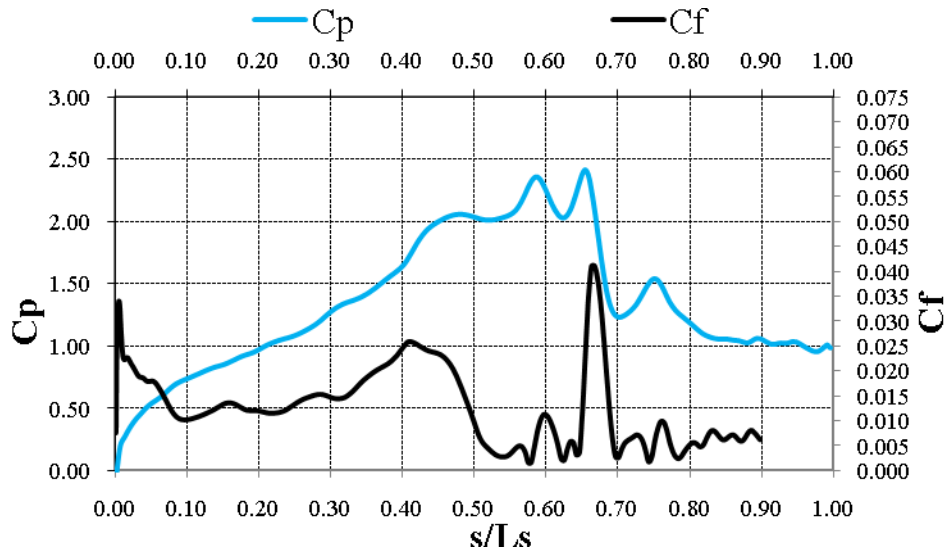
Fig. 24-11 Comparison of Instantaneous C$_p$ and C$_f$ on suction surface for Re=50,000, LFSTI: a) Contours of mean C$_f$ b) Contours of mean C$_p$ c)Q-criterion, Cp Contours d)Q-criterion, x-velocity Contours
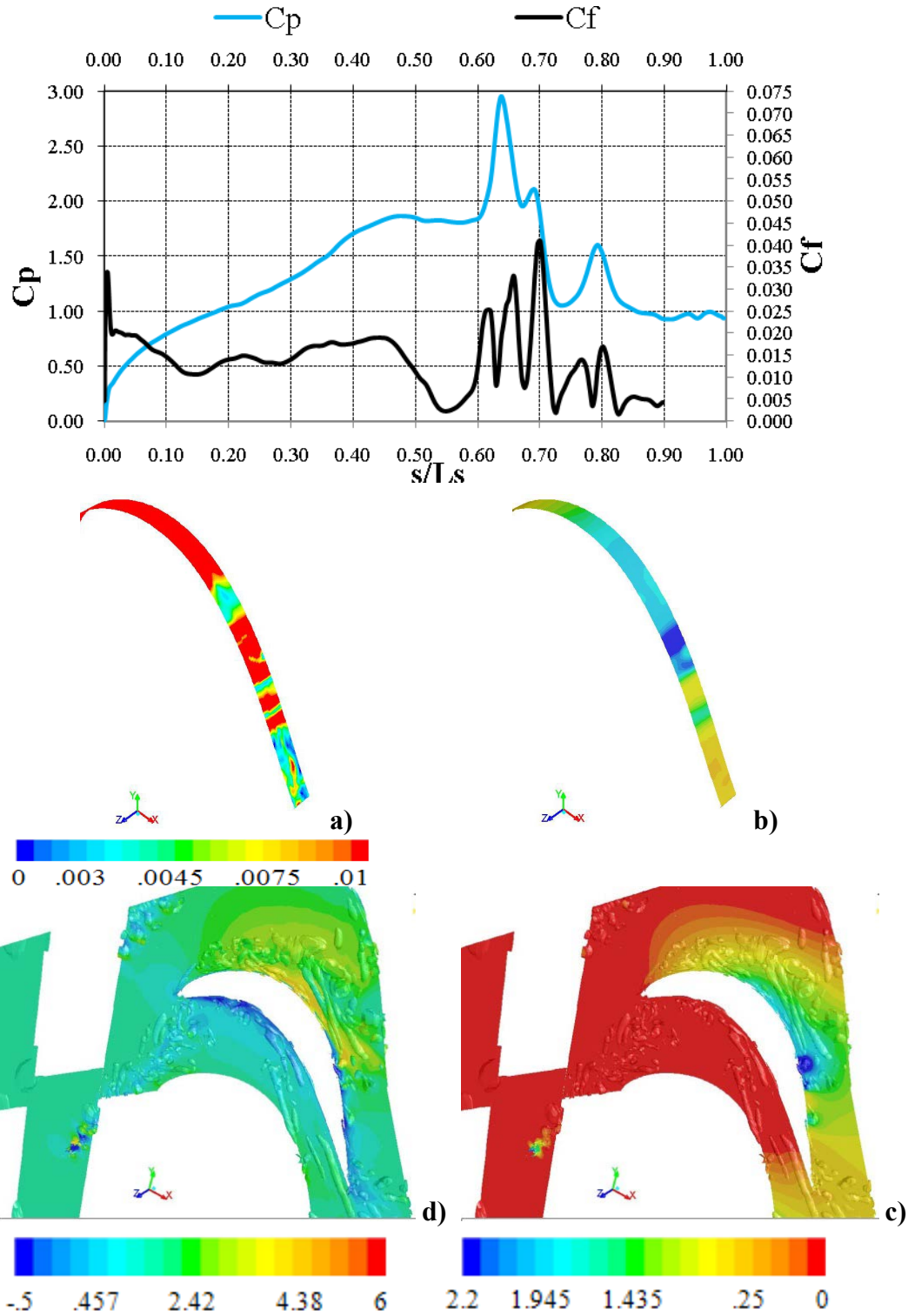
Fig. 24-12 Comparison of Instantaneous C_p and C_f on suction surface for Re=50,000, LFSTI: a) Contours of mean C_f b) Contours of mean C_p c)Q-criterion, Cp Contours d)Q-criterion, x-velocity Contours
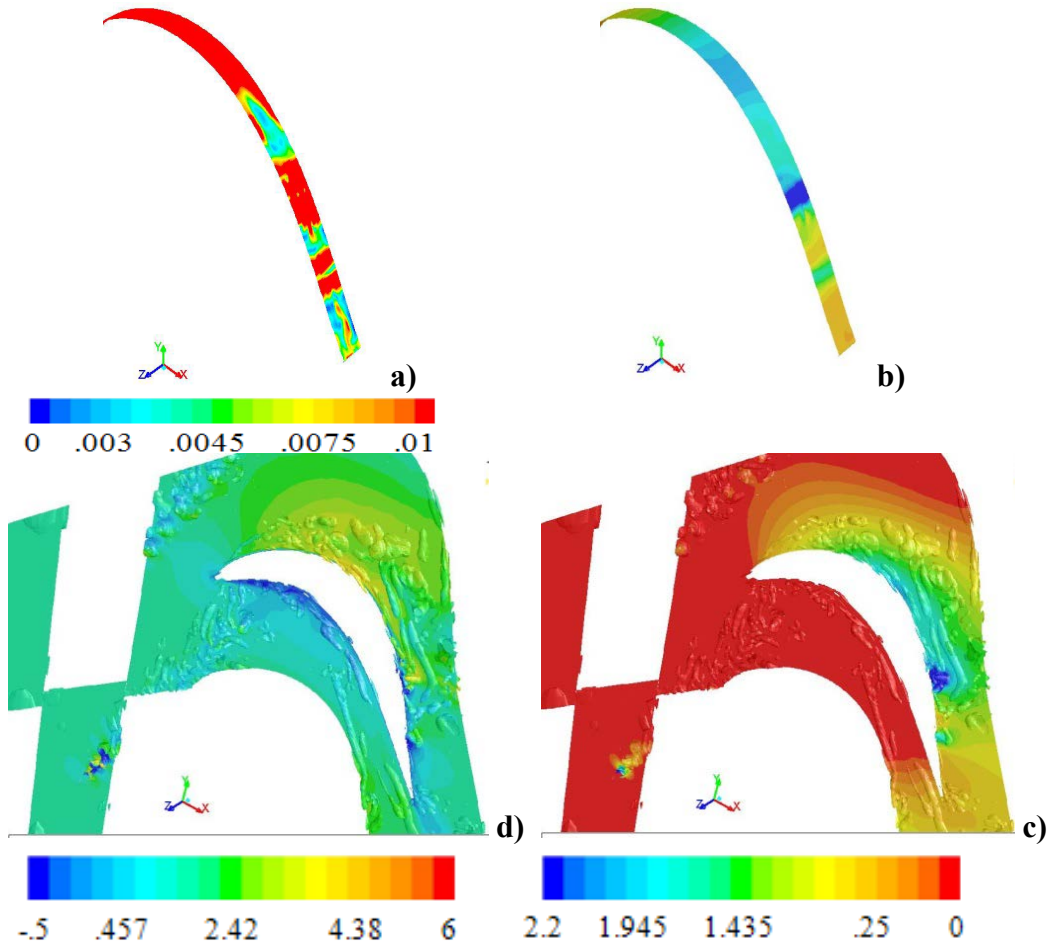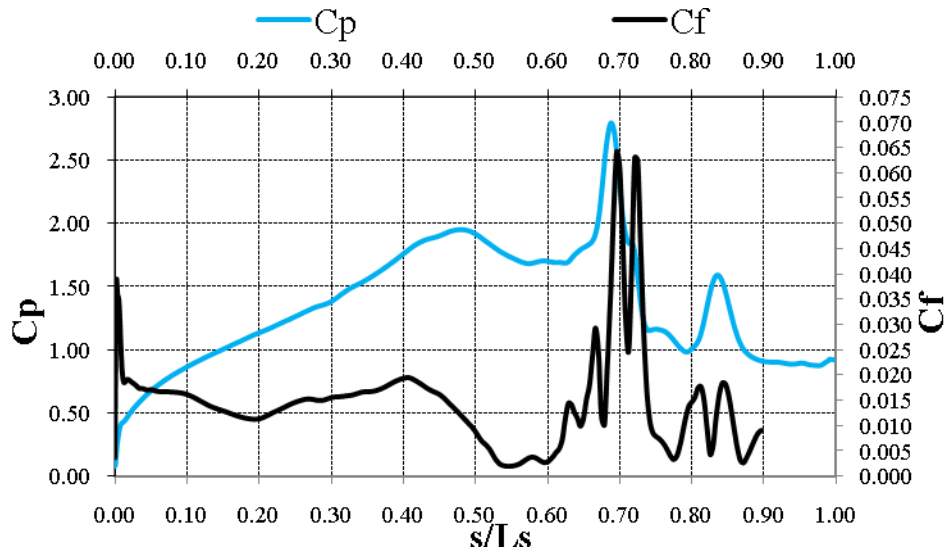
Fig. 24-13 Comparison of Instantaneous C_p and C_f on suction surface for Re=50,000, LFST: a) Contours of mean C_f b) Contours of mean C_p c)Q-criterion, Cp Contours d)Q-criterion, x-velocity Contours
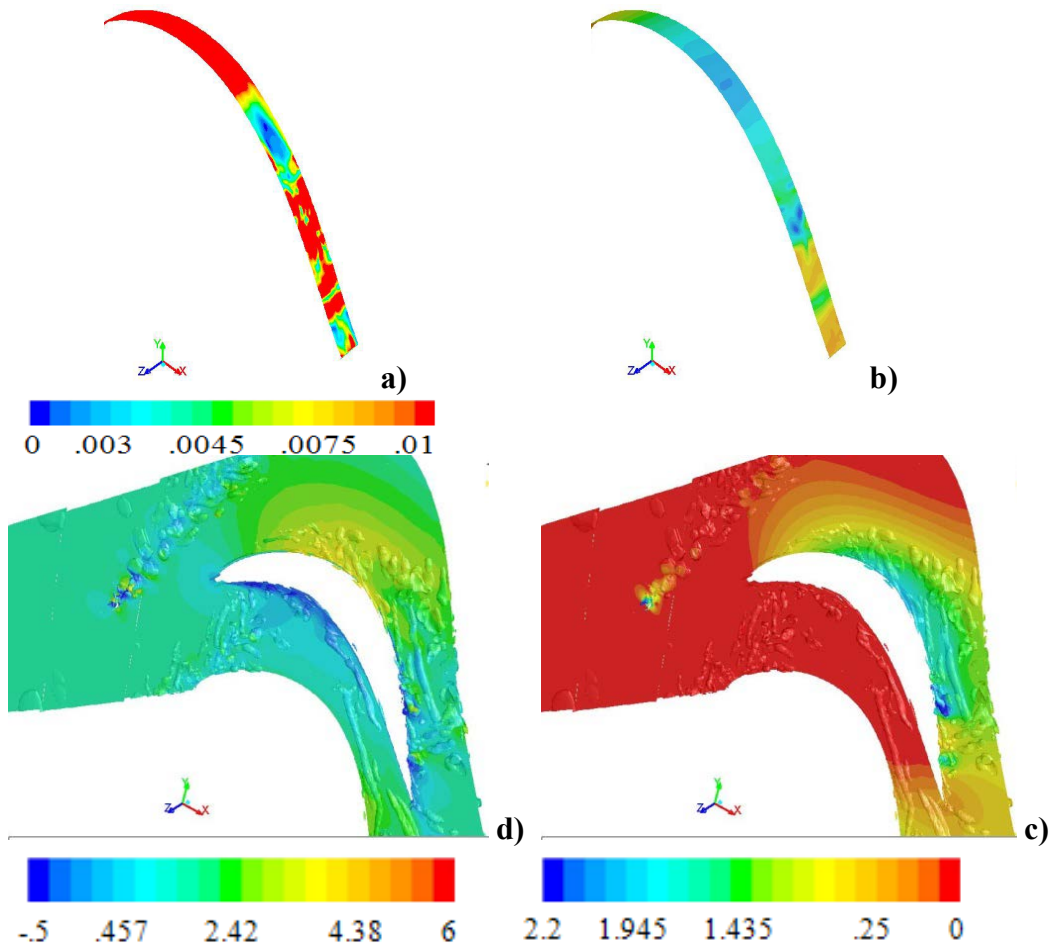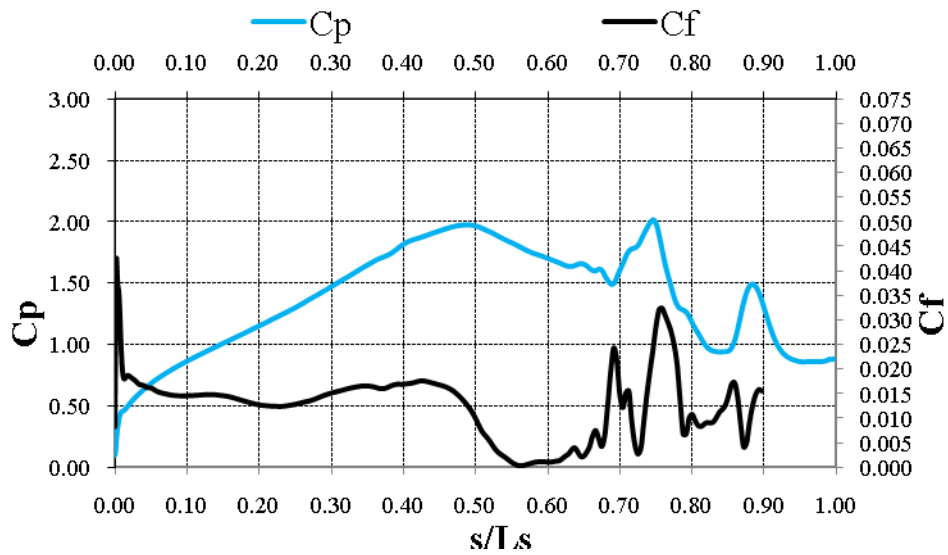
Fig. 24-14 Comparison of Instantaneous C_p and C_f on suction surface for Re=50,000, LFSTI: a) Contours of mean C_f b) Contours of mean C_p c)Q-criterion, Cp Contours d)Q-criterion, x-velocity Contours

Re=50,000, F=0.548

HFSTI

In switching to Re=50,000 HFSTI inlet flow conditions, like switching from Re=25000, LFSTI to HFSTI, the wake profile (Figure 25) does not change very much. In this HFSTI case, the wake deficit is predicted to be slightly lower than the LFSTI case, and the wake is predicted to be slightly wider. However, the overall trend and shape of the wake matches the profiles seen in all the cases thus far.

The experimental data showed very little change in the data as far as magnitudes and locations of the suction peak, separation, and reattachment points. However, in switching the CFD model to a HFSTI inlet flow, the result is that instead of slightly under-predicting the magnitude of Cp, it slightly over-predicts these values. However this over-prediction is very slight at the suction peak, separation and reattachment point, and the prediction of the locations of these events is nearly identical to the experimental data. The over-prediction on the leading edge is consistent with that was seen in the LFSTI which under-predicted the values from leading edge until reattachment, however the LFSTI had very good matching at the trailing edge, where in this HFSTI case it over-predicts these magnitudes all the way through the airfoil suction surface. This is also seen to be the trend on the pressure side, which when switching from LFSTI to HFSTI in the Re=25,000 cases, the ability to predict the pressure distribution on the pressure side surface also decreased. These effects show a trend that the high freestream turbulence that is imposed at the inlet of the domain will help in showing the interaction of this turbulence with the boundary layer over a suction peak and separation bubble, however it also seems to show more interaction with the areas of laminar flow, thus causing the

discrepancies in these regions. For this paper, the interaction of the flow with the boundary layer is the focus of the results, thus the reason for HFSTI inlet conditions used for the remainder of the cases.

When looking at the total pressure loss coefficient in Figure 27, the slightly over-predicted pressure leads to a slight over-prediction in the magnitude of the loss, however the amplitude of the curve varies by less than 10%. This consistent matching is also seen in Figures 28a and 28b which show velocity profiles and u' profiles respectively. The profiles themselves are very consistent with the trend the data shows as rod to blade spacing is reduced and show the same similar shape as does the LFSTI case.

When looking at the Cp and C_f values plotted on the same graph, as seen in Figure 29, the same trend of an inflection in the C_f downward slope is seen at the point where the separation bubble plateau begins. The C_f values then slowly decline to zero with a small length near zero slightly downstream from the zero point, then a sharp increase in C_f occurs which indicates the start of transition. Right before the C_f reaches a subsequent peak, the plateau in Cp ends, showing where reattachment occurs. In the previous plots, this point was seen as an additional inflection point, however since in this case the peak C_f is so close to the reattachment point it is just seen as more of a rounding off of the curve up to the peak. The upstream trends of a peak in C_f just before the suction peak, and the trailing edge trends of a steady amount of turbulence noted by fluctuations in the C_f along with attached flow through the end are the same as seen previously.

Since the HFSTI flow has the same mean flow properties and seems to model the data with similar consistency as the LFSTI case, the instantaneous plots below represent

20% advancements in time per cycle rather than the 10% plots shown for LFSTI since most of the details shown are consistent between the two.

With that said, Figure 30-1 shows a wake just reaching the leading edge of the airfoil, without any wake effect present over most of the suction side, with an exception for the very trailing edge. A clear suction peak is present, along with a small plateau in the C_p values before a reattachment is seen at .6Ls. This plateau is associated with near zero C_f values, with a zero C_f point. At about .58Ls a sharp increase is seen in C_f and right before its peak at .61Ls, reattachment is observed. Looking at the contours, this separation bubble is present across the entire span of the airfoil.

In Figure 30-2 the wake can be seen affecting the upstream portion of the airfoil surface along with starting to collapse down and compress the suction peak. This collapsing effect also puts a shear force over the suction peak and separation bubble, pushing it farther downstream, however the wake has yet to impinge enough into the boundary layer to suppress the separation. This is evident to have happened by Figure 30-3, which shows the pressure bubble being rolled up and compressed down the aft portion of the airfoil. The pressure bubble still shows some attachment to the surface on the contour C_p plots, which results in a turbulent spike in the C_f values in that region. Trailing behind this turbulent peak is the expected calmed zone, which, though near zero C_f, is suppressant to separation. The wake has moved far enough downstream for the suction peak to start its re-growth as well as the re-growth C_f peak.

In Figure 30-4, it can be seen that even though the suction bubble only has a faint attachment to the surface still (looking at the surface C_p contours), it still has enough of an effect to cause a spike in the C_p and C_f values at that point. Since this turbulent peak

is still evident, the calmed zone remains attached to the surface. This area is close to becoming separated by Figure 30-5, however there seems to be enough turbulence on the trailing edge to keep the flow from separating. This is evident by the lack of any dark blue contours on the surface, along with the fact that the C_f graph never hits zero nor is any sort of plateau evident in the Cp plot. It is clear that flow does separate eventually though because in Figure 30-6, as the next wake is starting to impinge on the surface, the suction peak again in compressed in magnitude and the separation bubble is sheared downstream, as seen in Figure 30-1.

It can be seen that in switching from LFSTI to HFSTI that the experimental differences are minimal for a Re=50,000 flow, as is predicted in CFD. There is a slight change in the prediction of the magnitude of the pressure profile over the suction surface, however, with this change in magnitude also results in excellent prediction of the suction peak value as well as the location of separation and reattachment. In looking at the instantaneous plots, further insight into the effect of the suction bubble and its affect on the suction surface as it is rolled off the trailing edge of the airfoil is shown. It can be seen that as long as the pressure bubble exists on the surface, a turbulent spike is also present, followed by a calm region, that though close to zero C_f, it near separates from the surface.
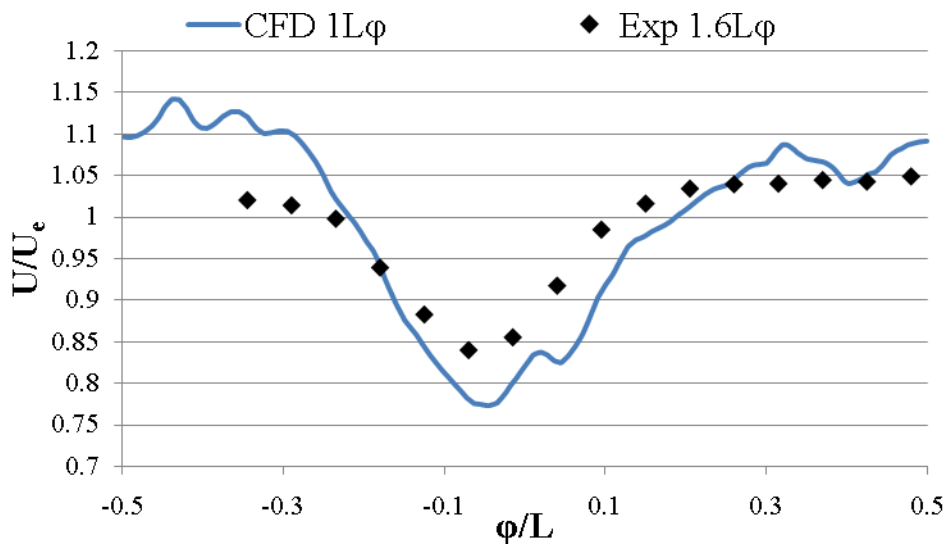
Fig 25 Rod Wake Velocity Magnitude for Re=50,000, HFSTI: Comparison of LES, $1L_{\varphi}$ to Experimental $1.6L_{\varphi}$
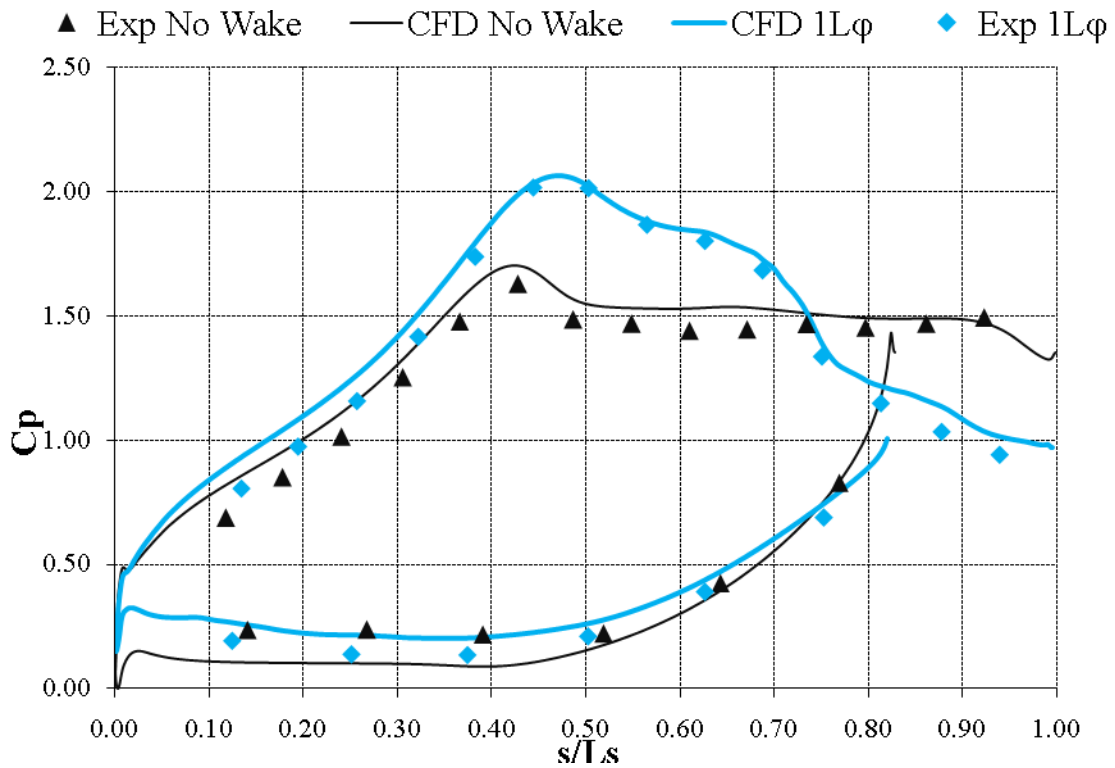
Fig. 26 C_p profiles for Re=50,000, HFSTI: Comparison between LES and Experimental data
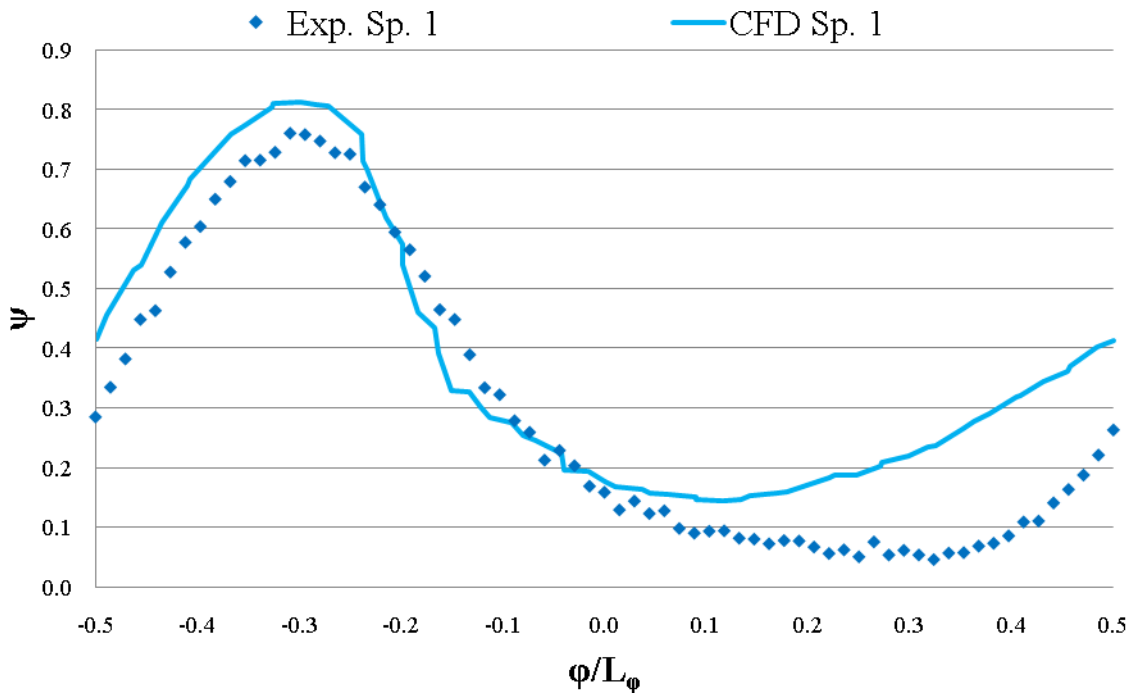
Fig. 27 Total Pressure Loss Coefficient for Re=50,000, HFSTI: Comparison between LES and Experimental Data
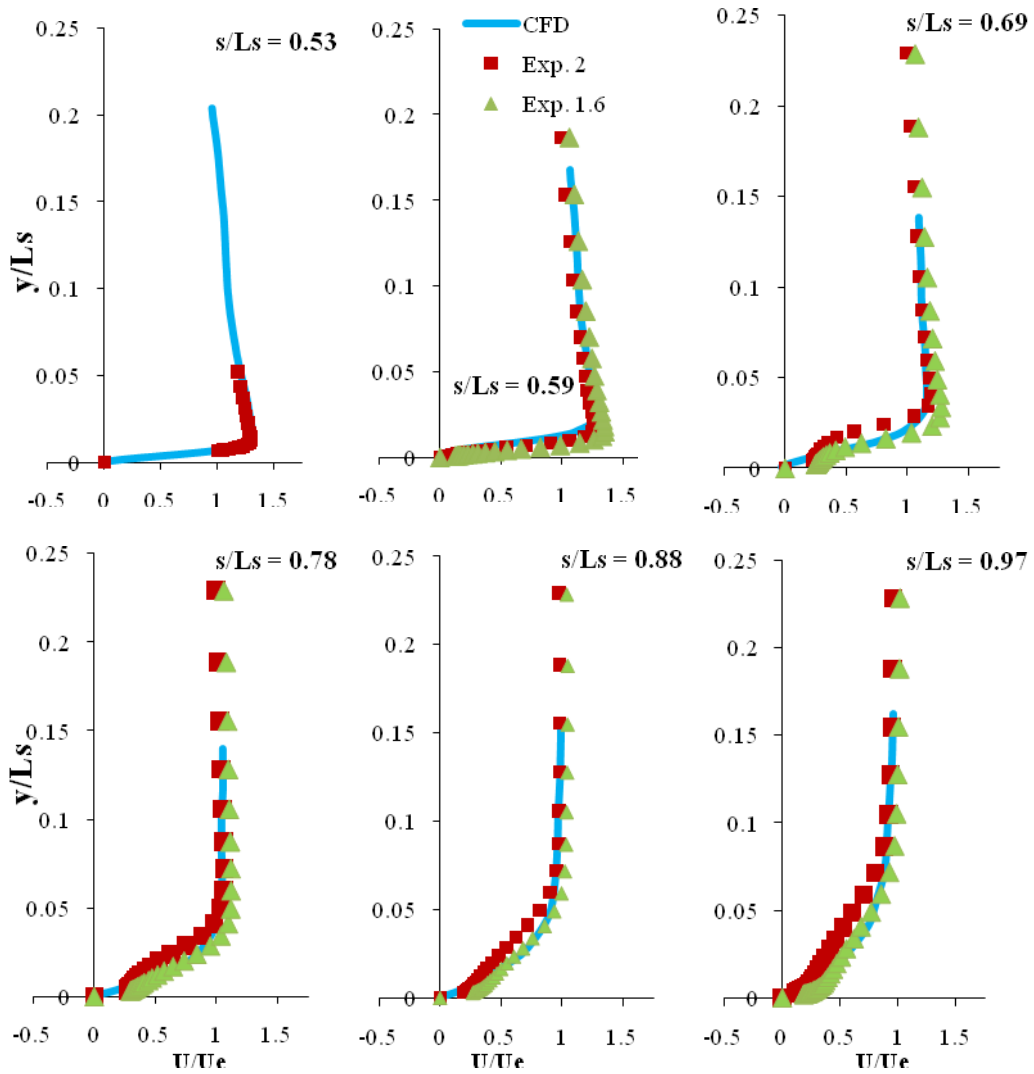
a)

Fig. 28 Time averaged velocity profiles at six streamwise stations for Re=50,000, HFSTI: Comparison between CFD (LES) and Experimental data: a - Mean, b - RMS
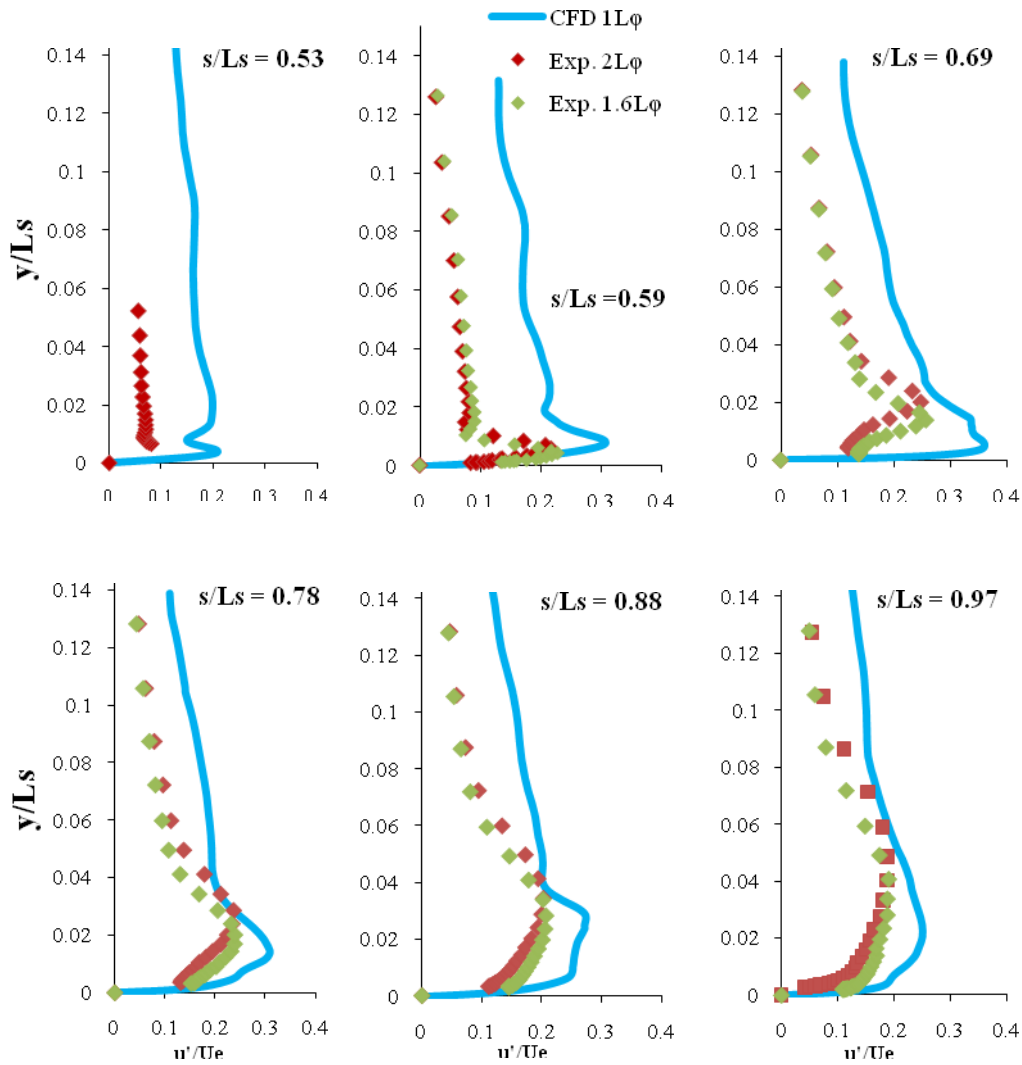
b)
Fig. 28 Time averaged velocity profiles at six streamwise stations for Re=50,000, HFSTI: Comparison between CFD (LES) and Experimental data: a - Mean, b - RMS
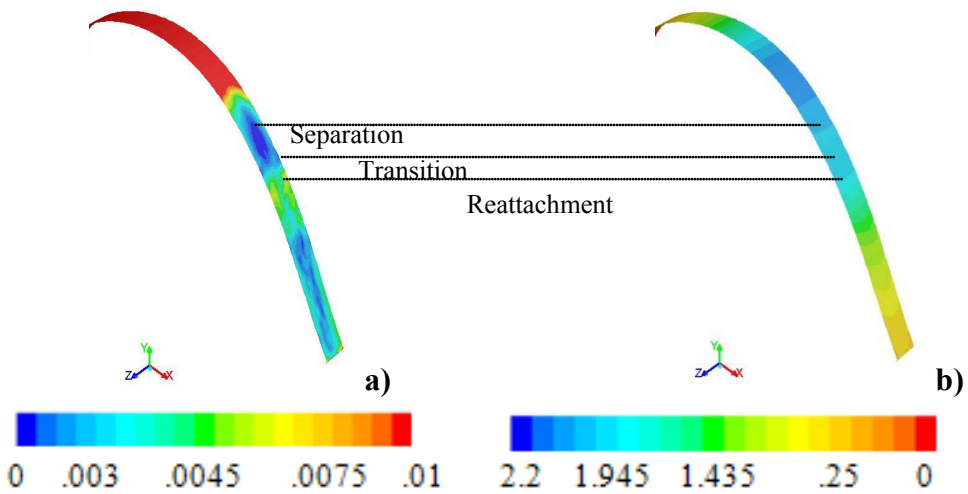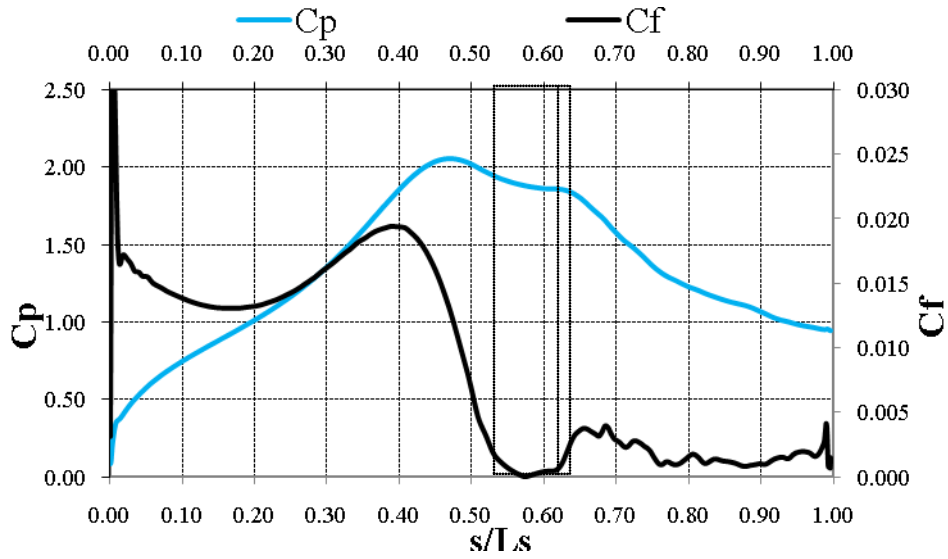
Fig. 29 Comparison of Mean C_p and C_f on suction surface for Re=50,000, HFSTI: a) Contours of mean C_f b) Contours of mean C_p
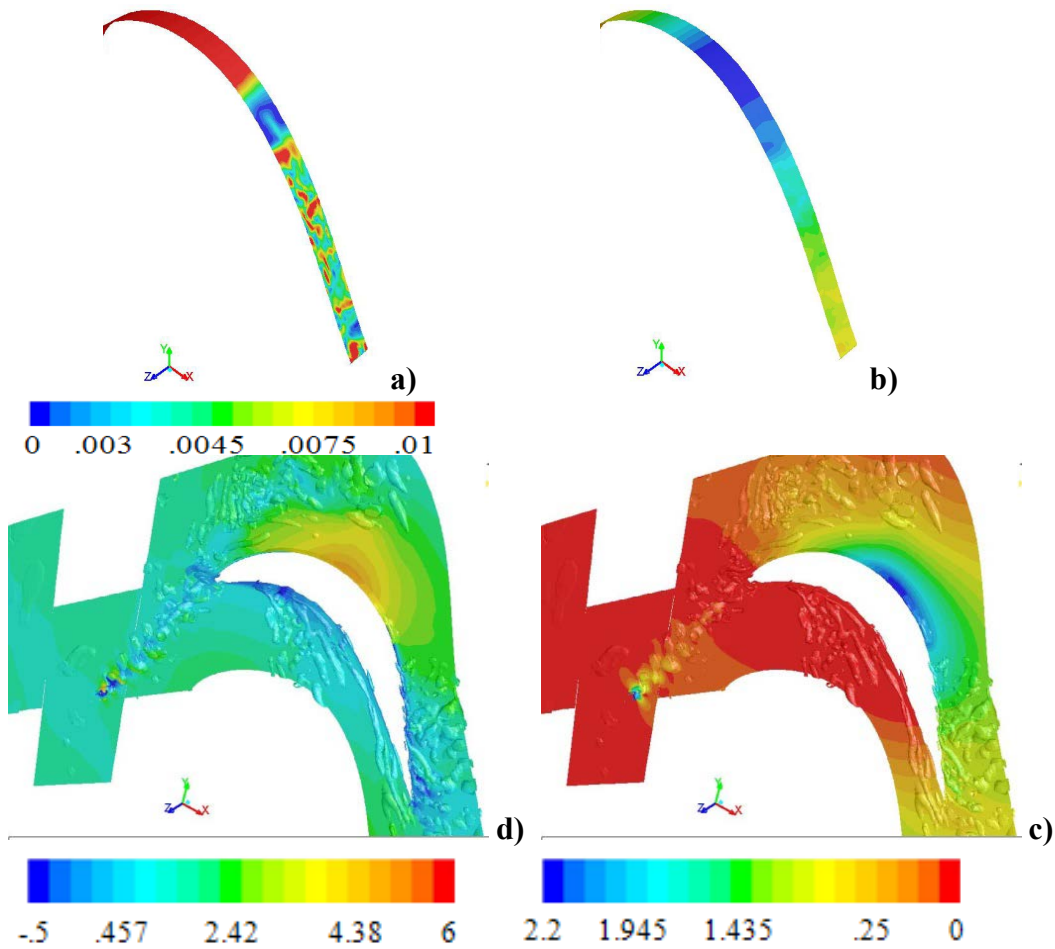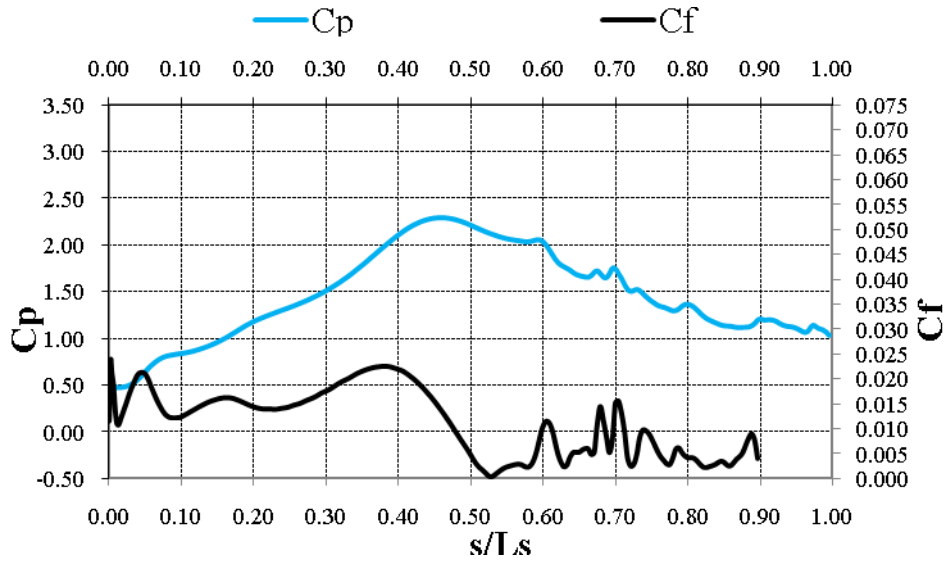
Fig. 30-1 Comparison of Instantaneous C_p and C_f on suction surface for Re=50,000, HFSTI: a) Contours of mean C_f b) Contours of mean C_p c)Q-criterion, Cp Contours d)Q-criterion, x-velocity Contours
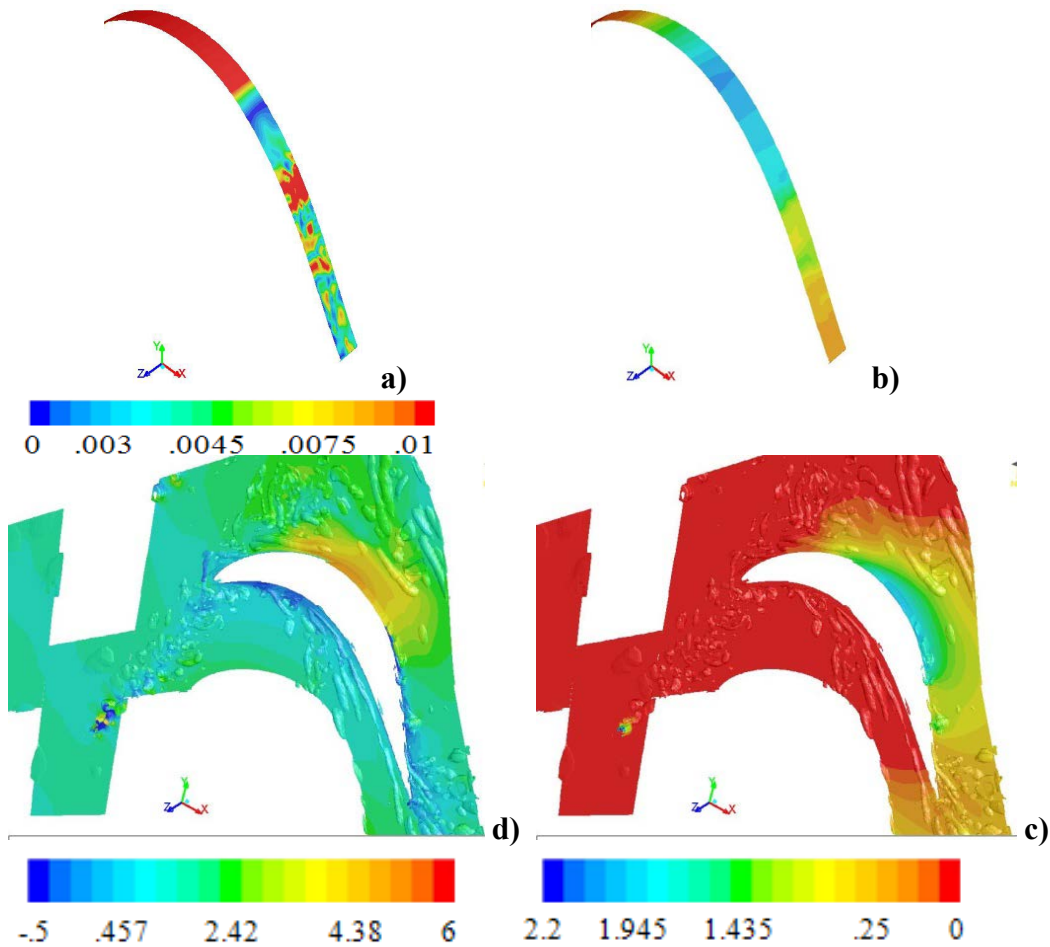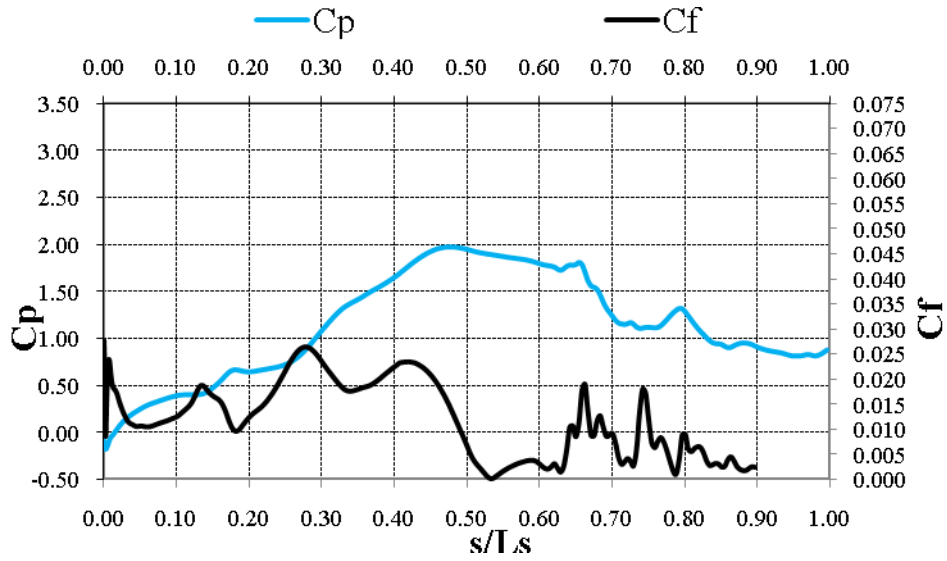
Fig. 30-2 Comparison of Instantaneous C_p and C_f on suction surface for Re=50,000, HFSTI: a) Contours of mean C_f b) Contours of mean C_p c)Q-criterion, C_p Contours d)Q-criterion, x-velocity Contours
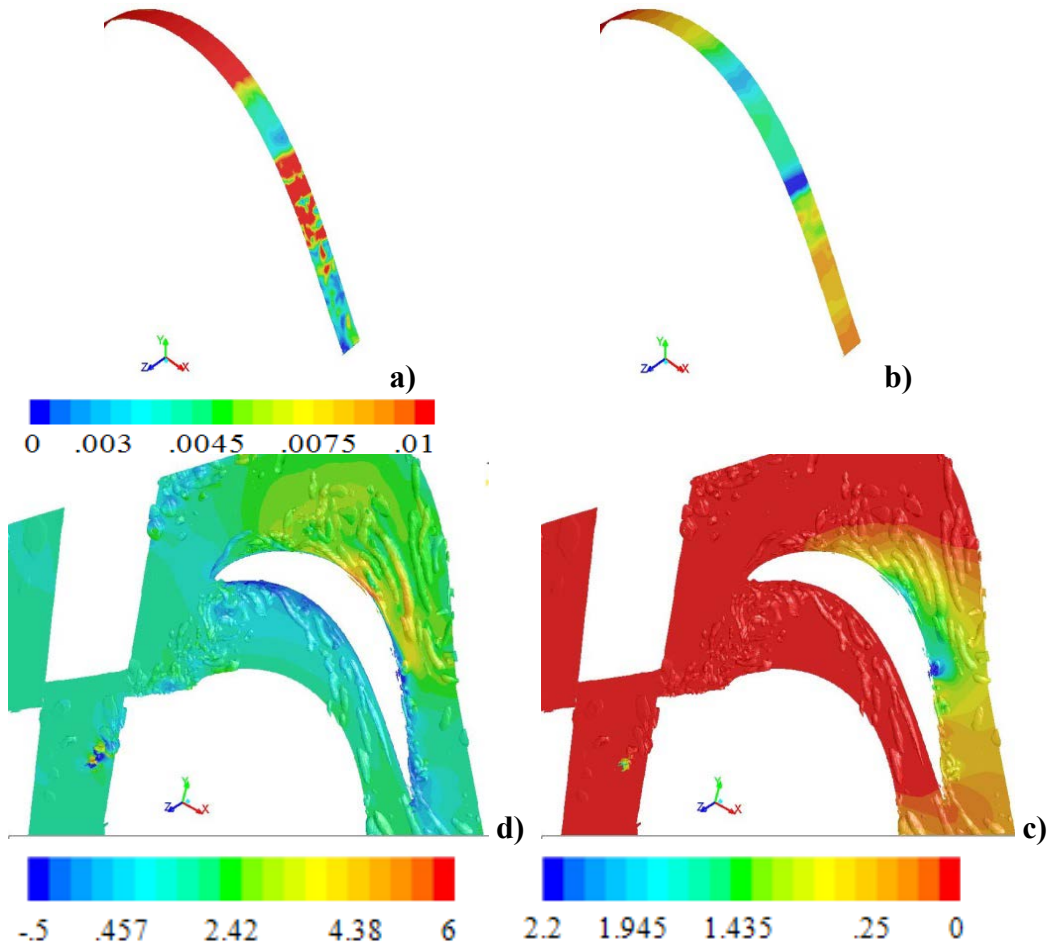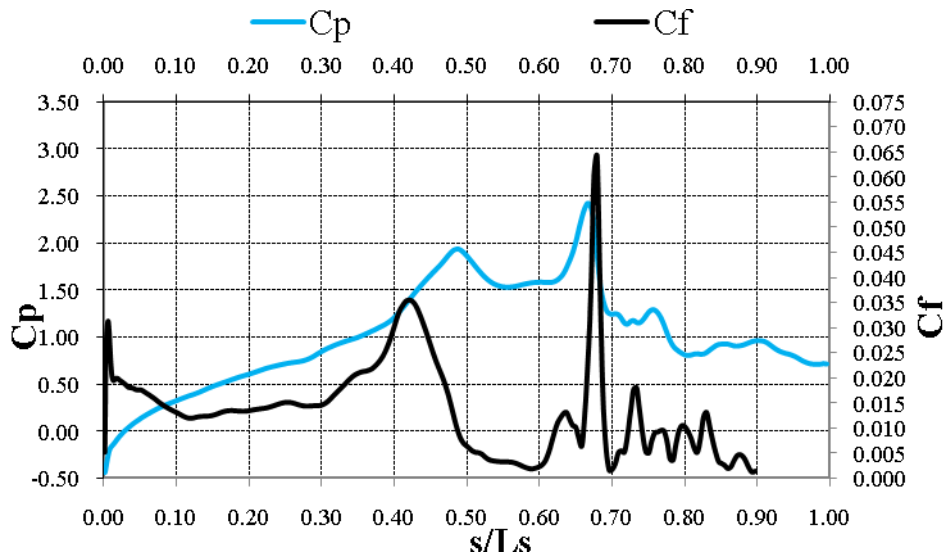
Fig. 30-3 Comparison of Instantaneous C$_p$ and C$_f$ on suction surface for Re=50,000, HFSTI: a) Contours of mean C$_f$ b) Contours of mean C$_p$ c)Q-criterion, Cp Contours d)Q-criterion, x-velocity Contours
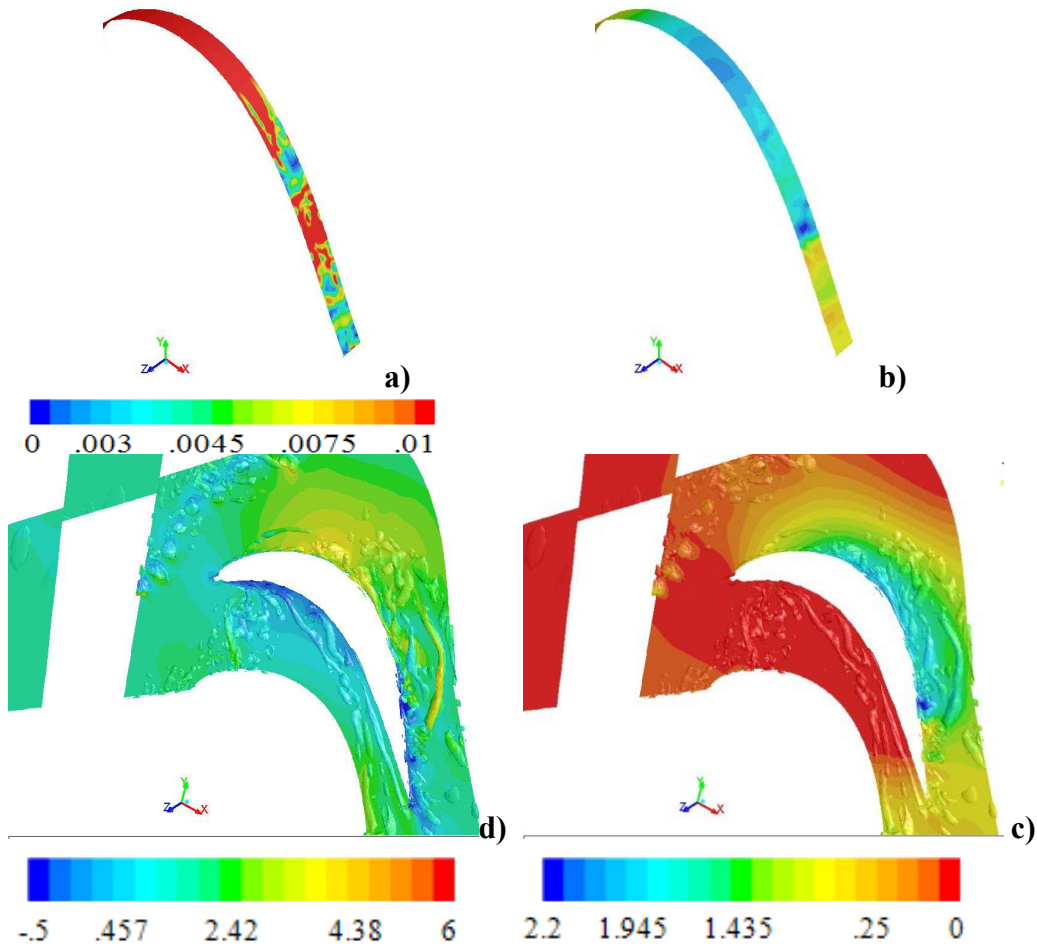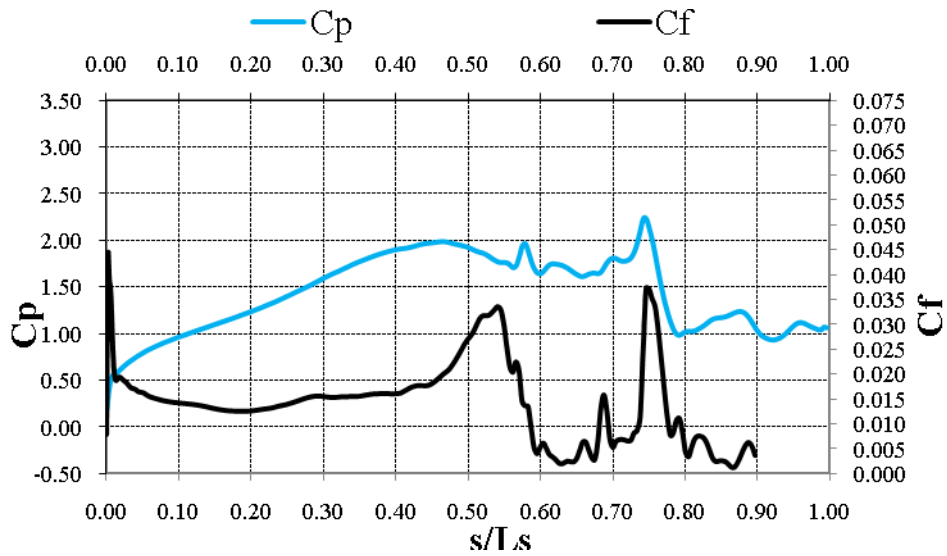
Fig. 30-4 Comparison of Instantaneous C_p and C_f on suction surface for Re=50,000, HFSTI: a) Contours of mean C_f b) Contours of mean C_p c)Q-criterion, Cp Contours d)Q-criterion, x-velocity Contours
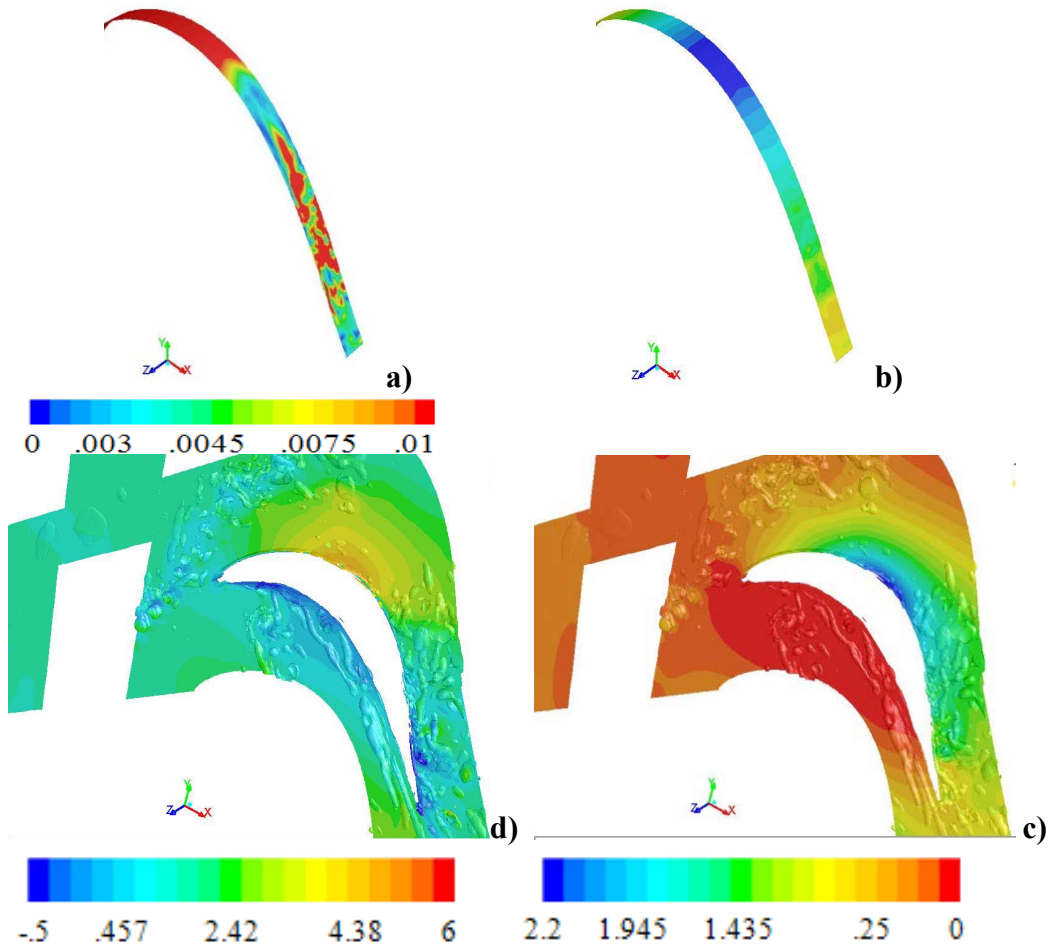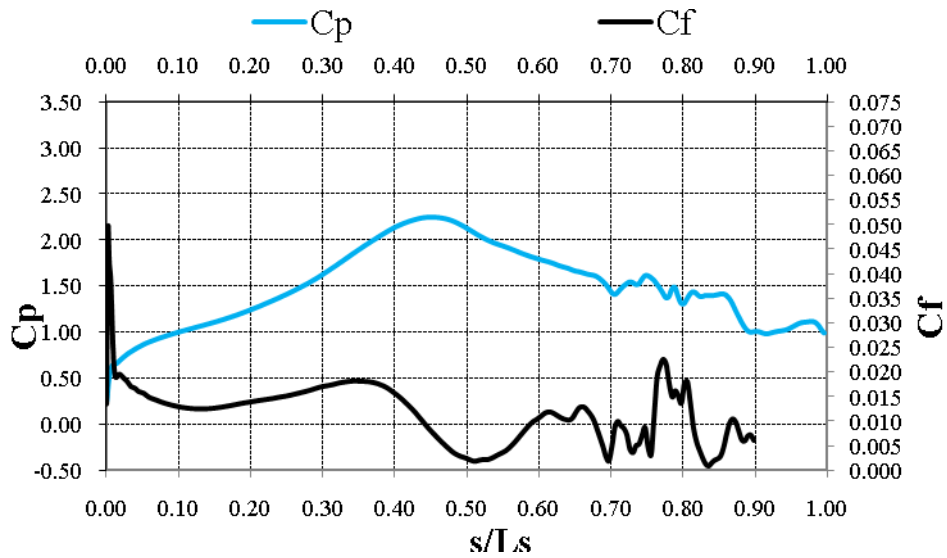
Fig. 30-5 Comparison of Instantaneous C_p and C_f on suction surface for Re=50,000, HFSTI: a) Contours of mean C_f b) Contours of mean C_p c)Q-criterion, Cp Contours d)Q-criterion, x-velocity Contours
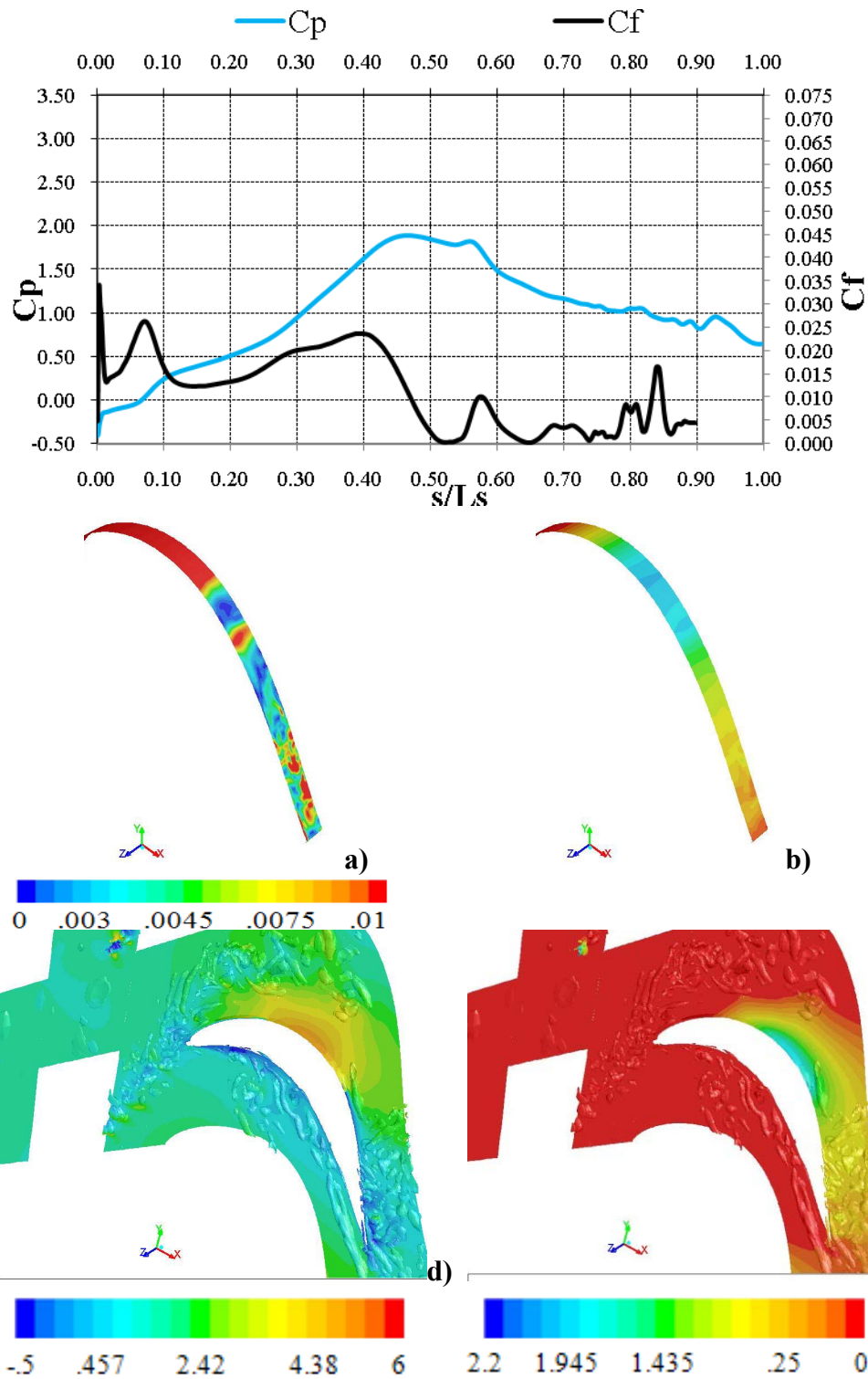
Fig. 30-6 Comparison of Instantaneous C_p and C_f on suction surface for Re=50,000, HFSTI: a) Contours of mean C_f b) Contours of mean C_p c)Q-criterion, Cp Contours d)Q-criterion, x-velocity Contours
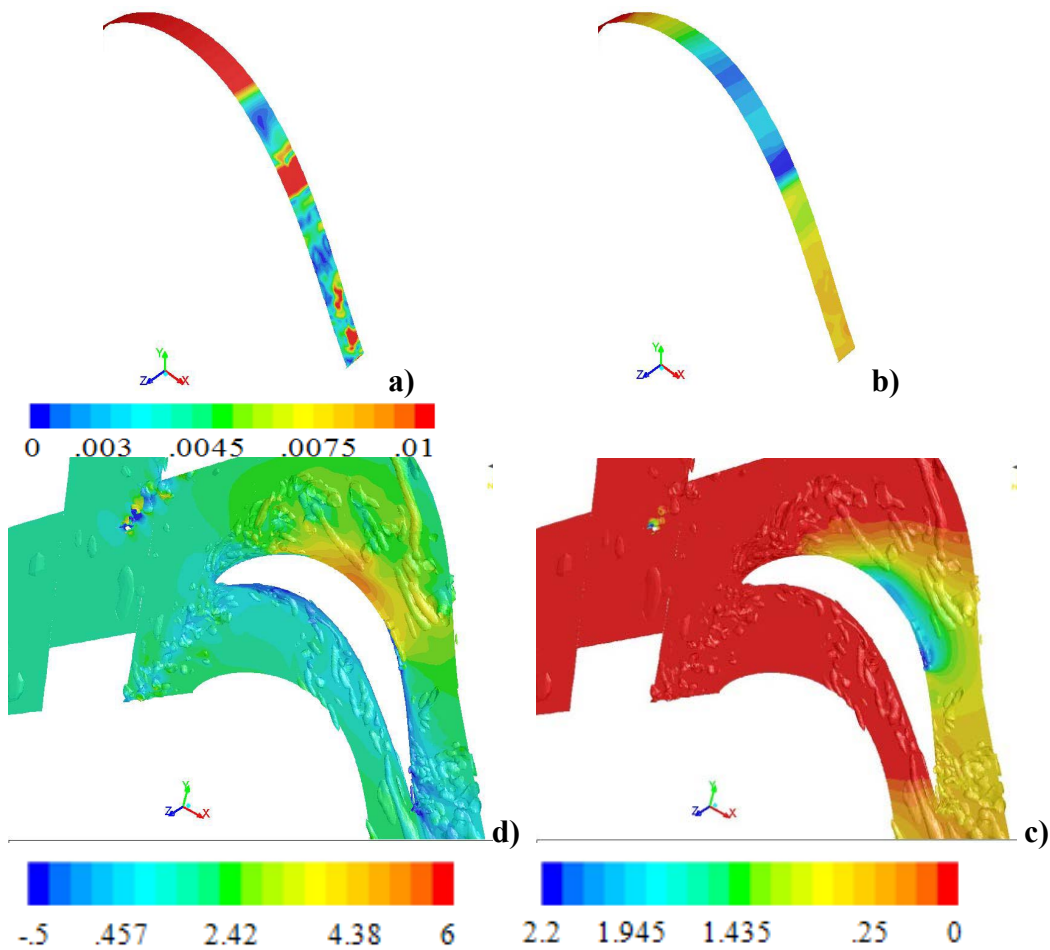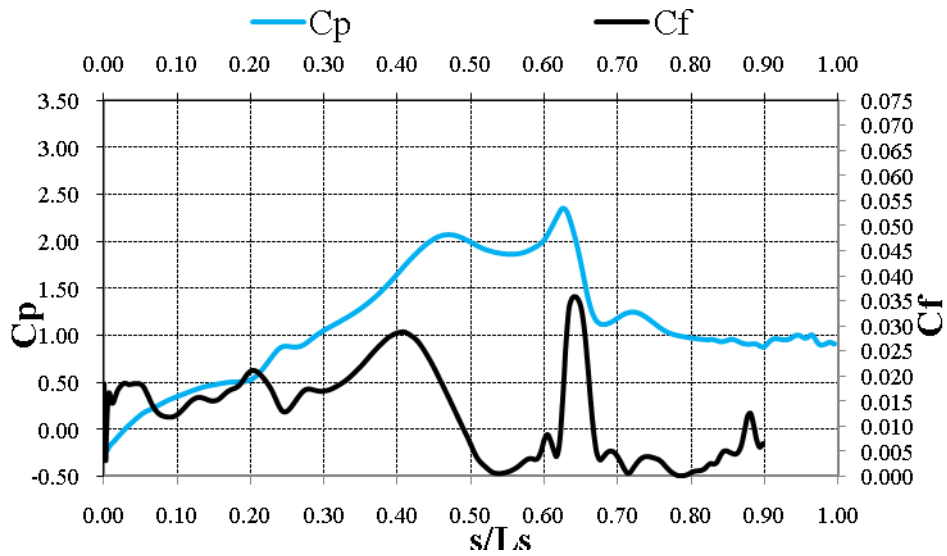
Fig. 30-7 Comparison of Instantaneous C$_p$ and C$_f$ on suction surface for Re=50,000, HFSTI: a) Contours of mean C$_f$ b) Contours of mean C$_p$ c)Q-criterion, Cp Contours d)Q-criterion, x-velocity Contours

Re50,000 HFSTI

F = 0.698

The initial analysis of increasing the rod speed, and thus the wake passing frequency, F, was chosen for an arbitrary increase in rod speed of 25%. This produces a wake passing frequency of F=0.698 and the effect of these results will be compared against the Re=50,000, HFSTI CFD results. The inlet conditions for these cases match the Re=50,000 HFSTI case since it was felt it did a better job at predicting the location of the significant events over the suction surface, like separation and reattachment.

The first thing to analyze is to make sure that the wake being produced at this speed is still consistent with the rest of the results seen so it can be determined that a realistic wake effect is being observed on the suction surface. In looking at Figure 31, the rod wake velocity profile is very consistent with the Re=50,000, F=0.548 wake that was produced in the previous section. The magnitude of this wake is seen to be slightly less than the base case, but the width seems to be just about the same size.

In looking at the mean Cp plot comparison on Figure 32 it is evident that increasing the wake passing frequency has nearly eliminated the separation plateau bubble over the suction surface. Not only has this increase in the amount of turbulence in the cascade passage allow for greater suppression of the separation bubble, it also has computationally produced results nearly the same as the experimental data. On the leading edge up to the suction peak and towards the trailing edge of the airfoil, this Re=50,000, HFSTI case actually models the experimental Re=50,000 case with a wake passing frequency of F=0.548 better than does the results for the CFD model of this case shown in the previous section. This shows that the mean effect of the wake in these

regions is to drive down these predicted magnitudes, since the Re=50,000, HFSTI case with F=0.548 had less of a wake presence and over-predicted the magnitudes on these surfaces.

In Figure 34 there is a better indication of the severity of the separation that occurs on the suction surface and where reattachment takes place. Due to the reduction in the separation bubble to nearly no separation at all, the amount of total pressure loss seen in Figure 33 is reduced by about 60 percent from the experimental data loss of .7Ψ. It is seen from the mean C_f plot that the same characteristics of an inflection in the C_f curve occurs where the Cp plot tends to level out some. The C_f values then decrease until it does finally hit zero, indicating that separation is still present on the suction surface of this blade, even if the plateau of a suction bubble is not very well defined. The following transition and reattachment happen shortly after the C_f zero point, which along with the contours of C_f, indicate that the separation is more a local event over the surface and not a long separation bubble.

In analyzing the instantaneous plots, Figure 35-1 shows a wake approaching the passage as another is just making its way past the suction peak. The Cp magnitude at the suction peak had been suppressed by the wake and is already starting to reform even though the previous suction bubble is not even half way down the aft side of the suction surface. The wake has rolled up and compressed this bubble to form the three Cp peaks expected, and the C_f shows high levels of turbulence in this region as well. Trailing behind this turbulent peak is the calmed region, which remains attached to the surface even though it has a minimal C_f.

By Figure 3, or 50 percent of a cycle, even though the overall amount of time that has passed is much less than in the F=0.548 case, the suction peak has reformed and the previous suction bubble has been completely rolled off the suction surface. This results in the calmed region detaching from the surface, even though a high level of turbulence still exists on the aft portion of the airfoil. Looking at the C_f contours it can be seen that these points of separation do not span the entire width of the blade, forming a very defined zero band that is present in a long separation bubble. This fact along with the fact that the Cp plot doesn't show the presence of a plateau indicates that these separation bubbles are very short and local bubbles over the surface. However by Figure 4, the zero band is more defined across the width, and even though the wake has begun to collapse upon the suction peak, the same form of a separation bubble being sheared downstream is present.

Therefore, even though the wake passing frequency was increased and the mean Cp plot barely indicates a separation of flow over the suction surface, it is clear that as a wake passes over the aft portion of the airfoil and rolls the suction bubble off the surface, the flow does start to experience small separated zones which eventual form into a separation bubble before the arrival of the next wake.
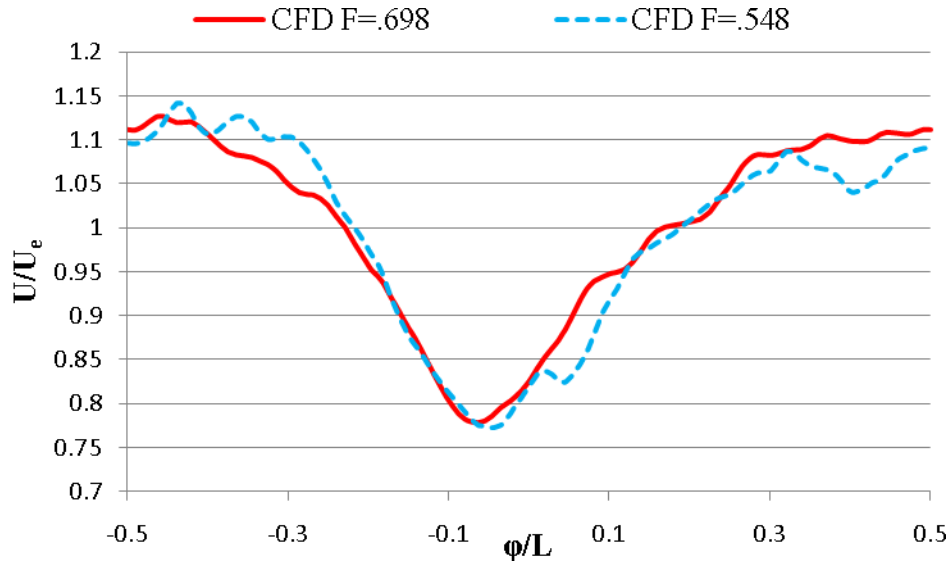
Fig. 31 Rod Wake Velocity Magnitude for Re=50,000, HFSTI: Comparison of LES, F=0.548 to LES, F=0.698.
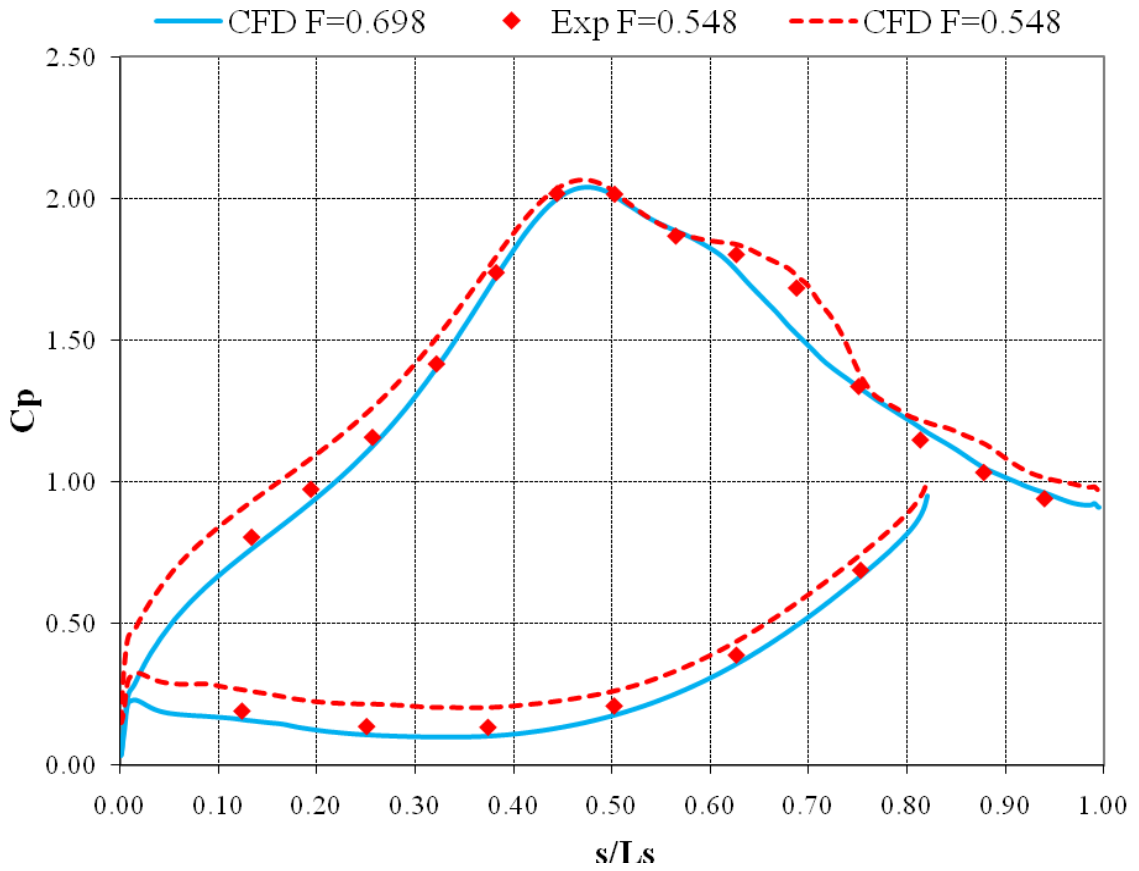
Fig. 32 C_p profiles for Re=50,000, HFSTI: Comparison between LES, F=0.548 to LES, F=0.698.
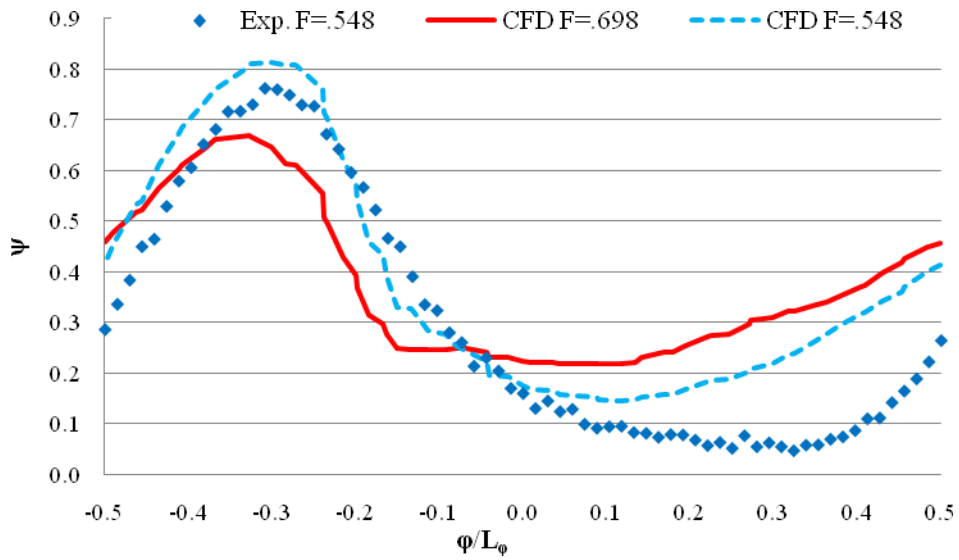
Fig. 33 Total Pressure Loss Coefficient for Re=50,000, HFSTI: Comparison between LES, F=0.548 to LES, F=0.698.
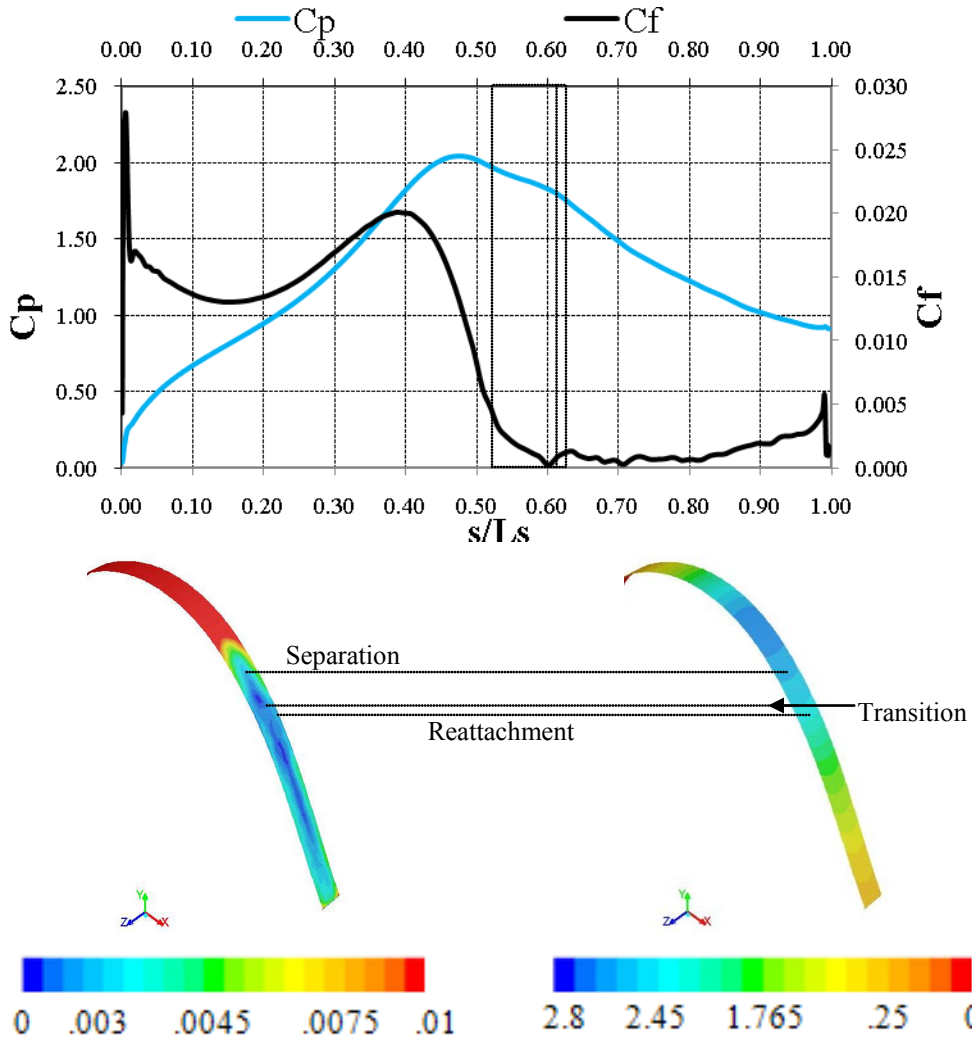
Fig. 34 Comparison of Mean C_p and C_f on suction surface for Re=50,000, HFSTI, F=0.698: a) Contours of mean C_f b) Contours of mean C_p.
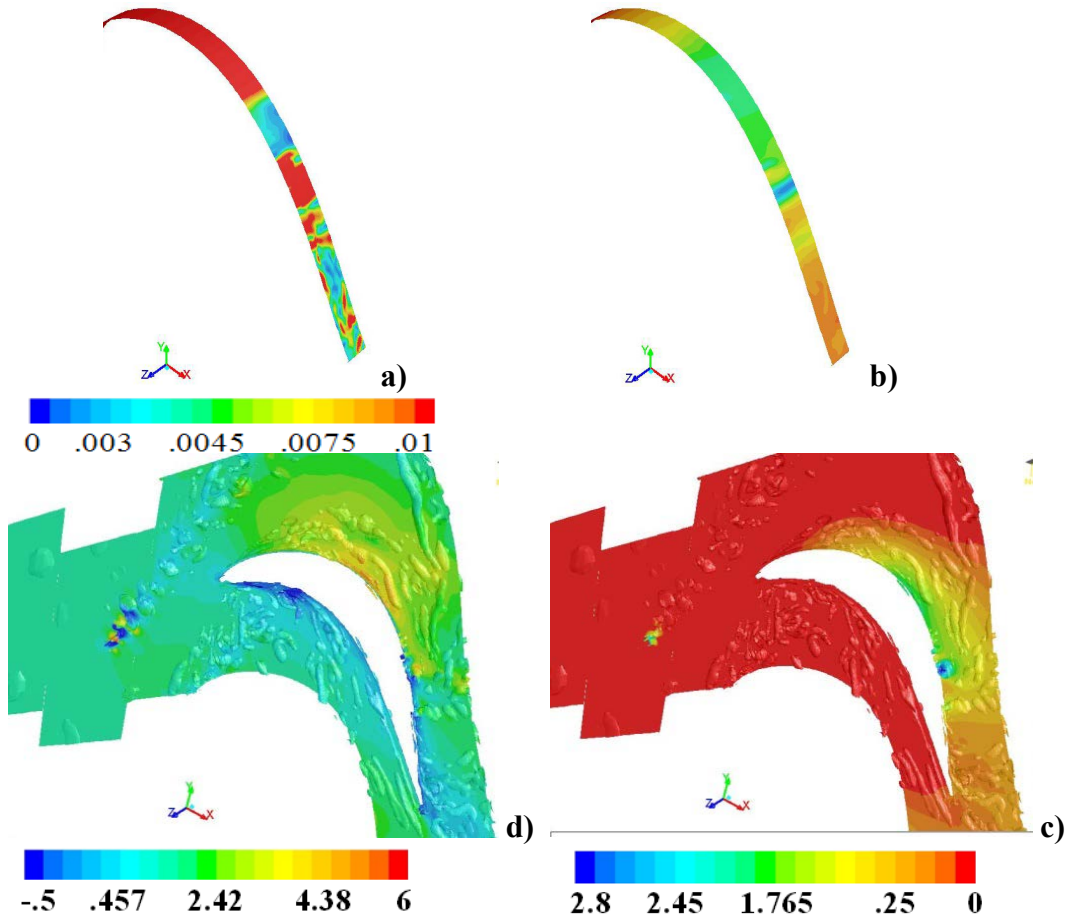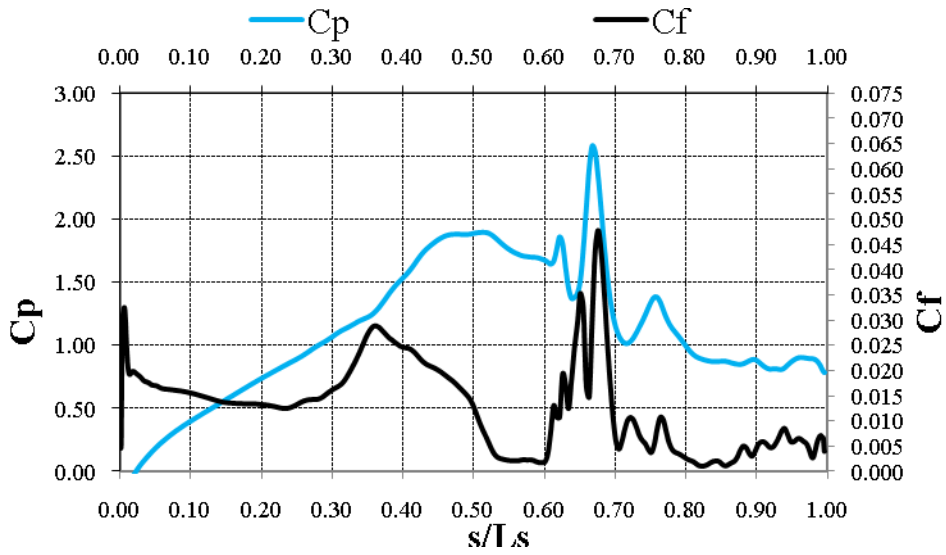
Fig. 35-1 Comparison of Instantaneous C$_p$ and C$_f$ on suction surface for Re=50,000, HFSTI, F=0.698: a) Contours of mean C$_f$ b) Contours of mean C$_p$ c)Q-criterion, Cp Contours d)Q-criterion, x-velocity Contours
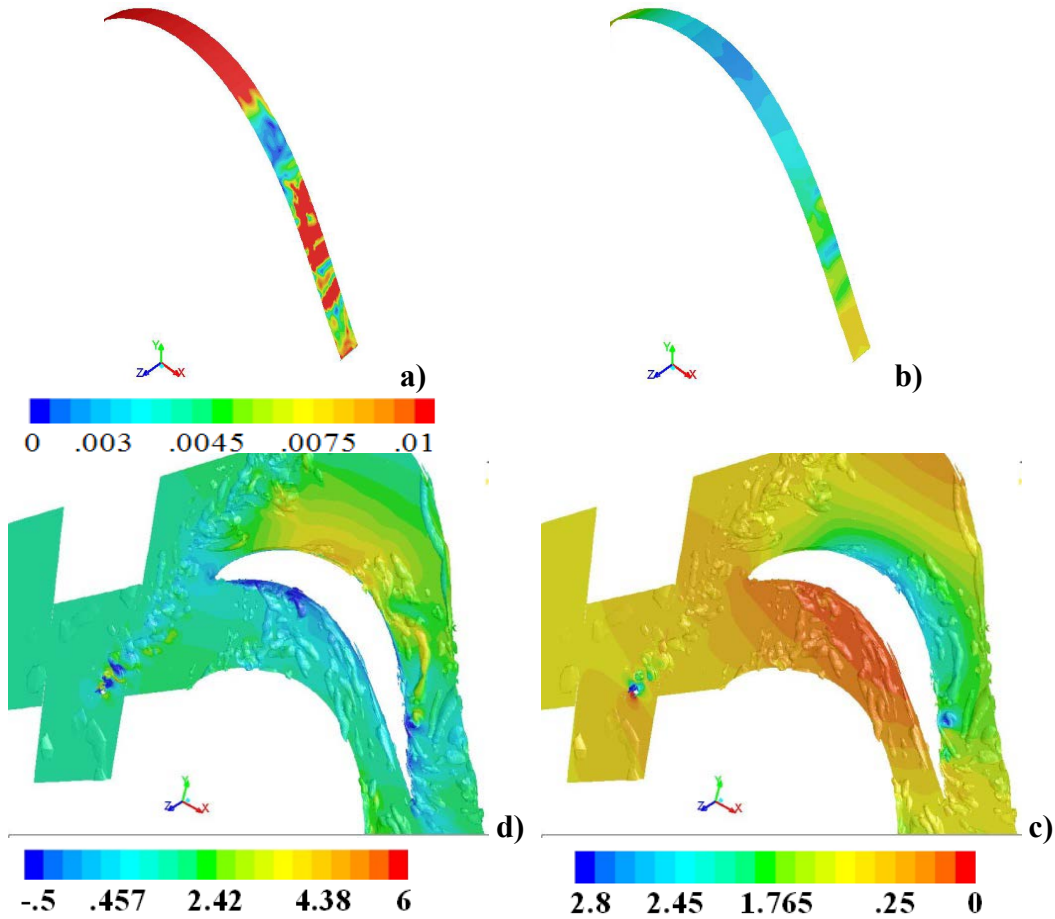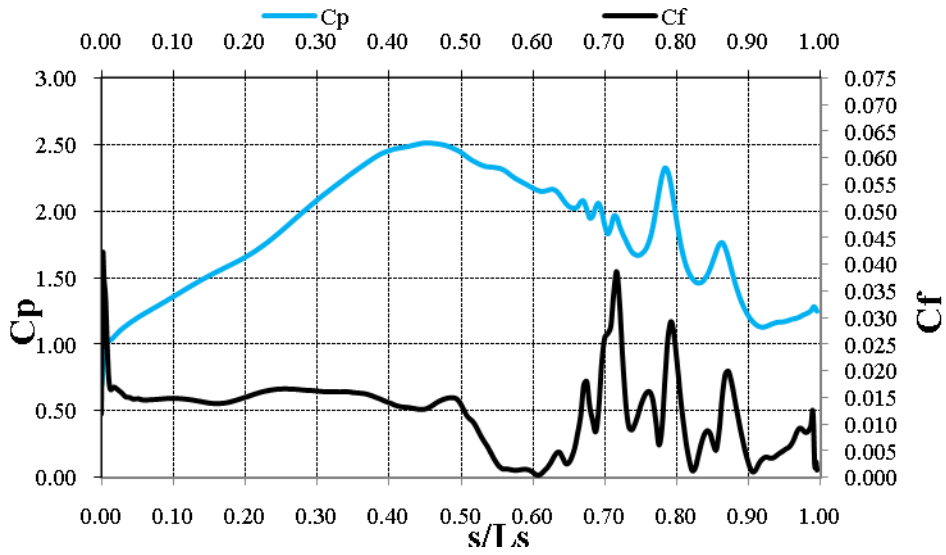
Fig. 35-2 Comparison of Instantaneous C_p and C_f on suction surface for Re=50,000, HFSTI, F=0.698: a) Contours of mean C_f b) Contours of mean C_p c)Q-criterion, Cp Contours d)Q-criterion, x-velocity Contours
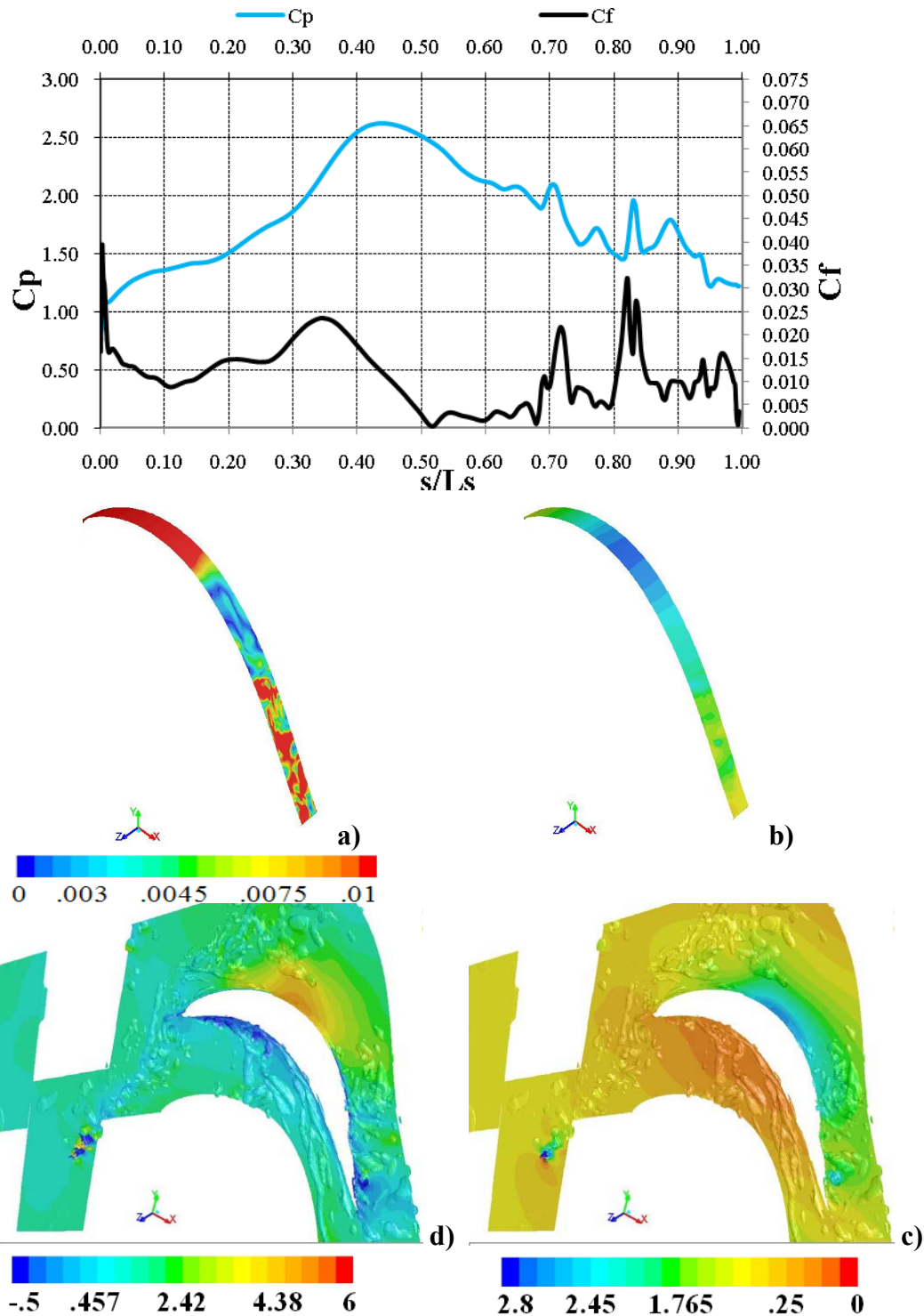
Fig. 35-3 Comparison of Instantaneous C_p and C_f on suction surface for Re=50,000, HFSTI, F=0.698: a) Contours of mean C_f b) Contours of mean C_p c)Q-criterion, Cp Contours d)Q-criterion, x-velocity Contours
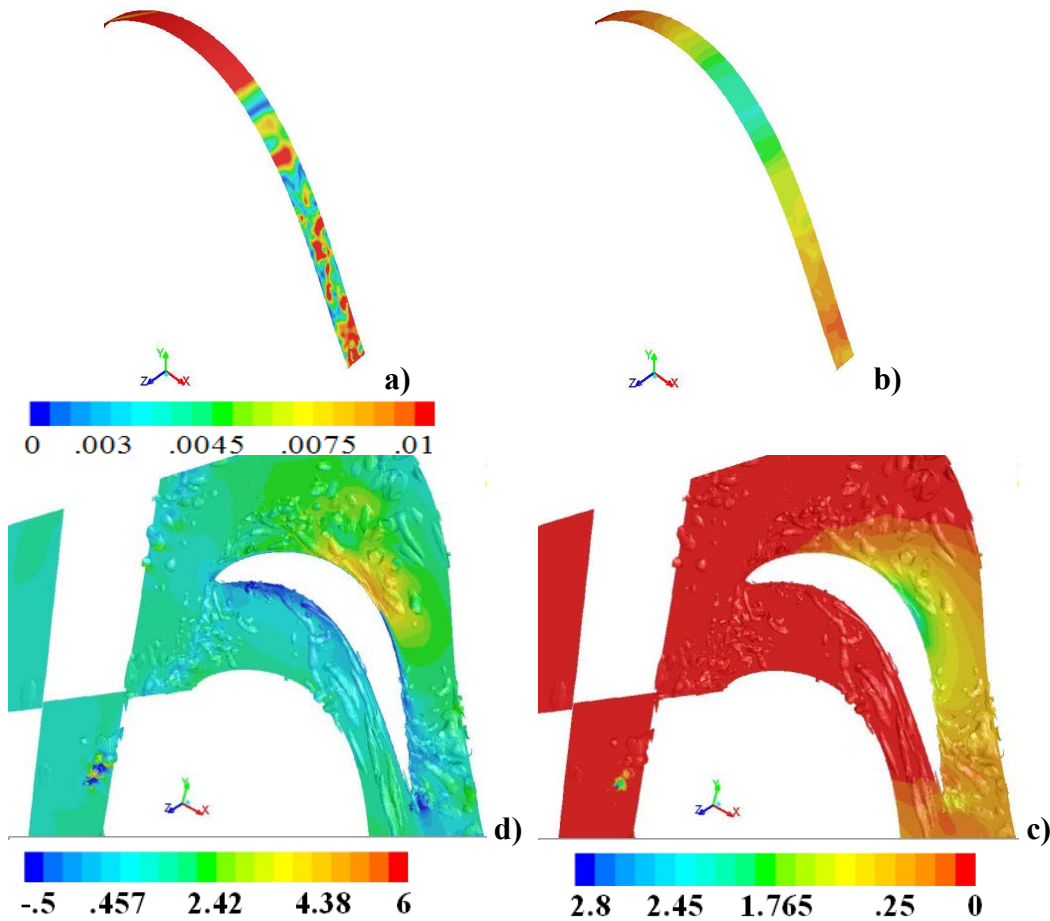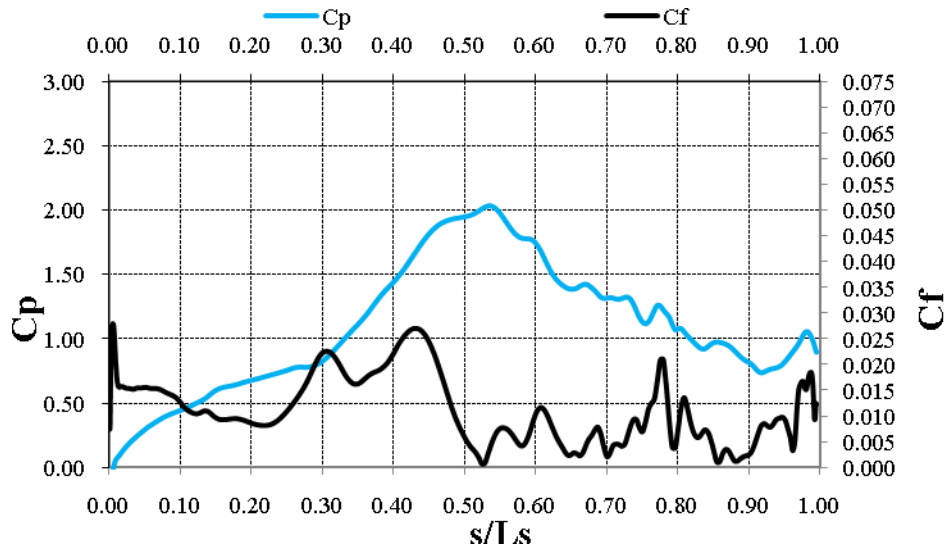
Fig. 35-4 Comparison of Instantaneous C_p and C_f on suction surface for Re=50,000, HFSTI, F=0.698: a) Contours of mean C_f b) Contours of mean C_p c)Q-criterion, Cp Contours d)Q-criterion, x-velocity Contours
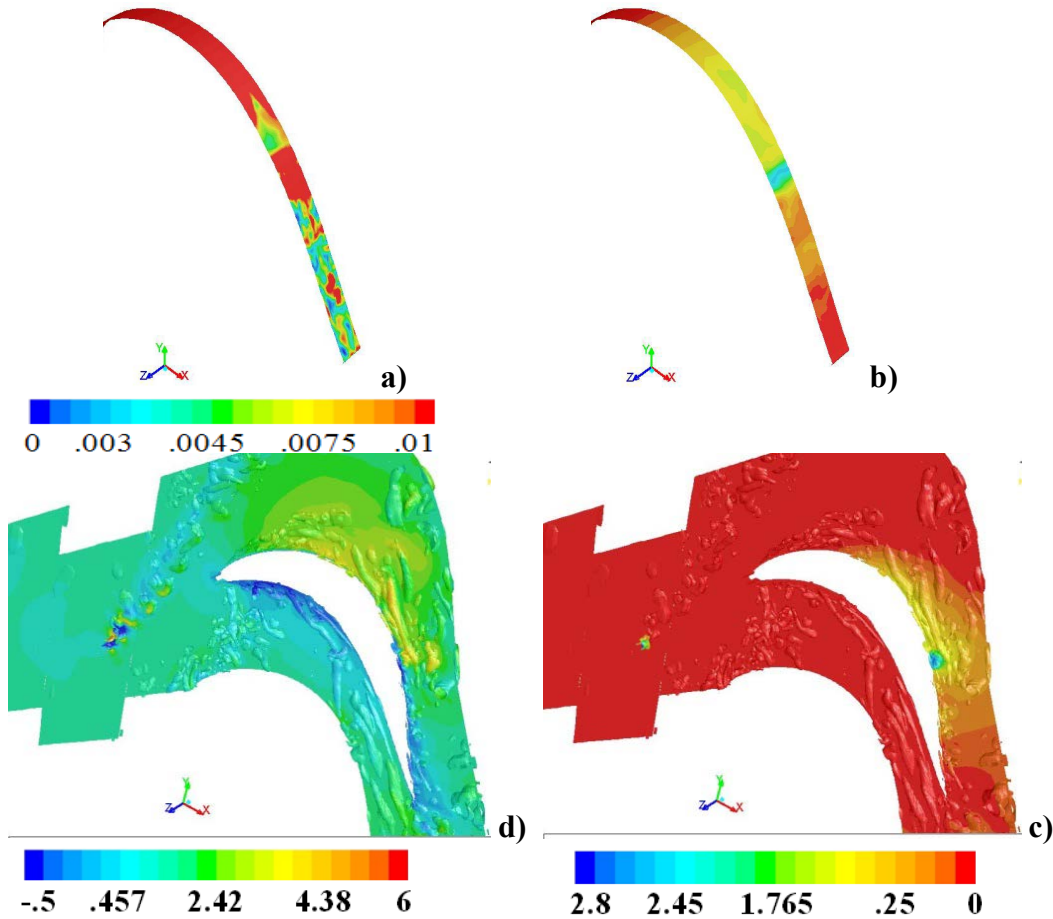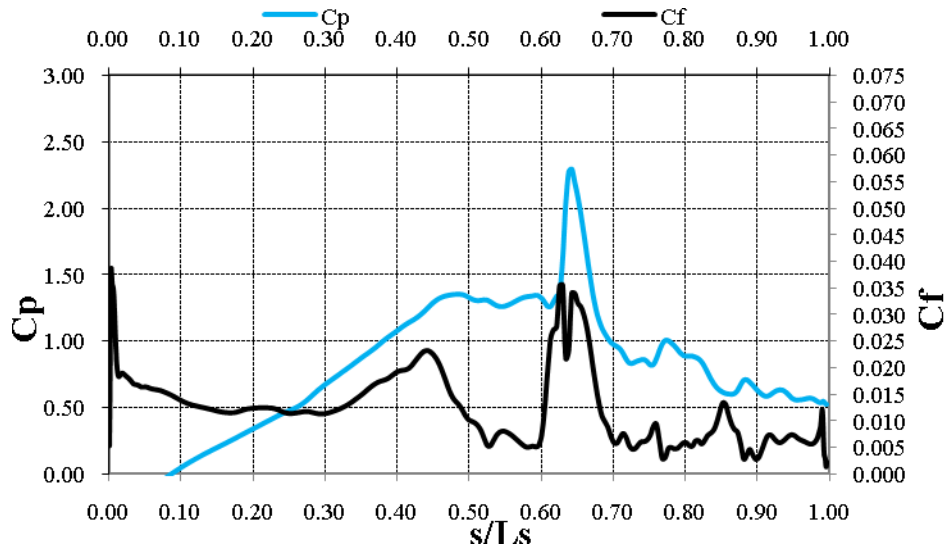
Fig. 35-5 Comparison of Instantaneous C_p and C_f on suction surface for Re=50,000, HFSTI, F=0.698: a) Contours of mean C_f b) Contours of mean C_p c)Q-criterion, Cp Contours d)Q-criterion, x-velocity Contours

Re50,000, HFSTI

F=0.917

The final case run was to increase the rod speed about another 33% percent on top of the wake passing frequency of F=0.689. The results did not show much of a variation as one can see in Figure 37b. The rod wake velocity profile took the same shape that had been seen in the previous cases, and has nearly the same width and magnitude as the rod passing frequency of F=0.698. This identical profile gives a good explanation of why the rest of the data between these two cases is also very similar.

In Figure 37a, the mean Cp profiles seem to match the experimental data for F=0.548 at the suction peak and after reattachment, however this case does not match the leading edge or pressure side quite as well as the F=0.689 case. The differences between all three of these cases can be seen clearly in Figure 37b. Here, it is evident that increasing the rod passing frequency from F=0.548 to F=0.689 played a significant role in reducing the separation bubble, however a further increase in rod speed only created the slightest of difference between F=0.689 and F=0.917. Again, this similar Cp profile lead to a similar prediction in the reduction of the total pressure loss coefficient seen in Figure 38.

The biggest discrepancy between the F=0.689 case and the F=0.917 case comes in the mean C_f plot. In the F=0.689 plot, once the C_f hit a zero point it had a noticeable increase, with an associated "reattachment peak" downstream after. However here in the F=0.917 case, the C_f value hits zero and then stays right near zero for the majority of the downstream portion of the surface. This makes trying to find a transition zone out of the separated point near impossible to dictate, and like in the F=0.689 case, since the Cp plot

only shows the slightest inflection towards a plateau and then again towards a reattachment, says that these separated zones must be very small and local. This is also indicated by the C_f contour plots.

In looking through the instantaneous plots, this constant near zero C_f value over the aft portion of the suction surface becomes evident. From Figure 40-1, one can see a wake on the forward portion of the airfoil as the previous wake is just making it off the trailing edged. The suction peak is well defined as is the proceeding C_f peak. However, downstream of the peak there is a large area where the C_f values stay near and hit zero. These areas do not form a well defined band across the width of the blade which is evident when a full separation bubble is present, thus these areas of zero C_f are much more local instances.

In Figure 40-2, one can once again see a rolled up suction bubble being compressed and moved down the suction surface. The associated turbulent peak and calmed region are also evident. It is in this calmed region over the suction peak and in the turbulent peak that the C_f values ever really get much above the zero line. Again, Figure 40-3 shows that as the suction bubble separates from the suction surface, the calmed region starts to have points that show detachment from the surface. Right before another wake reaches the suction peak, the most prominent zero C_f band across the suction surface can been seen in Figure 40-4. This band is also accompanied by a slight inflection towards a plateau in the Cp plot, thus indicating a slightly large separated region. Right before another wake approaches the peak in Figure 40-6, this is also evident with an even stronger presence of a plateau and a large region of C_f values at or near

zero. This shows that a separation bubble still does have a chance to form even at these high wake passing frequencies.

In these higher wake passing frequency cases, one thing that is noticeable is that with a strong formation of a suction peak bubble, the wake seems to make its way up the suction surface much more as compared to having the wake in the free stream collapse down on the suction peak. This could be a reason why further increasing the rod speed did not show much difference in the results. Nevertheless, these increased rod speeds did suppress a bubble growth for the majority of a wake cycle, with only a small fraction of time where separation seemed present right as another wake arrived at the suction peak.
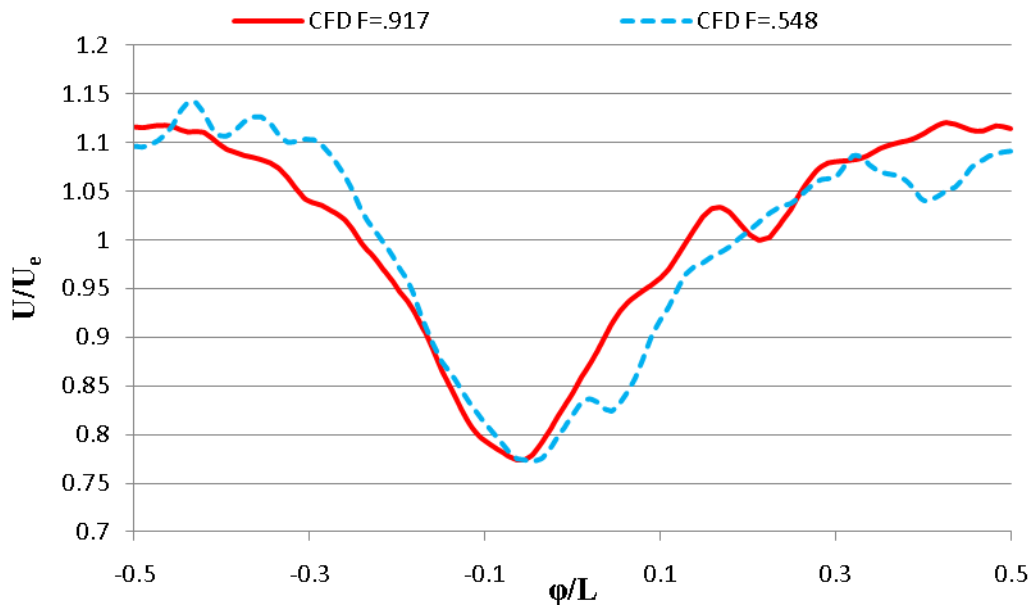
Fig 36 Rod Wake Velocity Magnitude for Re=50,000, HFSTI: Comparison of LES, F=0.548 to LES, F=0.917.
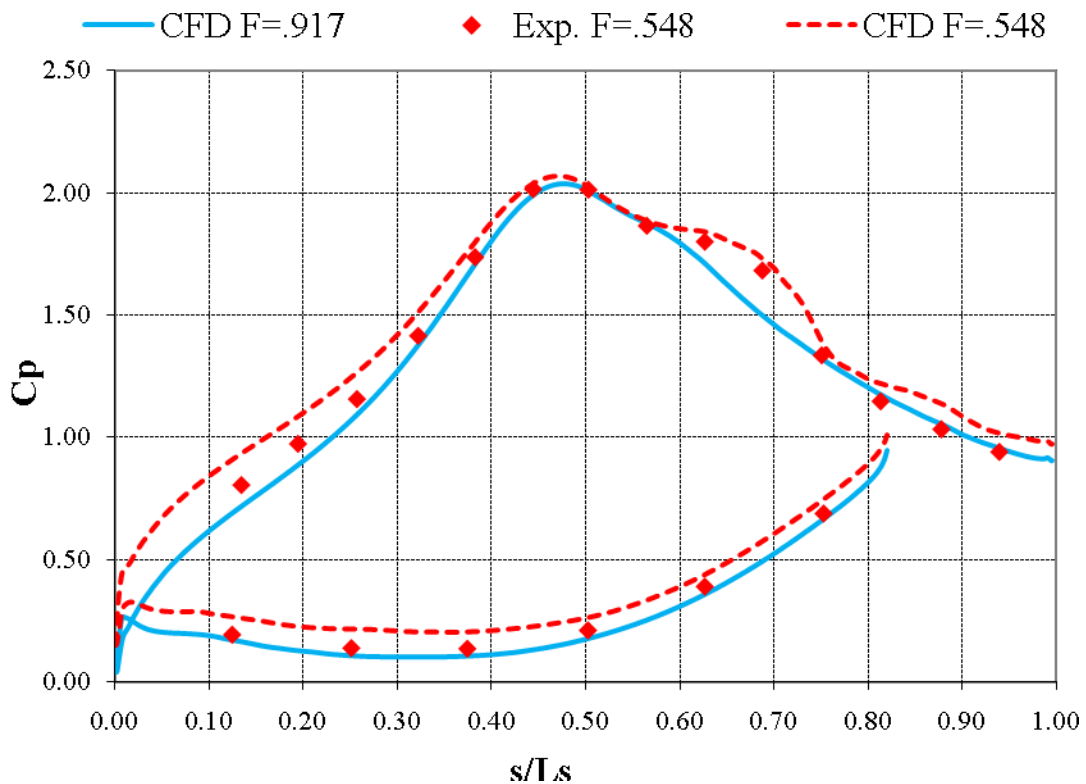
Fig. 37a C_p profiles for Re=50,000, HFSTI: Comparison between Experimental and LES, F=0.548 to LES, F=0.917.
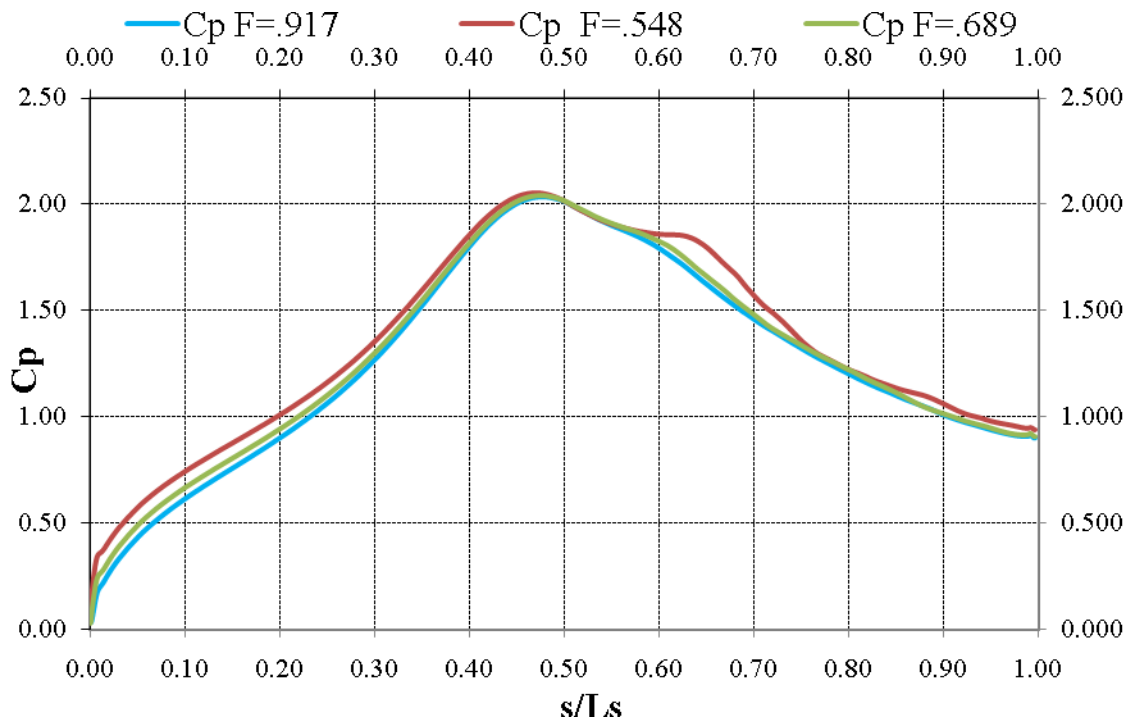
Fig. 37b C_p profiles for Re=50,000, HFSTI: Comparison between LES, F=0.548, F=0.689 and F=0.917.
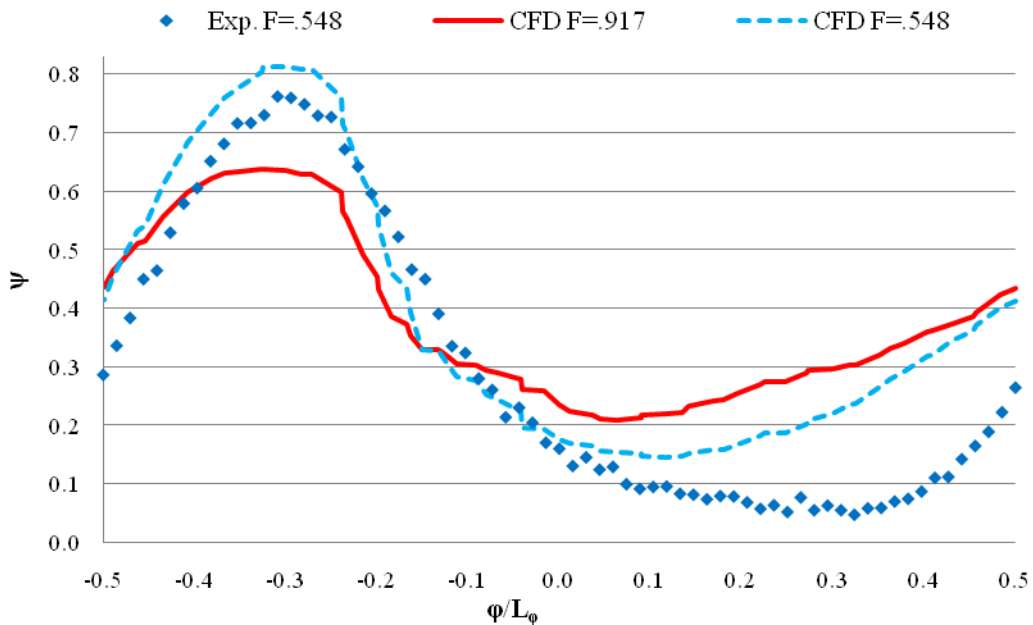
Fig. 38 Total Pressure Loss Coefficient for Re=50,000, HFSTI: Comparison between LES, F=0.548 to LES, F=0.917.
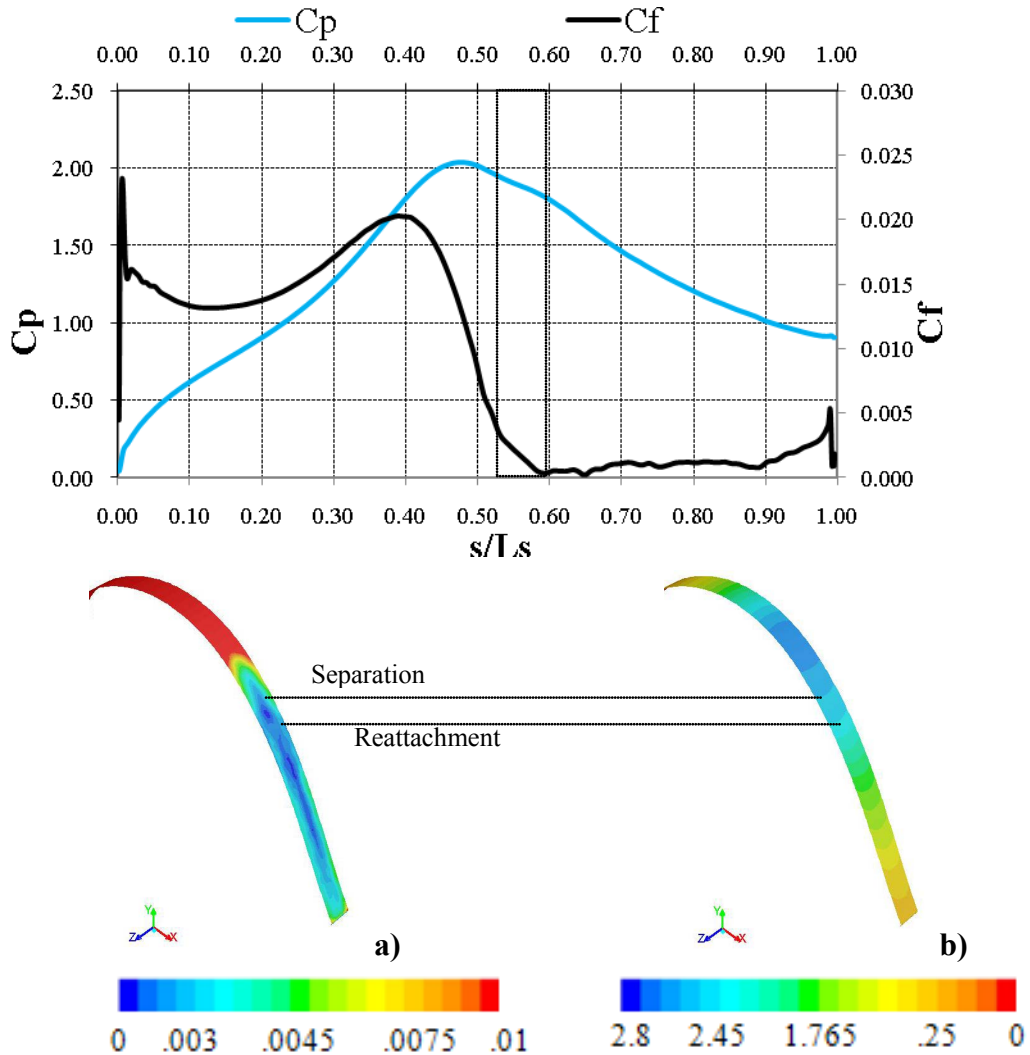
Fig. 39 Comparison of Mean C_p and C_f on suction surface for Re=50,000, HFSTI, F=0.917: a) Contours of mean C_f b) Contours of mean C_p.
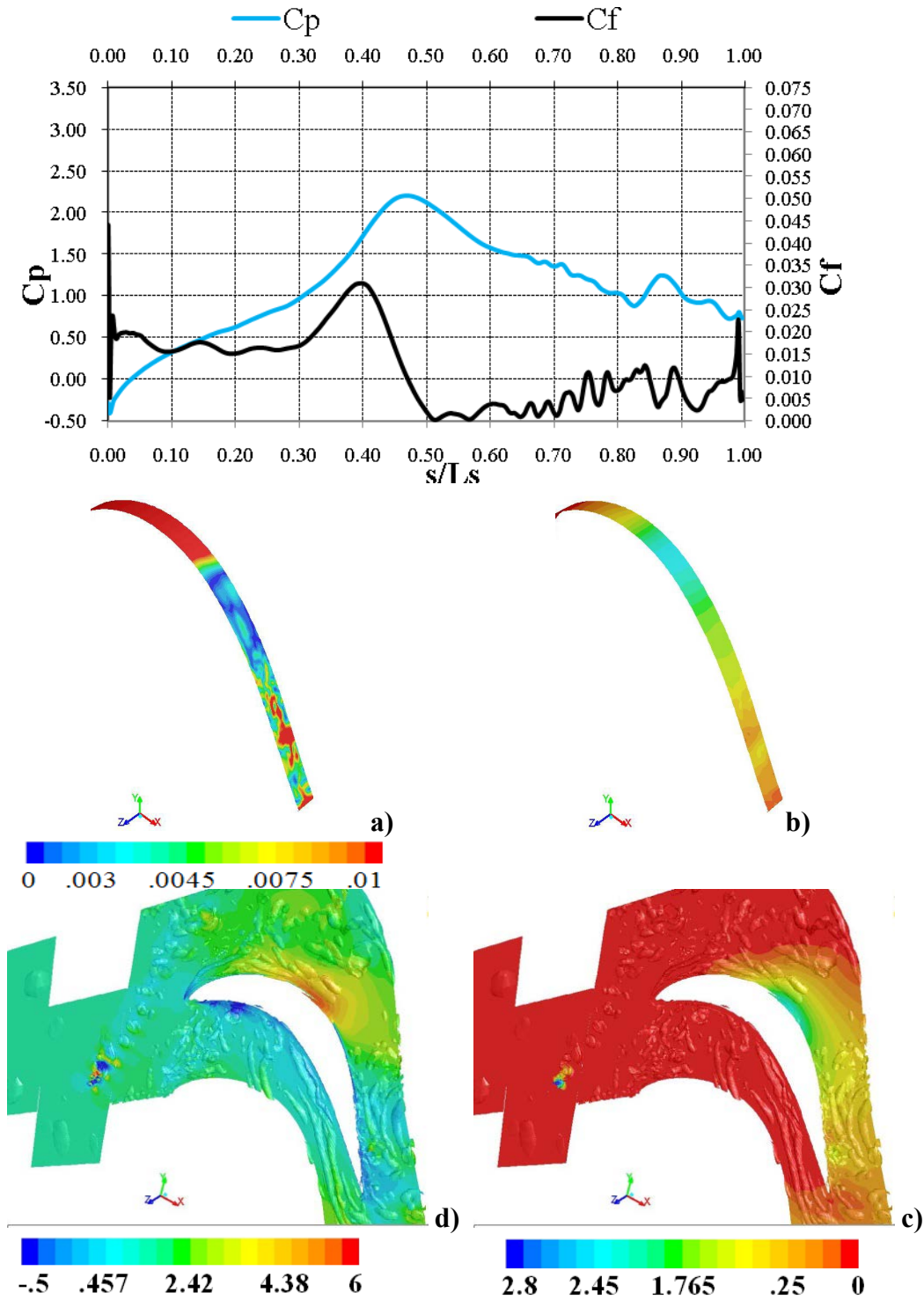
Fig. 40-1 Comparison of Instantaneous C_p and C_f on suction surface for Re=50,000, HFSTI, F=0.917: a) Contours of mean C_f b) Contours of mean C_p c)Q-criterion, Cp Contours d)Q-criterion, x-velocity Contours
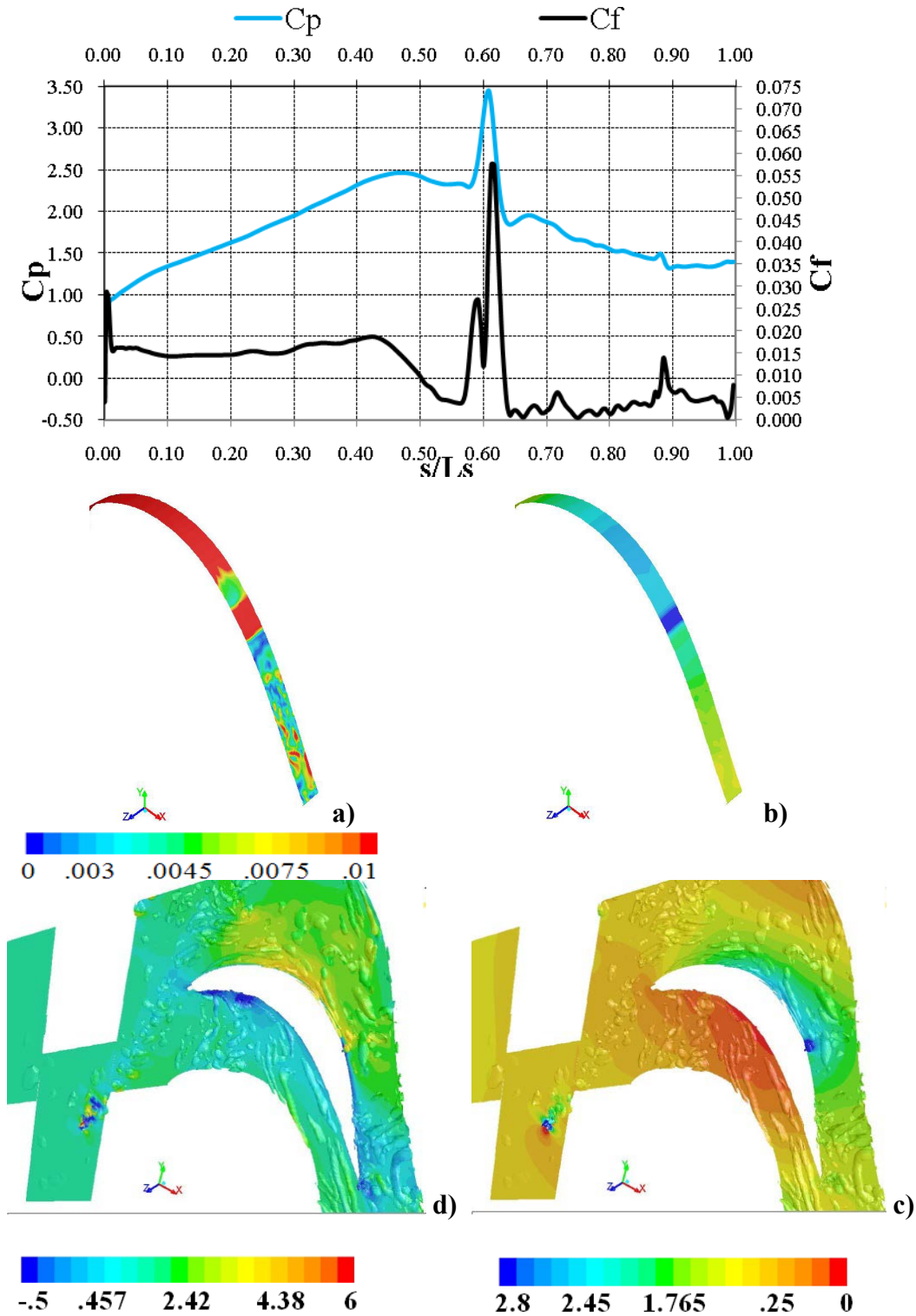
Fig. 40-2 Comparison of Instantaneous C_p and C_f on suction surface for Re=50,000, HFSTI, F=0.917: a) Contours of mean C_f b) Contours of mean C_p c)Q-criterion, Cp Contours d)Q-criterion, x-velocity Contours
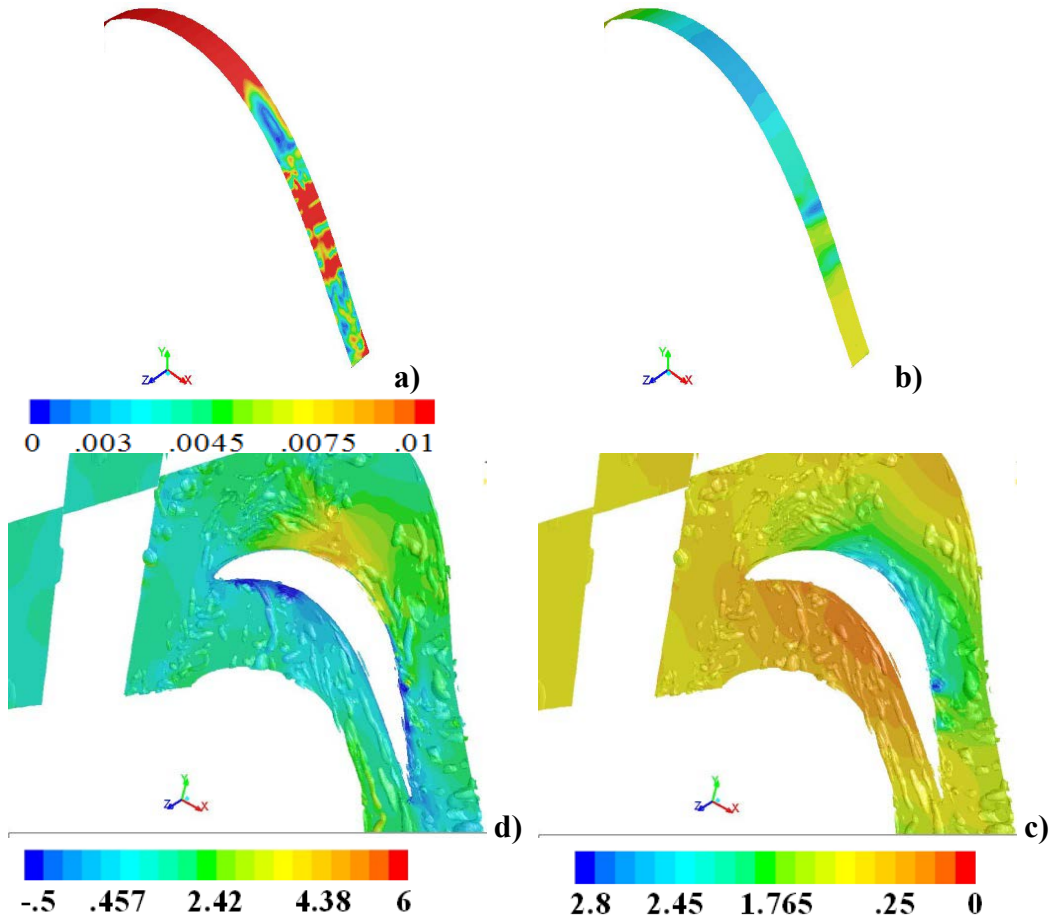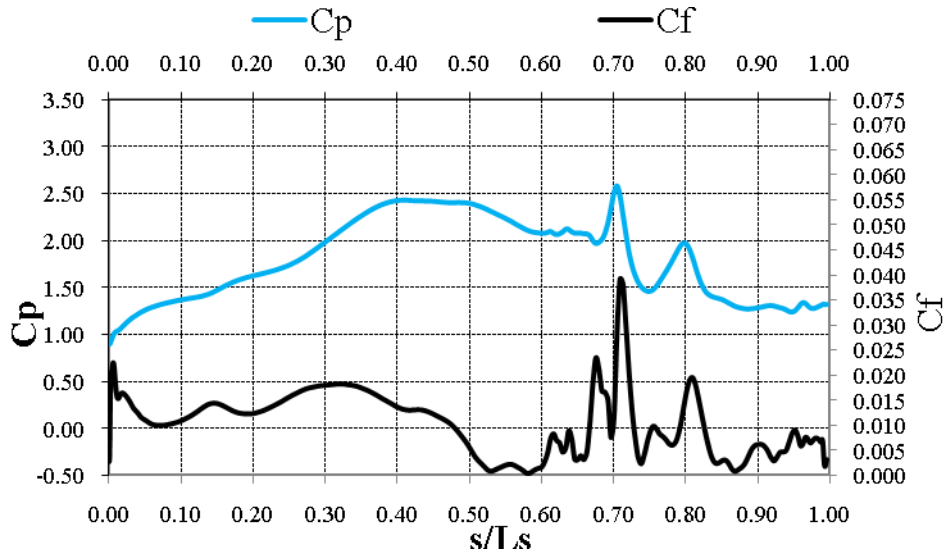
Fig. 40-3 Comparison of Instantaneous C_p and C_f on suction surface for Re=50,000, HFSTI, F=0.917: a) Contours of mean C_f b) Contours of mean C_p c)Q-criterion, Cp Contours d)Q-criterion, x-velocity Contours
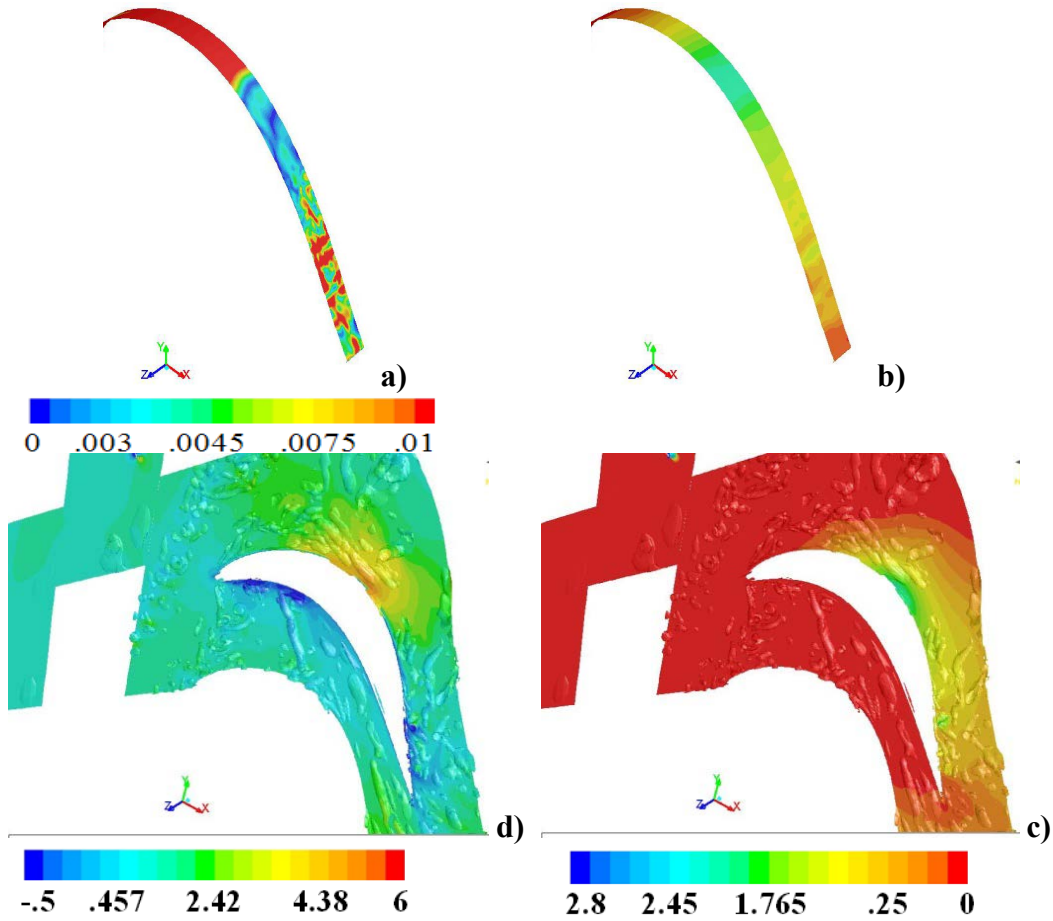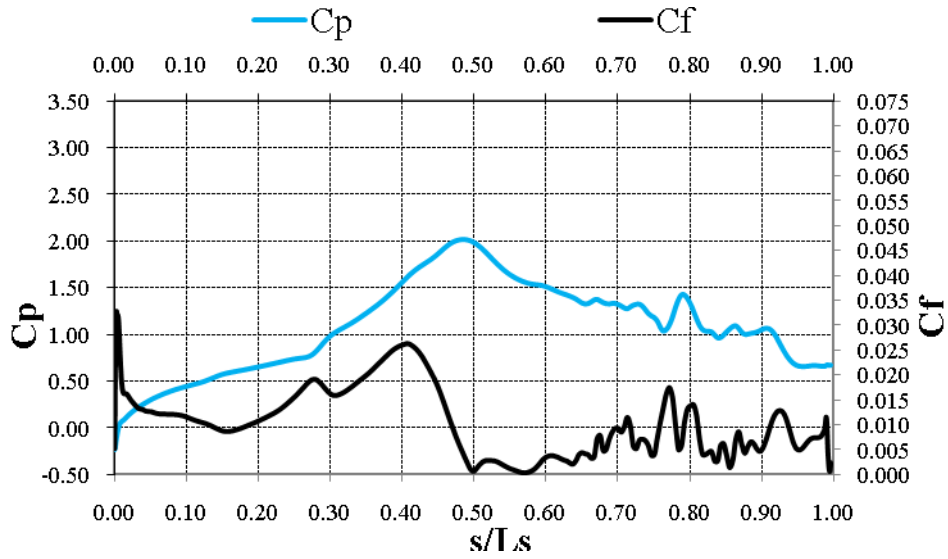
Fig. 40-4 Comparison of Instantaneous C_p and C_f on suction surface for Re=50,000, HFSTI, F=0.917: a) Contours of mean C_f b) Contours of mean C_p c)Q-criterion, Cp Contours d)Q-criterion, x-velocity Contours
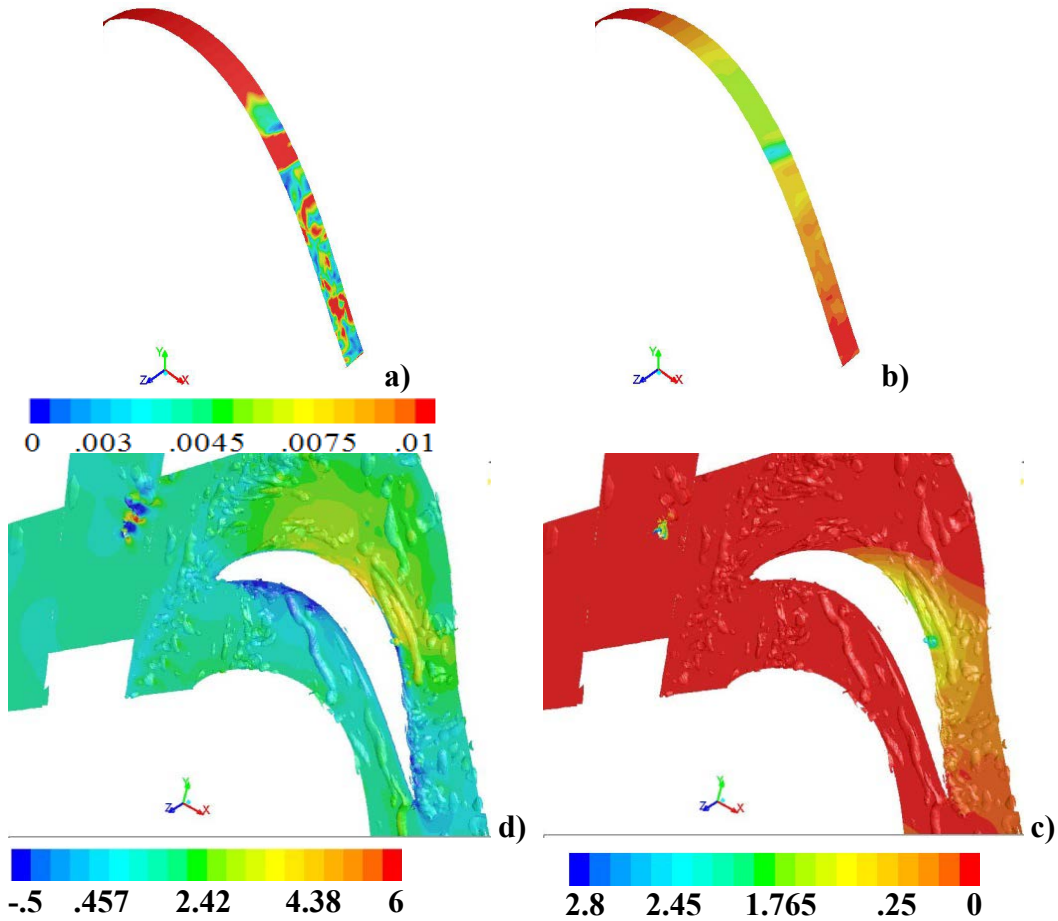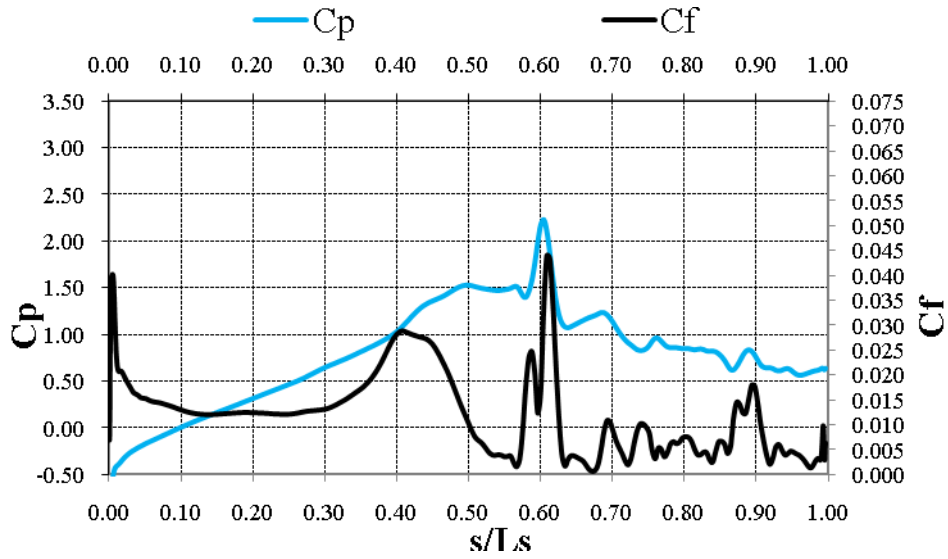
Fig. 40-5 Comparison of Instantaneous C_p and C_f on suction surface for Re=50,000, HFSTI, F=0.917: a) Contours of mean C_f b) Contours of mean C_p c)Q-criterion, Cp Contours d)Q-criterion, x-velocity Contours
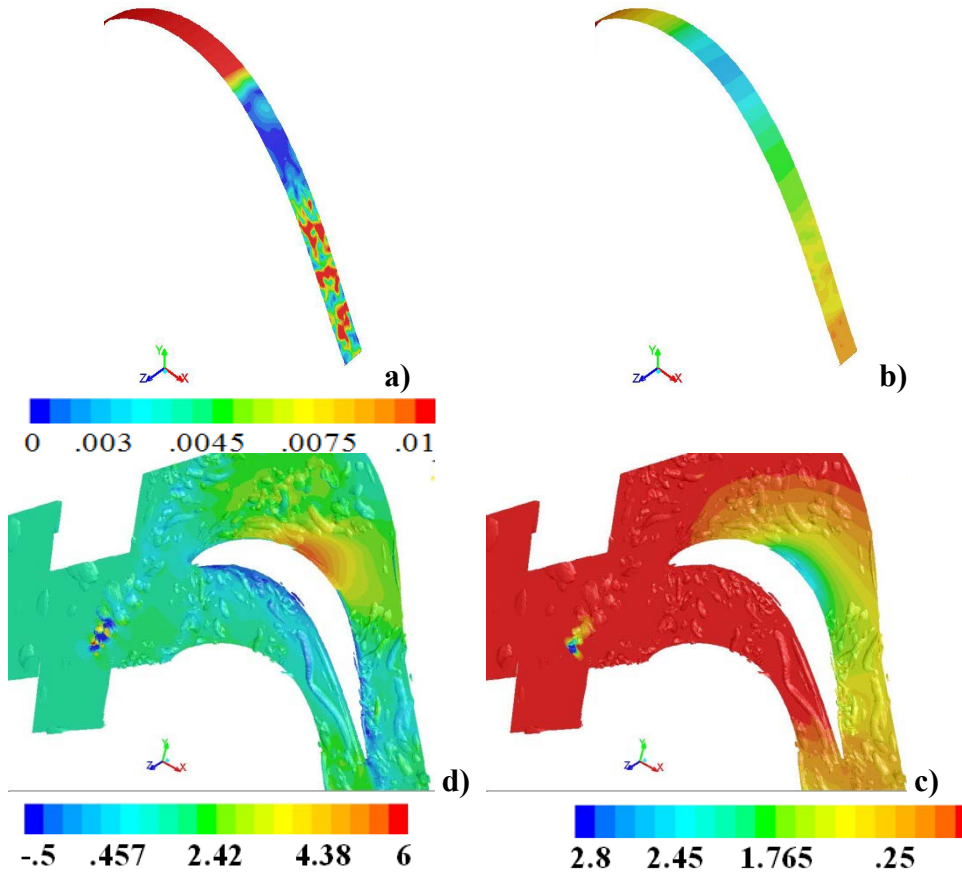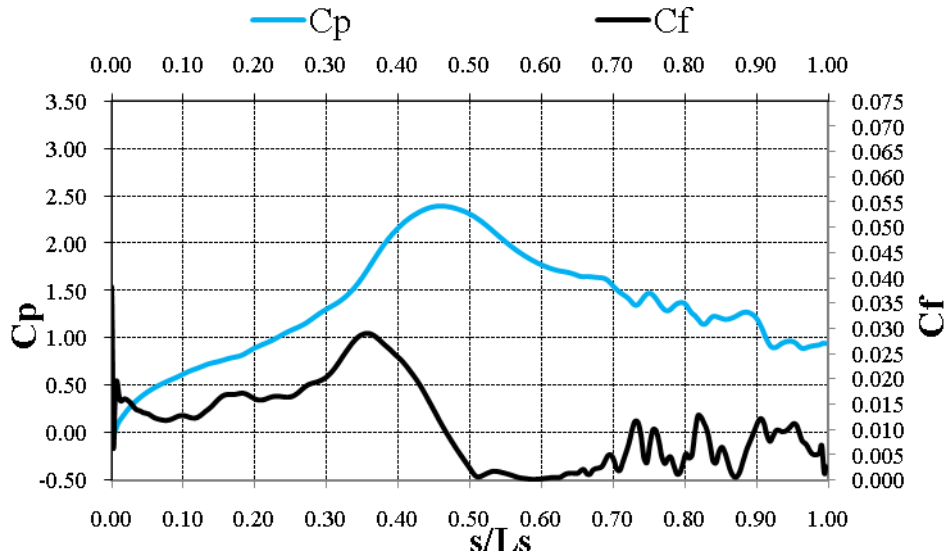
Fig. 40-6
Comparison of Instantaneous C_p and C_f on suction surface for Re=50,000, HFSTI, F=0.917: a) Contours of mean C_f b) Contours of mean C_p c)Q-criterion, Cp Contours d)Q-criterion, x-velocity Contours

Conclusion

In simulating a wake/blade interaction in the same computational domain, the first challenge was to create a mesh that was fine enough to capture the wake vortex shedding off of a wake generating rod and propagate it downstream to the airfoil. Once this geometry was established in 2D, it was then projected in the z-direction to create the 3D domain.

Overall the 2D URANS results showed the proper trend of interaction between the wake and the suction surface of the airfoil with the mean coefficient of pressure profiles (Cp) indicating a reattachment after separation. These trends were only marginally accurate in comparison to the experimental data for both Re=25,000 and Re=50,000 cases since the predicted magnitude of the Cp profile and the location of reattachment were not very consistent with the experimental data. This was mainly attributed to the lack of ability to take into account the three dimensionality of a wake structure and its subsequent interaction with the boundary layer. Thus the mesh was then projected into a 3D domain and the same URANS (Trans-SST) model was run at the same time step as in the 2D cases. These 3D URANS cases were unable to capture any wake vortex shedding off of the rod, which had been seen in cases run by Ladreau [2005]. It was determined that in order to capture the wake, the time step size would have to be reduced to levels associated with a LES turbulence, thus the remainder of the cases were run using LES since the computational cost savings of using a URANS model with a larger time step were diminished.

In the Re=25,000, 3D cases the results showed better matching in the predicted magnitude of the mean Cp profile over the suction surface, however the predicted

magnitude of the separation bubble and its location of reattachment still lacked in consistency with the experimental data. Switching from a low freestream turbulence intensity model (LFSTI) to a high (HFSTI), showed marginal improvements, however overall the results were still consistently inaccurate. This lack of ability to properly predict turbulent flow in low Reynolds' number flow has been noted in the past, thus the remainder of the cases were run at Re=50,000.

These Re=50,000 cases showed excellent consistency in both magnitude and predicted location of separation and reattachment in the mean C_p profiles. The predicted total pressure loss still varied slightly from the experimental data, however this was to be expected to the fact the computational domain is set up as a repeating periodic domain, thus not taking into account the effects of the endwalls and tailboard of the actual experimental domain. Due to the exceptional prediction in mean results, the instantaneous profiles of C_p and C_f were examined to see the affect the wake has over the suction surface as it passes through the cascade passage.

These instantaneous results showed that as a wake reaches the suction peak of the suction surface, it collapses down, compressing the peak C_p value of the suction bubble, eventually rolling it up into three defined peaks. These peaks first experience a shear, stretching effect and eventually beginning to roll down the aft side of the suction surface, remaining attached to the surface and being further compressed and increasing in C_p magnitude. The correlating effect on the C_f values over these events show that as the suction bubble in broken down and compressed, the three defined suction peaks are associated with defined peaks in the C_f values, thus showing a high amount of turbulence in this region. Trailing behind this turbulent peak is the predicted calmed region

described by Hodson and Howell [2005]. This calmed region remains near zero in C_f value, but shows resistance to separation as long as the suction bubble being remains attached to the surface. As this bubble is eventually rolled off of the surface, the calmed regions shows an immediate location of separation with a zero C_f value. This spotted separation grows and eventually spans across the width of the suction surface as the Cp values start to show a defined separation bubble, indicated by a "plateau" in the Cp profile. Also indicated by the C_f profile is that where separation is indicated to start, an inflection in the decreasing C_f values is also indicated, leveling out the curve as it approaches, hits, and recovers from a zero C_f value. As it starts to increase out of this zero value, another inflection incurs in the curve slightly before reattachment is indicated on the Cp values. This inflection shows a start of a sharp increase in C_f and indicates the start of transition in the boundary layer. Reattachment occurs just before another peak in the C_f values, which then shows turbulence in the flow as it stays attached to the trailing edge.

Finally, Re=50,000 cases were simulated with an increase in the rod speed and thus increasing the wake passing frequency to see what additional affect this would have on the suction surface. Initially about a 25% increase in rod speed significantly reduced the separation bubble to near nonexistent in the mean Cp values, however a slight indication of one still was present. Increase the rod speed an additional 25% on top of this showed little effect. These results showed that even with an increase in the wake passing frequency and an increase in turbulence in the cascade passage, any amount of time in between wakes was enough for the suction peak to re-grow to its peak magnitude, and some separation to occur.

Bibliography

ANSYS Fluent Documentation, 2009

Bons, J.P., Pluim, J., Gompertz, K. and Bloxham, M., 2008, "The Application of Flow Control to an Aft-Loaded Low Pressure Turbine Cascade with Unsteady Wakes", *ASME Paper GT2008-50864*.

Clark J.P., 2007

Hodson, H.P., and Howell, R.J., 2005, "Bladerow Interactions, Transition, and High-Lift Aerofoils in Low-Pressure Turbine," Annual Review of Fluid Mechanics, **37**, pp. 71-98.

Ibrahim, M.B., Kartuzova, O. and Volino, R.J., 2008, "Experimental and Computational Investigations of Separation and Transition on a Highly Loaded Low Pressure Turbine Airfoil: Part 1 – Low Freestream Turbulence Intensity", *ASME Paper IMECE2008-68879*.

Ibrahim, M.B., Kartuzova, O., Doucet, D.J. and Volino, R.J., 2010, "Les Flow Control Simulations For Highly Loaded Low Pressure Turbine Airfoil (L1a) Using Pulsed Vortex Generator Jets"**,** *ASME Paper GT2010-23015*.

Kaszeta, R. W., Simon, T. W., and Ashpis, D. E., 2001, "Experimental Investigation of Transition to Turbulence as Affected by Passing Wakes," Proceedings of ASME Turbo Expo 2001, ASME, New York, ASME Paper No. 2001-GT-0195.

Kaszeta, R. W., and Simon, T. W., 2002, "Experimental Investigation of Transition to Turbulence as Affected by Passing Wakes," NASA Contractor Report, NASA-CR-2002-212104, Cleveland.

Kartuzova, O.V., 2010, "A computational study for the utilization of jet pulsations in gas turbine film cooling and flow control," Ph.D. thesis, Cleveland State University, Cleveland, OH.

Kim S.E., 2004, "Large eddy simulation using unstructured meshes and dynamic subgridscale turbulence models." *Technical Report AIAA-2004-2548, American Institute of Aeronautics and Astronautics*, 34th Fluid Dynamics Conference and Exhibit.

Kim, W.W. and Menon, S.,1997, "Application of the localized dynamic subgrid-scale model to turbulent wall-bounded flows." *Technical Report AIAA-97-0210, American Institute of Aeronautics and Astronautics*, 35th Aerospace Sciences Meeting, Reno, NV.

Langtry, R.B., 2006, "A Correlation-Based Transition Model using Local Variables for Unstructured Parallelized CFD codes", Ph.D. Thesis, Stuttgart University.

Ladreau, S., 2005, "Unsteady RANS modeling of wake-blade interaction: computational requirements and limitations." Computers and Fluids 34. 3-21.

Menter, F.R., Langtry, R.B., Likki, S.R., Suzen, Y.B., Huang, P.G., and Völker, S., 2006, "A Correlation based Transition Model using Local Variables Part 1- Model Formulation", ASME *Journal of Turbomachinery*, **128**, pp. 413-422.

Pluim, J., Memory, C., Bons, J., and Chen, J.P., "Designing a High Fidelity Wake Simulator for Research Using Linear Cascades," *ASME Paper GT2009-52276*, 2009.

Rodi, W., 2006, "DNS and LES of some Engineering Flows", Fluid Dynamics Research, Vol. 38, pp. 145-173.

Sarkar, S., 2009, "Influent of Wake Structure on Unsteady Flow in a Low Pressure Turbine Blade Passage," *ASME J. Turbomachinery*, 131, October 2009.

Stieger, R. D., 2002, "The Effects of Wakes on Separating Boundary Layers in Low-Pressure Turbines," Ph.D. Dissertation, Cambridge University, Eng. Dept, Cambridge, UK

Stieger, R., Hollis, D. and Hodson, H., 2003, "Unsteady Surface Pressures Due to Wake Induced Transition in Laminar Separation bubble on a LP Turbine Cascade", *ASME Paper No. GT2003-38303.*

Suzen, Y.B. and Huang, P.G., 2005, "Numerical Simulation of Unsteady Wake/Blade Interactions in Low-Pressure Turbine Flows Using and Intermittency Transport Equation", Journal of Turbomachinery, Vol. 127, pp. 431-444.

Volino, R.J., Kartuzova, O. and Ibrahim, M.B., 2008, "Experimental and Computational Investigations of Separation and Transition on a Highly Loaded Low Pressure Turbine Airfoil: Part 2 – High Freestream Turbulence Intensity", *ASME Paper IMECE2008-68776*.

Volino, R.J., 2008, "Separated Flow Measurements on a Highly Loaded Low-Pressure Turbine Airfoil," *ASME Paper GT2008-51445*.

Volino, R.J., 2010, "Effect of Unsteady Wakes on Boundary Layer Separation on a Very High Lift Low Pressure Turbine Airfoil", *ASME Paper GT2010-23573*.

REPORT DOCUMENTATION PAGE				Form Approved OMB No. 0704-0188

The public reporting burden for this collection of information is estimated to average 1 hour per response, including the time for reviewing instructions, searching existing data sources, gathering and maintaining the data needed, and completing and reviewing the collection of information. Send comments regarding this burden estimate or any other aspect of this collection of information, including suggestions for reducing this burden, to Department of Defense, Washington Headquarters Services, Directorate for Information Operations and Reports (0704-0188), 1215 Jefferson Davis Highway, Suite 1204, Arlington, VA 22202-4302. Respondents should be aware that notwithstanding any other provision of law, no person shall be subject to any penalty for failing to comply with a collection of information if it does not display a currently valid OMB control number.
PLEASE DO NOT RETURN YOUR FORM TO THE ABOVE ADDRESS.

1. REPORT DATE (DD-MM-YYYY) 01-09-2012	2. REPORT TYPE Final Contractor Report	3. DATES COVERED (From - To) January 2007 to September 2010

4. TITLE AND SUBTITLE CFD Simulations for the Effect of Unsteady Wakes on the Boundary Layer of a Highly Loaded Low Pressure Turbine Airfoil (L1A) Final Report	5a. CONTRACT NUMBER NNC07IA10I; N00189-07-P-A253
	5b. GRANT NUMBER DE-FC26-06NT42853
	5c. PROGRAM ELEMENT NUMBER
6. AUTHOR(S) Vinci, Samuel, J.	5d. PROJECT NUMBER
	5e. TASK NUMBER
	5f. WORK UNIT NUMBER WBS 561581.02.08.03.47.02.01

7. PERFORMING ORGANIZATION NAME(S) AND ADDRESS(ES) Cleveland State University 2121 Euclid Avenue Cleveland, Ohio 44115	8. PERFORMING ORGANIZATION REPORT NUMBER E-18088

9. SPONSORING/MONITORING AGENCY NAME(S) AND ADDRESS(ES) National Aeronautics and Space Administration Washington, DC 20546-0001	10. SPONSORING/MONITOR'S ACRONYM(S) NASA
	11. SPONSORING/MONITORING REPORT NUMBER NASA/CR-2012-217417

12. DISTRIBUTION/AVAILABILITY STATEMENT
Unclassified-Unlimited
Subject Categories: 02, 05, 07, and 34
Available electronically at http://www.sti.nasa.gov
This publication is available from the NASA Center for AeroSpace Information, 443-757-5802

13. SUPPLEMENTARY NOTES
This report was submitted as a thesis in partial fulfillment of the requirements for the degree Master of Science to the Cleveland State University, Department of Mechanical Engineering, Cleveland, Ohio, May 2010. Grant technical monitors, Anthony J. Strazisar, Office of the Chief Scientist, Glenn Research Center, organization code ASOO, James D. Heidmann, Aeropropulsion Division, Glenn Research Center, organization code RTTO, David E. Ashpis, Aeropropulsion Division, Glenn Research Center, organization code RTTO, ashpis@nasa.gov

14. ABSTRACT
This report is the third part of a three-part final report of research performed under an NRA cooperative Agreement contract. The first part was published as NASA/CR-2012-217415. The second part was published as NASA/CR-2012-217416. The study of the very high lift low-pressure turbine airfoil L1A in the presence of unsteady wakes was performed computationally and compared against experimental results. The experiments were conducted in a low speed wind tunnel under high (4.9%) and then low (0.6%) freestream turbulence intensity for Reynolds number equal to 25,000 and 50,000. The experimental and computational data have shown that in cases without wakes, the boundary layer separated without reattachment. The CFD was done with LES and URANS utilizing the finite-volume code ANSYS Fluent (ANSYS, Inc.) under the same freestream turbulence and Reynolds number conditions as the experiment but only at a rod to blade spacing of 1. With wakes, separation was largely suppressed, particularly if the wake passing frequency was sufficiently high. This was validated in the 3D CFD efforts by comparing the experimental results for the pressure coefficients and velocity profiles, which were reasonable for all cases examined. The 2D CFD efforts failed to capture the three dimensionality effects of the wake and thus were less consistent with the experimental data. The effect of the freestream turbulence intensity levels also showed a little more consistency with the experimental data at higher intensities when compared with the low intensity cases. Additional cases with higher wake passing frequencies which were not run experimentally were simulated. The results showed that an initial 25% increase from the experimental wake passing greatly reduced the size of the separation bubble, nearly completely suppressing it.

15. SUBJECT TERMS
Gas turbines; Turbomachinery; Turbine; Low pressure turbine; Turbulence; Flow control; Synthetic jets; CFD; LES; Turbulence models; Wakes; Separation; Vortex generated jets

16. SECURITY CLASSIFICATION OF:			17. LIMITATION OF ABSTRACT	18. NUMBER OF PAGES	19a. NAME OF RESPONSIBLE PERSON STI Help Desk (email:help@sti.nasa.gov)
a. REPORT U	b. ABSTRACT U	c. THIS PAGE U	UU	132	19b. TELEPHONE NUMBER (include area code) 443-757-5802

Standard Form 298 (Rev. 8-98)
Prescribed by ANSI Std. Z39-18